ISSN 1949-8470 (online)

World Journal of *Radiology*

World J Radiol 2017 December 28; 9(12): 416-458

Published by Baishideng Publishing Group Inc

WJR World Journal of Radiology

A peer-reviewed, online, open-access journal of Radiology

Editorial Board

2014-2017

The *World Journal of Radiology* Editorial Board consists of 365 members, representing a team of worldwide experts in radiology. They are from 36 countries, including Afghanistan (1), Argentina (2), Australia (5), Austria (7), Belgium (2), Brazil (8), Canada (6), Chile (1), China (43), Croatia (1), Denmark (4), Egypt (6), France (5), Germany (22), Greece (10), India (12), Iran (6), Ireland (2), Israel (3), Italy (47), Japan (13), Netherlands (1), New Zealand (1), Pakistan (1), Poland (2), Portugal (1), Serbia (1), Singapore (3), Slovakia (1), South Korea (18), Spain (4), Sweden (2), Switzerland (4), Thailand (1), Turkey (26), United Kingdom (11), and United States (82).

Yue-Qi Zhu, *Shanghai*

Croatia

Goran Kusec, Osijek

Denmark

Poul E Andersen, *Odense*
Lars J Petersen, *Aalborg*
Thomas Z Ramsoy, *Frederiksberg*
Morten Ziebell, *Copenhagen*

Egypt

Mohamed F Bazeed, *Mansoura*
Mohamed Abou El-Ghar, *Mansoura*
Reem HA Mohamed, *Cairo*
Mohamed R Nouh, *Alexandria*
Ahmed AKA Razek, *Mansoura*
Ashraf A Zytoon, *Shebin El-Koom*

France

Sabine F Bensamoun, *Compiègne*
Romaric Loffroy, *Dijon*
Stephanie Nougaret, *Montpellier*
Hassane Oudadesse, *Rennes*
Vincent Vinh-Hung, *Fort-de-France*

Germany

Henryk Barthel, *Leipzig*
Peter Bannas, *Hamburg*
Martin Beeres, *Frankfurt*
Ilja F Ciernik, *Dessau*
A Dimitrakopoulou-Strauss, *Heidelberg*
Peter A Fasching, *Erlanegn*
Andreas G Schreyer, *Regensburg*
Philipp Heusch, *Duesseldorf*
Sonja M Kirchhoff, *Munich*
Sebastian Ley, *Munich*
Adel Maataoui, *Frankfurt am Main*
Stephan M Meckel, *Freiburg*
Hans W Muller, *Duesseldorf*
Kay Raum, *Berlin*
Dirk Rades, *Luebeck*
Marc-Ulrich Regier, *Hamburg*
Alexey Surov, *Halle*
Martin Walter, *Magdeburg*
Axel Wetter, *Essen*
Christoph Zilkens, *Düsseldorf*

Greece

Panagiotis Antoniou, *Thessaloniki*
Nikos Efthimiou, *Athens*
Dimitris Karnabatidis, *Patras*
George Latsios, *Athens*
Stylianos Megremis, *Iraklion*
Alexander D Rapidis, *Athens*
Kiki Theodorou, *Larissa*
Ioannis A Tsalafoutas, *Athens*
Evanthia E Tripoliti, *Ioannina*
Athina C Tsili, *Ioannina*

India

Ritesh Agarwal, *Chandigarh*
Chandan J Das, *New Delhi*
Prathamesh V Joshi, *Mumbai*
Naveen Kalra, *Chandigarh*
Chandrasekharan Kesavadas, *Trivandrum*
Jyoti Kumar, *New Delhi*
Atin Kumar, *New Delhi*
Kaushala P Mishra, *Allahabad*
Daya N Sharma, *New Delhi*
Binit Sureka, *New Delhi*
Sanjay Sharma, *New Delhi*
Raja R Yadav, *Allahabad*

Iran

Majid Assadi, *Bushehr*
SeyedReza Najafizadeh, *Tehran*
Mohammad Ali Oghabian, *Tehran*
Amir Reza Radmard, *Tehran*
Ramin Sadeghi, *Mashhad*
Hadi Rokni Yazdi, *Tehran*

Ireland

Tadhg Gleeson, *Wexford*
Frederik JAI Vernimmen, *Cork*

Israel

Dafna Ben Bashat, *Tel Aviv*
Amit Gefen, *Tel Aviv*
Tamar Sella, *Jerusalem*

Italy

Adriano Alippi, *Rome*
Dante Amelio, *Trento*
Michele Anzidei, *Rome*
Filippo F Angileri, *Messinas*
Stefano Arcangeli, *Rome*
Roberto Azzoni, *San Donato milanese*
Tommaso V Bartolotta, *Palermo*
Tommaso Bartalena, *Imola*
Livia Bernardin, *San Bonifacio*
Federico Boschi, *Verona*
Sergio Casciaro, *Lecce*
Emanuele Casciani, *Rome*
Musa M Can, *Napoli*
Alberto Cuocolo, *Napoli*
Michele Ferrara, *Coppito*
Mauro Feola, *Fossano*
Giampiero Francica, *Castel Volturno*
Luigi De Gennaro, *Rome*
Giulio Giovannetti, *Pisa*
Francesca Iacobellis, *Napoli*
Formato Invernizzi, *Monza Brianza*
Francesco Lassandro, *Naples*
Lorenzo Livi, *Florence*
Pier P Mainenti, *Napoli*
Laura Marzetti, *Chieti*
Giuseppe Malinverni, *Crescentino*
Enrica Milanesi, *Turin*
Giovanni Morana, *Treviso*
Lorenzo Monti, *Milan*
Silvia D Morbelli, *Genoa*
Barbara Palumbo, *Perugia*
Cecilia Parazzini, *Milan*
Stefano Pergolizzi, *Messina*
Antonio Pinto, *Naples*
Camillo Porcaro, *Rome*
Carlo C Quattrocchi, *Rome*
Alberto Rebonato, *Perugia*
Giuseppe Rizzo, *Rome*
Roberto De Rosa, *Naples*
Domenico Rubello, *Rovigo*
Andrea Salvati, *Bari*
Sergio Sartori, *Ferrara*
Luca M Sconfienza, *Milano*
Giovanni Storto, *Rionero*
Nicola Sverzellati, *Parma*
Alberto S Tagliafico, *Genova*
Nicola Troisi, *Florence*

Japan

Yasuhiko Hori, *Chiba*
Hidetoshi Ikeda, *Koriyama*
Masahito Kawabori, *Sapporo*
Tamotsu Kamishima, *Sapporo*
Hiro Kiyosue, *Yufu*
Yasunori Minami, *Osaka-sayama*
Yasuhiro Morimoto, *Kitakyushu*
Satoru Murata, *Tokyo*
Shigeki Nagamachi, *Miyazaki*
Hiroshi Onishi, *Yamanashi*
Morio Sato, *Wakayama Shi*
Yoshito Tsushima, *Maebashi*
Masahiro Yanagawa, *Suita*

Netherlands

Willem Jan van Rooij, *Tilburg*

New Zealand

W Howell Round, *Hamilton*

Pakistan

Wazir Muhammad, *Abbottabad*

Poland

Maciej S Baglaj, *Wroclaw*

Piotr Czauderna, *Gdansk*

Portugal

Joao Manuel RS Tavares, *Porto*

Serbia

Olivera Ciraj-Bjelac, *Belgrade*

Singapore

Gopinathan Anil, *Singapore*
Terence KB Teo, *Singapore*
Cher Heng Tan, *Singapore*

Slovakia

Stefan Sivak, *Martin*

South Korea

Ki Seok Choo, *Busan*
Seung Hong Choi, *Seoul*
Dae-Seob Choi, *Jinju*
Hong-Seok Jang, *Seoul*
Yong Jeong, *Daejeon*
Chan Kyo Kim, *Seoul*
Se Hyung Kim, *Seoul*
Joong-Seok Kim, *Seoul*
Sang Eun Kim, *Seongnam*
Sung Joon Kwon, *Seoul*
Jeong Min Lee, *Seoul*
In Sook Lee, *Busan*
Noh Park, *Goyang*
Chang Min Park, *Seoul*
Sung Bin Park, *Seoul*
Deuk Jae Sung, *Seoul*
Choongsoo Shin, *Seoul*
Kwon-Ha Yoon, *Iksan*

Spain

Miguel A De Gregorio, *Zaragoza*
Antonio Luna, *Jaén*
Enrique Marco de Lucas, *Santander*
Fernando Ruiz Santiago, *Granada*

Sweden

Dmitry Grishenkov, *Stockholm*
Tie-Qiang Li, *Stockholm*

Switzerland

Nicolau Beckmann, *Basel*
Christian Boy, *Bern*
Giorgio Treglia, *Bellinzona*

Stephan Ulmer, *Kiel*

Thailand

Sirianong Namwongprom, *Chiang Mai*

Turkey

Kubilay Aydin, *Istanbul*
Ramazan Akdemir, *Sakarya*
Serhat Avcu, *Ankara*
Ayse Aralasmak, *Istanbul*
Oktay Algin, *Ankara*
Nevbahar Akcar, *Meselik*
Bilal Battal, *Ankara*
Zulkif Bozgeyik, *Elazig*
Nazan Ciledag, Aakara
Fuldem Y Donmez, *Ankara*
Gulgun Engin, *Istanbul*
Ahmet Y Goktay, *Izmir*
Oguzhan G Gumustas, *Bursa*
Kaan Gunduz, *Ankara*
Pelin Ozcan Kara, *Mersin*
Kivanc Kamburoglu, *Ankara*
Ozgur Kilickesmez, *Istanbul*
Furuzan Numan, *Istanbul*
Cem Onal, *Adana*
Ozgur Oztekin, *Izmir*
Seda Ozbek (Boruban), *Konya*
Selda Sarikaya, *Zonguldak*
Figen Taser, *Kutahya*
Baran Tokar, *Eskisehir*
Ender Uysal, *Istanbul*
Ensar Yekeler, *Istanbul*

United Kingdom

Indran Davagnanam, *London*
M DC Valdés Hernández, *Edinburgh*
Alan Jackson, *Manchester*
Suneil Jain, *Belfast*
Long R Jiao, *London*
Miltiadis Krokidis, *Cambridge*
Pradesh Kumar, *Liverpool*
Peter D Kuzmich, *Derby*
Georgios Plataniotis, *Brighton*
Vanessa Sluming, *Liverpool*

United States

Garima Agrawal, *Saint Louis*
James R Brasic, *Baltimore*
Rajendra D Badgaiyan, *Buffalo*
Ulas Bagci, *Bethesda*
Anat Biegon, *Stony Brook*
Ramon Casanova, *Winston Salem*
Wenli Cai, *Boston*
Zheng Chang, *Durham*
Corey J Chakarun, *Long Beach*
Kai Chen, *Los Angeles*
Hyun-Soon Chong, *Chicago*
Marco Cura, *Dallas*
Ravi R Desai, *Bensalem*
Delia DeBuc, *Miami*
Carlo N De Cecco, *Charleston*
Timm-Michael L Dickfeld, *Baltimore*
Subba R Digumarthy, *Boston*
Huy M Do, *Stanford*
Todd A Faasse, *Grand Rapids*
Salomao Faintuch, *Boston*
Girish M Fatterpekar, *New York*
Dhakshinamoorthy Ganeshan, *Houston*
Robert J Griffin, *Little Rock*
Andrew J Gunn, *Boston*
Sandeep S Hedgire, *Boston*
Timothy J Hoffman, *Columbia*
Mai-Lan Ho, *San Francisco*
Juebin Huang, *Jackson*
Abid Irshad, *Charleston*
Matilde Inglese, *New York*
El-Sayed H Ibrahim, *Jacksonville*
Paul R Julsrud, *Rochester*
Pamela T Johnson, *Baltimore*
Ming-Hung Kao, *Tempe*
Sunil Krishnan, *Houston*
Richard A Komoroski, *Cincinnati*
Sandi A Kwee, *Honolulu*
King Kim, *Ft. Lauderdale*
Guozheng Liu, *Worcester*
Yiyan Liu, *Newark*
Venkatesh Mani, *New York*
Lian-Sheng Ma, *Pleasanton*
Rachna Madan, *Boston*
Zeyad A Metwalli, *Houston*
Yilong Ma, *Manhasset*
Hui Mao, *Atlanta*
Feroze B Mohamed, *Philadelphia*
Gul Moonis, *Boston*
John L Nosher, *New Brunswick*
Rahmi Oklu, *Boston*
Aytekin Oto, *Chicago*
Bishnuhari Paudyal, *Philadelphia*
Rajul Pandya, *Youngstown*
Chong-Xian Pan, *Sacramento*
Jay J Pillai, *Baltimore*
Neal Prakash, *Duarte*
Reza Rahbar, *Boston*
Ali S Raja, *Boston*
Gustavo J Rodriguez, *El Paso*
David J Sahn, *Portlsand*
Steven Schild, *Scottsdale*
Ali R Sepahdari, *Los Angeles*
Li Shen, *Indianapolis*
JP Sheehan, *Charlottesville*
Atul B Shinagare, *Boston*
Sarabjeet Singh, *Boston*
Charles J Smith, *Columbia*
Kenji Suzuki, *Chicago*
Monvadi Srichai-Parsia, *Washington*
Sree H Tirumani, *Boston*
Hebert A Vargas, *New York*
Sachit Verma, *Philadelphia*
Yoichi Watanabe, *Minneapolis*
Li Wang, *Chapel Hill*
Carol C Wu, *Boston*
Shoujun Xu, *Houston*
Min Yao, *Cleveland*
Xiaofeng Yang, *Atlanta*
Qingbao Yu, *Albuquerque*
Aifeng Zhang, *Chicago*
Chao Zhou, *Bethlehem*
Hongming Zhuang, *Philadelphia*

WJR World Journal of Radiology

Contents

Monthly Volume 9 Number 12 December 28, 2017

REVIEW

MINIREVIEWS

CASE REPORT

World Journal of Radiology
Volume 9 Number 12 December 28, 2017

Contents

NAME OF JOURNAL
World Journal of Radiology

ISSN
ISSN 1949-8470 (online)

LAUNCH DATE
January 31, 2009

FREQUENCY
Monthly

EDITORIAL OFFICE
Xiu-Xia Song, Director
World Journal of Radiology
Baishideng Publishing Group Inc
7901 Stoneridge Drive, Suite 501, Pleasanton, CA 94588, USA
Telephone: +1-925-2238242
Fax: +1-925-2238243
E-mail: editorialoffice@wjgnet.com
Help Desk: http://www.f6publishing.com/helpdesk
http://www.wjgnet.com

PUBLISHER
Baishideng Publishing Group Inc
7901 Stoneridge Drive, Suite 501,
Pleasanton, CA 94588, USA
Telephone: +1-925-2238242
Fax: +1-925-2238243
E-mail: bpgoffice@wjgnet.com
Help Desk: http://www.f6publishing.com/helpdesk
http://www.wjgnet.com

PUBLICATION DATE
December 28, 2017

INSTRUCTIONS TO AUTHORS
http://www.wjgnet.com/bpg/gerinfo/204

ONLINE SUBMISSION
http://www.f6publishing.com

World Journal of Radiology

Submit a Manuscript: http://www.f6publishing.com

World J Radiol 2017 December 28; 9(12): 416-425

DOI: 10.4329/wjr.v9.i12.416

ISSN 1949-8470 (online)

REVIEW

Dynamic contrast-enhanced magnetic resonance imaging of prostate cancer: A review of current methods and applications

Yousef Mazaheri, Oguz Akin, Hedvig Hricak

Yousef Mazaheri, Department of Medical Physics and Radiology, Memorial Sloan Kettering Cancer Center, New York, NY 10065, United States

Oguz Akin, Hedvig Hricak, Department of Radiology, Memorial Sloan Kettering Cancer Center, New York, NY 10065, United States

ORCID number: Yousef Mazaheri (0000-0002-8493-1608); Oguz Akin (0000-0002-2041-6199); Hedvig Hricak (0000-0003-2240-9694).

Author contributions: All authors are the guarantors of integrity of entire study; Mazaheri Y designed the study; Mazaheri Y and Akin O performed data analysis/interpretation; Mazaheri Y and Akin O performed the literature research; all authors contributed to manuscript drafting or manuscript revision for important intellectual content; all authors gave manuscript final version approval and manuscript editing; all authors take responsibility for the integrity of the data and the accuracy of the data analysis.

Conflict-of-interest statement: This manuscript is not published anywhere else; all authors conform that there is no conflict of interests (including none for related to commercial, personal, political, intellectual, or religious interests).

Manuscript source: Unsolicited manuscript

Correspondence to: Yousef Mazaheri, PhD, Department of Medical Physics and Radiology, Memorial Sloan Kettering Cancer Center, 1275 York Avenue, New York, NY 10065, United States. mazahery@mskcc.org
Telephone: +1-646-8884520
Fax: +1-646-8885139

Received: May 17, 2017
Peer-review started: May 19, 2017
First decision: July 3, 2017
Revised: August 3, 2017
Accepted: October 17, 2017
Article in press: October 17, 2017
Published online: December 28, 2017

Abstract

In many areas of oncology, dynamic contrast-enhanced magnetic resonance imaging (DCE-MRI) has proven to be a clinically useful, non-invasive functional imaging technique to quantify tumor vasculature and tumor perfusion characteristics. Tumor angiogenesis is an essential process for tumor growth, proliferation, and metastasis. Malignant lesions demonstrate rapid extravasation of contrast from the intravascular space to the capillary bed due to leaky capillaries associated with tumor neovascularity. DCE-MRI has the potential to provide information regarding blood flow, areas of hypoperfusion, and variations in endothelial permeability and microvessel density to aid treatment selection, enable frequent monitoring during treatment and assess response to targeted therapy following treatment. This review will discuss the current status of DCE-MRI in cancer imaging, with a focus on its use in imaging prostate malignancies as well as weaknesses that limit its widespread clinical use. The latest techniques for quantification of DCE-MRI parameters will be reviewed and compared.

Key words: Prostate cancer; Prostate magnetic resonance imaging; Tumor angiogenesis; Dynamic contrast-enhanced magnetic resonance imaging; K_{ep} = rate constant between extracellular extravascular space and plasma space; K^{trans} = volume transfer constant

Core tip: Dynamic contrast-enhanced magnetic resonance imaging (DCE-MRI) of prostate cancer can characterize tissue vascularity with important clinical application including aid in the detection, localization and staging, assessment of tumor aggressiveness, and assessment of treatment response. The current lack of standardized acquisition and analysis methods should be addressed to encourage more wide spread use of DCE-MRI in prostate cancer imaging.

Mazaheri Y, Akin O, Hricak H. Dynamic contrast-enhanced magnetic resonance imaging of prostate cancer: A review of current methods and applications. *World J Radiol* 2017; 9(12): 416-425 Available from: URL: http://www.wjgnet.com/1949-8470/full/v9/i12/416.htm DOI: http://dx.doi.org/10.4329/wjr.v9.i12.416

INTRODUCTION

This review describes dynamic contrast-enhanced magnetic resonance imaging (DCE-MRI) techniques for aiding prostate cancer management. First, we review methodologies for the acquisition and analysis of DCE-MRI data, including a commonly used model for the quantification of DCE-MRI data sets. Second, we discuss several current and potential future clinical applications of DCE-MRI and pharmacokinetic parametric maps in prostate cancer imaging. These include: (1) Primary tumor detection, localization, and staging; (2) risk assessment; (3) treatment planning; (4) treatment response assessment; and (5) detection of residual or locally recurrent cancer after treatment. Finally, we present an overview of the challenges of DCE-MRI in the management of prostate cancer and future directions.

BASIC CONCEPTS

To characterize tumor vasculature, a number of paramagnetic agents have been approved for routine clinical use. The most commonly-used contrast agents are gadolinium (Gd) chelates of low molecular weight. The mechanism of most T_1 methods involves characterization of the influxes and out-fluxes of the contrast agent and of the extracellular extravascular volume fraction within the tumor vasculature. In conventional contrast-enhanced imaging, data are acquired before contrast administration and again one or two times after contrast administration. An intravenous line may be set up during or prior to the exam to allow the injection of gadolinium contrast [gadolinium-diethylenetriamine pentaacetic acid (Gd-DTPA)] during a magnetic resonance (MR) acquisition. For some patients, Gd-DTPA may be injected into the arm by a nurse, just as is done for many routine clinical MRI exams. Gd-DTPA is administered into the right antecubital vein.

DCE-MRI is the acquisition of sequential images during the passage of a contrast agent within a tissue of interest. DCE-MRI data are acquired rapidly during imaging following IV injection of the contrast agent and allow modeling of the passage of the contrast agent. Numerous pharmacokinetic models have been proposed for quantitative analysis of the observed signal intensity changes following contrast agent administration and for estimating pharmacokinetic parameters[1,2]. For a comprehensive review of DCE-MRI tracer kinetic models see[3] as well as a recent article by Sourbron and Buckley[4].

IMAGING STRATEGIES: RAPID DYNAMIC CONTRAST-ENHANCED IMAGING

In "dynamic" contrast-enhanced MR imaging, 3D T_1-weighted fast spoiled gradient-echo MRI sequences are obtained every 5-10 s before, during, and several minutes after administration of contrast in a sequential or "dynamic" fashion for a period of up to 10 min. Acquisition times of greater than 15 s are generally not used due to difficulty detecting early enhancement and capillary transit time of < 5 s. Contrast agents create shorter relaxation times, resulting in a brightening of T_1 signal on images. Contrast signal depends on both extravasation of contrast as well as velocity of blood flow to the target area[5,6]. There is no consensus on the best method for acquiring DCE-MRI data.

QUANTIFICATION OF DCE-MRI DATA

The assessment of signal enhancement after contrast injection can be performed through a semi-quantitative analysis of signal intensity changes over time. In this approach parameters, including curve shape, maximum signal intensity, wash-in (or upslope) and washout rates, as well as the initial area under the signal intensity curve or contrast medium concentration (IAUGC) curve, are estimated. Alternatively, it is possible to use a quantitative approach, which is based on pharmacokinetic modeling of the contrast agent. Numerous pharmacokinetic models have been proposed for quantitative analysis of signal intensity changes and for estimating pharmacokinetic parameters[1,2].

Semi-quantitative/model-free method

Data modeling impacts the accuracy of parameters derived from DCE-MR images, which depends on both temporal sampling and signal intensity from the injected contrast agent. As an alternative to data modeling, data can be compared in a semi-quantitative method by using pixel-by-pixel analysis[4,6]. From the corresponding signal intensity–time curves, enhancement kinetic parameters, semi-quantitative parameters are estimated. The typical parameters estimated for the semi-quantitative or non-model-based analysis include peak enhancement (PE), time-to-peak (TTP), wash-in, washout, and IAUGC. PE refers to the maximum signal intensity value between contrast arrivals, normalized by subtraction of the baseline

signal intensity. The quantity TTP is the corresponding time when the peak-enhancement is observed. The enhancement-slope and washout-slope allow for the quantitative evaluation of the wash-in and wash-out of the contrast agent and refer to the steepness of the curve during wash-in and wash-out (until the end of the acquisition), respectively. Semi-quantitative parameters are readily calculated with post-processing software available from the manufacturer of the MR unit and do not require measurement of arterial input function or tissue T_1 relaxation. One notable disadvantage of semi-quantitative parameters is that they are estimated directly from the signal intensity measurements (or concentration if in addition T_1 maps are generated) without a physiological or empirical model. Another disadvantage is that these parameters are dependent on experimental factors such as hardware, sequence parameters, and contrast dose, which limit their comparability across different sites or different acquisitions under different experimental conditions.

The semi-quantitative analyses provide parameters of area under the curve, time to peak, maximum enhancement, and slope of regions of interest. Advantages of these analytical parameters are their ease of acquisition, good visual image quality, and the fact that they do not require additional information such as tissue T_1 or measurement of the arterial input function. However, variability in dosing, bolus time, sequence parameters, tissue characteristics or other factors could affect reproducibility, presenting problems when utilizing these descriptive parameters. Models have been utilized to quantify and standardize parameters of contrast agents.

Quantitative analysis of DCE-MRI

A number of methods have been presented in the literature for the acquisition and analysis of DCE-MRI data sets. In this section we will review the basic principles of DCE-MRI analysis and introduce a few widely used analysis methods.

Relationship between MR signal and contrast agent concentration

In contrast-enhanced MRI, the relationship between signal and contrast agent concentration is not linear. To estimate contrast agent concentration, required for quantification of DCE-MRI parameters, the relationship between T_1, signal intensity, and contrast agent concentration is applied. The signal intensity for a spoiled gradient echo in steady-state is given by: $S(\alpha) = M_0 [(1-E_1) \sin(\alpha)]/[1-E_1 \cos(\alpha)] \times e^{(-TE/T2^*)}$ [1].

Where $E1 = e^{-(TE/T1)}$, α is the flip angle, M_0 is the proton density, TR is the repetition time, TE is the echo time, and T_2^* is the effective transversal relaxation time. The change in relaxation rate per unit of contrast agent concentration is given by[7], assuming that the tracer concentration is to be linearly proportional to the change in the relaxation rate under the assumption of a fast exchange limit: $C(t) = (1/R_1)\{[1/T_1(t)] - [1/T_1(0)]\}$ [2].

Where $T_1(t)$ and $T_1(t)$ are the relaxation times with contrast agent at time *t*, and pre-enhancement, R_1 is the relaxivity in $(mM \cdot s)^{-1}$ taken to equal 4.5 mmol/s at 1.5-Tesla field strength, and C (t) is the concentration of the contrast agent.

Tofts model

Following the convention proposed by Tofts *et al*[8], a simple one-compartmental model of the tumor is used to predict the flow of the contrast agent into the EES as a function of time (Figure 1): $[d C_t(t)]/dt = K^{trans} \times \{C_p(t) - [C_t(t)/v_e]\}$ [8].

Where $C_p(t)$ is the tracer concentration in blood plasma $C_p = C_b/(1\text{-Hct})$, and the hematocrit (Hct) in tumors is typically assumed to equal 0.25[9]. K^{trans} (min) is the volume transfer constant between the blood plasma and the EES; K_{ep} (min) is the rate constant between the EES and the blood plasma and is given by: $K_{ep} = (K^{trans}/v_e)$ where v_e is the fractional volume of the EES. Intuitively, K^{trans} describes the diffusive transport of the contrast agent across the capillary endothelium. The solution to Eq.[8], with the assumption that the contribution to the concentration of the contrast agent due to plasma is negligible, is given by the following (referred to as the original Tofts model): $C_p(t) = K^{trans} \int_0^t C_p(u) \times \exp\{-[K^{trans}(t-u)]/v_e\} du$ [9].

Extended Tofts model (ETM)

In the case of tumors, the above-mentioned assumption is not valid, and thus the two-compartment extension of the Tofts model is required, where the tissue concentration is the sum of the contribution due to the plasma volume, v_p, as well as the fractional volume of the EES, v_e: $C_t(t) = v_p C_p(t) + v_e C_e(t)$ [10].

The extended Tofts model corresponds to two compartments with the assumption that the concentration of the contrast agent is derived from the EES and plasma, given by: $C_t(t) = K^{trans} \int_0^t C_p(u) \times \exp\{-[K^{trans}(t-u)]/v_e\} du + v_p C_p(t)$ [11].

Additional considerations in quantitative DCE-MRI

A number of factors need to be taken into account in the estimation of parameters from DCE-MRI.

Choice of arterial input function

Measurement of the patient-specific arterial input function (AIF) or plasma concentration requires localization of a large vessel that delivers blood to the organ of interest. Alternatively a bi-exponential AIF, $C_p(t)$, can be generated assuming a bi-exponent model given by[10] (Figure 2): $C_p(t) = D[a_1 \exp(-m_1 t) + a_2 \exp(-m_2 t)]$ [10].

Where *D* is the dose of the contrast agent (mmol/kg of body weight). This is referred to as a model-based AIF. The first term in this expression corresponds to the equilibration of contrast agent between blood and extracellular space (fast), while the second term

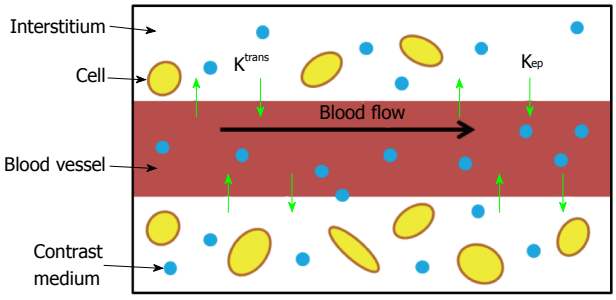

Figure 1 Schematic diagram of the Tofts kinetic model with the commonly used estimated parameters K^{trans} and k_{ep}.

corresponds to the removal of contrast agent from the plasma by the kidneys (slow). Substituting Eq.[10] into Eq.[8] and solving for $C_t(t)$ in the tumor tissue we obtain: $C_p(t) = D \times K^{trans} \Sigma^{2}_{i=1} \{[a_1 \exp(-m_i t) + a_2 \exp(-k_{ep} t)]/k_{ep}-m_i\}$ [11].

An alternative to calculating the bi-exponential AIF is to derive the AIF in a select population and extend it to future studies. This is referred to as a population average AIF. One study compared prostate DCE-MRI parameters obtained at 3 Tesla before biopsy using three AIF estimates: Patient-specific or individual AIF, population average AIF, and model-based AIF[11]. The study found patient-specific and population average AIFs had the highest sensitivity in predicting the biopsy results in prostate cancer, while the model-based bi-exponential AIF had the highest specificity. The areas under the ROC curves were not significantly different between any of the AIFs. In another study[12], investigators compared the effects of using population based AIF or semi-automated or fully automated image-based patient-specific AIF to calculate DCE-MRI parameters in the prostate; they found that K^{trans} estimates were more sensitive to the choice between population *vs* patient-specific AIF as compared to k_{ep}.

T_1 mapping

An estimate of the voxel contrast concentration in DCE-MRI requires T_1 estimation in order to convert signal intensity to T_1 values. T_1 relaxation times can be estimated from T_1 maps acquired prior to the injection of contrast. Typically, before contrast agent administration, a series of spoiled gradient echo volumes at different flip angles are acquired[13]. The steady-state signal is given by Eq.[1], which can be rearranged to yield: $S(\alpha)/\sin(\alpha) = E_1 [S(\alpha)/\tan(\alpha)] + M_0 \times (1-E_1) \times e^{(-TE/T^*2)}$ [12].

With a series of acquisitions at different flip angles, a linear fit of $S(\alpha)/\sin(\alpha)$ *vs* $S(\alpha)/\tan(\alpha)$ will allow estimation of T_1 from a linear fit $T_1 = -TR/\ln(m)$, where m is the slope between measurement points. At least two flip angles are required to estimate T_1 maps.

DCE-MRI of prostate

Studies on the use of dynamic or conventional contrast-enhanced MRI for prostate cancer have focused on localization and staging, assessment of prostate cancer aggressiveness, and assessment of treatment response (Figure 3). These studies suggest the many ways that contrast-enhanced MRI could be used to augment the value of a prostate MRI exam.

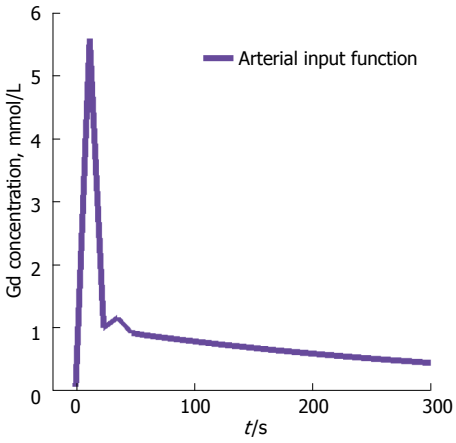

Figure 2 Model-based arterial input function. Shown is the model-based arterial input function, based on the Parker function.

Localization and staging

Numerous studies have investigated the accuracy of DCE-MRI in localization and staging of prostate cancer using DCE-MRI (Figures 4 and 5). In a study performed at 1.5 Tesla, the accuracy of DCE-MRI in tumor localization was found to be significantly higher than that of T2-weighted imaging (as well as significantly higher than that of quantitative spectroscopic imaging)[14]. The same group reported that accuracy in prostate cancer localization (again at 1.5 Tesla) was significantly higher with DCE–MRI and 3D MRSI than with T2-weighted imaging[14,15]. Using a 3.0-Tesla system, Kim *et al*[16] found that detection of prostate cancer in the peripheral zone was better with DCE-MRI than with T2-weighted imaging. Sensitivity, specificity, and accuracy were 55%, 88% and 70%, respectively, with T2-weighted MRI as compared to 73%, 77%, and 75%, respectively, with dynamic contrast-enhanced imaging. In another study phased-array coils were used for signal homogeneity to image patients on a 1.5 T system before biopsy; based on early and intense enhancement areas on T1-weighted DCE images, sensitivity, specificity, and positive and negative predictive values were 90%, 88%, 77% and 95%, respectively for the detection of foci greater than 0.5 cc *vs* 77%, 91%, 86% and 85% for the detection of foci greater than 0.2 cc[17]. Ocak *et al*[18] found the forward volume transfer constant (K^{trans}), the reverse reflux rate constant between extracellular space and plasma (k_{ep}), and the area under the gadolinium curve (AUGC) to be significantly higher in cancer than in the normal PZ. Engelbrecht *et al*[19] identified relative peak enhancement in the PZ and washout rate in the central gland as DCE-MRI parameters useful for prostate cancer detection and localization, but they did not find strong correlations between dynamic parameters in prostate

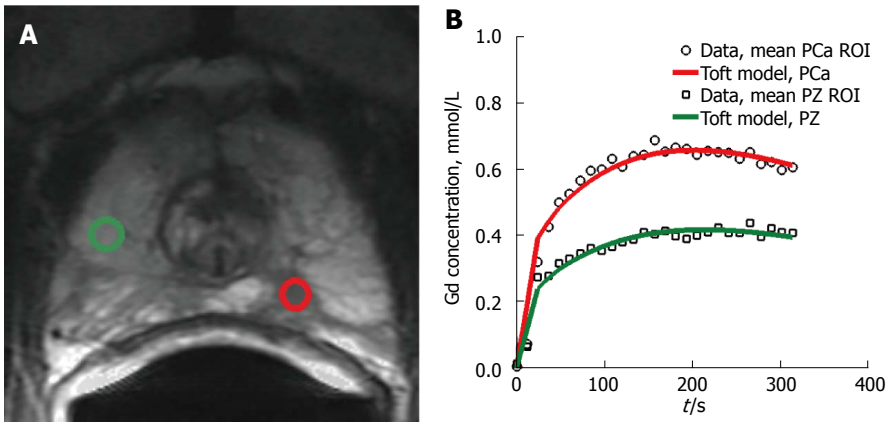

Figure 3 Example of enhancement kinetics pattern from two regions-of-interest. A: Transverse T2-weighted image. The green regions-of-interest (ROIs) corresponds to a benign PZ region. The red ROI corresponds to region with prostate cancer; B: Contrast curves of the two ROIs shown in A. The curves are characteristic of the types of time-intensity curves obtained with dynamic contrast-enhanced MRI. The green ROI shows moderately slow and slight enhancement wash-in pattern. This is characteristic for many benign, enhancing tissues, such as normal prostate tissue. The red ROI shows a rapid rise in signal intensity with subsequent wash-out as is typical in tumors.

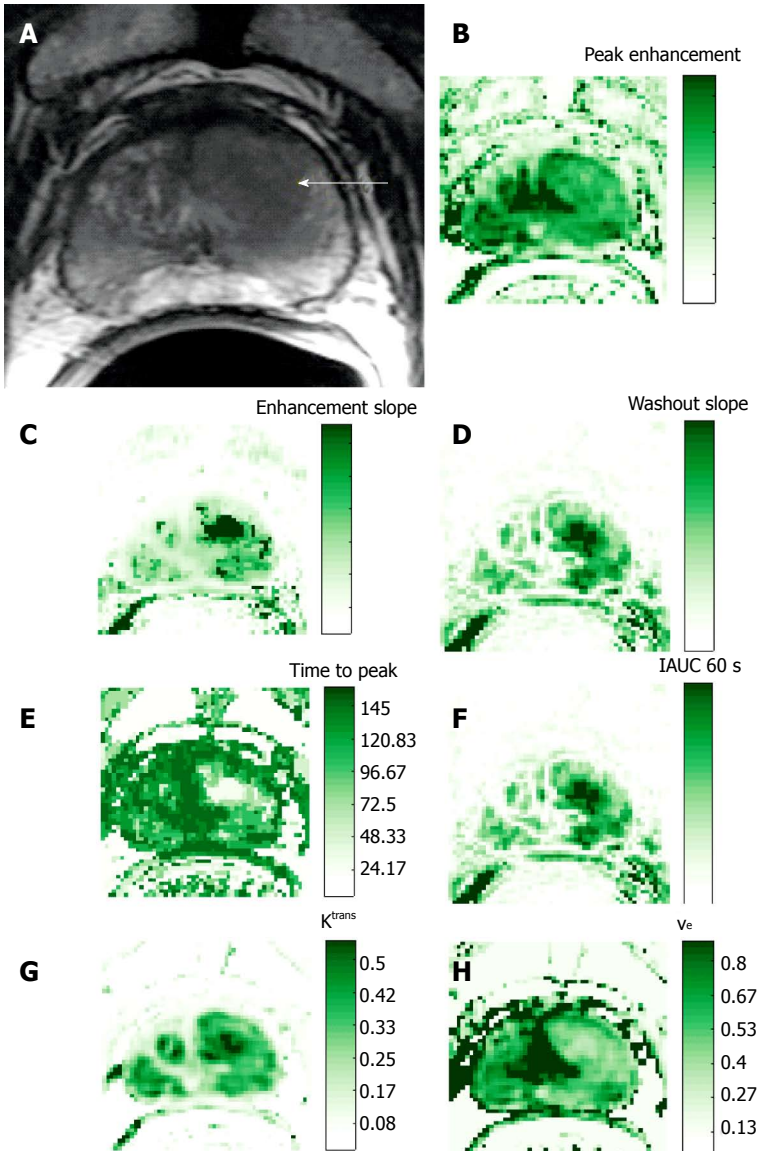

Figure 4 Representative 3T data in 63-year-old patient with prostate cancer (presurgical prostate-specific antigen level, 3.4 ng/mL). A: Transverse T2-weighted image. Pharmacokinetic parameter maps based on the semi-quantitative method and the Toft's kinetic model. Parametric maps for the semi-quantitative parameters, including; B: Peak-enhancement; C: Enhancement slope; D: Wash-out slope; E: Time-to-peak; and F: Intensity curve or contrast medium concentration at 60 s. Using the Toft's kinetic model, the pharmacokinetic parameter maps for G K^{trans} and H v_e are shown.

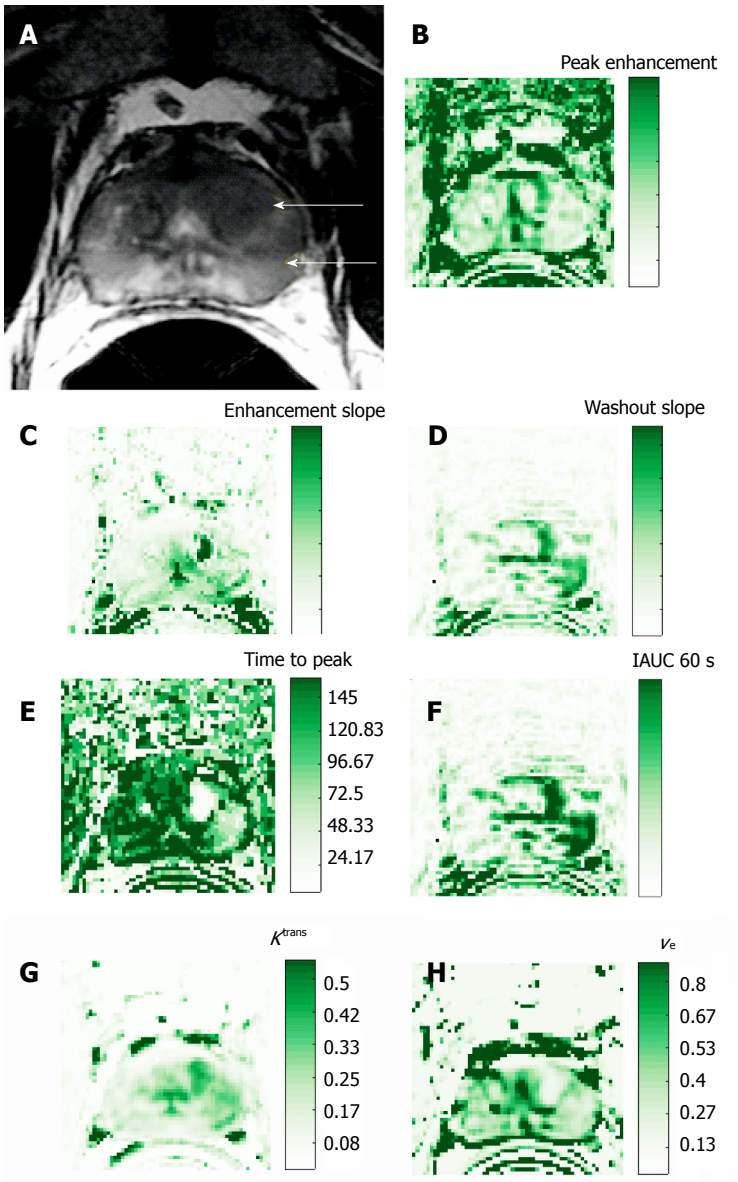

Figure 5 Representative 3T data in a 54-year-old prostate cancer patient [presurgical prostate-specific antigen level, 4.7 ng/mL; biopsy Gleason score, 7 (3 + 4)]. Pharmacokinetic parameter maps based on the semi-quantitative method and the Toft's kinetic model. Parametric maps for the semi-quantitative parameters, including B: Peak-enhancement; C: Enhancement slope; D: Wash-out slope; E: Time-to-peak; and F: Intensity curve or contrast medium concentration at 60 s. Using the Toft's kinetic model, the pharmacokinetic parameter maps for G K^{trans} and H v_e are shown.

cancer regions and tumor stage, Gleason score, patient age, tumor volume, or prostate-specific antigen. Alonzi *et al*[20] provided a table summarizing the early literature on prostate tumor localization.

With regard to staging of prostate cancer with DCE-MRI, one study compared the performance of an experienced reader to that of a less experienced reader[21]. The investigators found that for the experienced reader, the sensitivity, specificity, and accuracy of staging with dynamic contrast-enhanced MR imaging were 69%, 97%, and 87%, respectively, and were not significantly different from the corresponding values obtained with T2-weighted imaging alone. However, for the less experienced reader, the use of DCE-MRI parametric maps resulted in a significant improvement in the area under the receiver operating characteristic curve as compared to T2-weighted imaging alone. Bloch *et al*[22] presented findings from 1.5-Tesla high-spatial-resolution T2-weighted imaging and DCE-MR imaging in 32 patients. When the T2-weighted imaging and DCE-MR imaging data sets were combined, the mean sensitivity, specificity, *P* value, and negative predictive values for the assessment of extracapsular extension (ECE) were 86%, 95%, 90%, and 93%, respectively; the determination of ECE was significantly better when the data sets were combined than when T2-weighted imaging was used alone.

ROLE OF DCE-MRI IN THE PI-RADS (PROSTATE IMAGING REPORTING AND DATA SYSTEM) CLASSIFICATION

The European Society of Urogenital Radiology (ESUR) has provided a set of guidelines for MR imaging of the

prostate[23]. These guidelines provide recommendations for minimum standards of MR protocols as well outlining a structured reporting scheme, referred to as PI-RADS which are based on the BI-RADS classification for breast imaging. The reporting provides scores ranging from 1 to 5. The PI-RADS classification of DCE-MRI uses the time-resolved signal intensity curve to provide a qualitative analysis of the shape of the signal intensity curve. A score of 1 is assigned when the signal intensity curve increases gradually (Type Ⅰ curve). Score of 2 is assigned when there is progressive signal intensity stabilization followed by a slight and late decrease in signal intensity (Type Ⅱ curve). Score of 3 is assigned if the signal intensity curve demonstrates rapid washout after reaching peak enhancement (Type Ⅲ curve). Focal lesions which enhance according to Type Ⅱ or Ⅲ curves are assigned an additional point. Asymmetric lesions or unusually located lesions which enhance according to Type Ⅱ or Ⅲ curves receive an additional point[24].

Assessment of prostate cancer aggressiveness

The Gleason score, determined by histopathology, characterizes prostate cancer aggressiveness based on the microscopic appearance of the cancer tissue[25]. Together with other parameters, the Gleason score is used for prostate cancer staging, assessment of the patient's prognosis and treatment selection. Most commonly, the Gleason score is determined by biopsy, which is performed when an elevated serum prostate-specific antigen (PSA) level and/or an abnormal digital rectal examination (DRE) suggest that the patient may have prostate cancer. The biopsy Gleason score and the amount of cancer in each biopsy core are both important predictors of prostate cancer aggressiveness and rate of progression[26,27]. However, biopsy underestimates the Gleason score relative to the prostatectomy Gleason score in as many as 50% of cases[28]. Moreover, sextant biopsy samples mostly the posterior peripheral zone of the prostate, thereby potentially missing tumors in anterior portions of the gland.

A review of prior studies to identify associations between MRI perfusion parameters and Gleason score suggests no such associations have been consistently found[29-33]. An earlier study by Padhani *et al*[29] found only a weak correlation between MRI tumor stage and tumor vascular permeability. However, no correlation was observed between enhancement patterns (*i.e.*, both quantitive and semi-quantitive parameters) and Gleason score or PSA levels. Another study used an enhanced inversion-prepared dual-contrast gradient-echo sequence at 1.5 Tesla to perform DCE-MRI combined with dynamic susceptibility contrast (DSC) MR imaging, which allows simultaneous calculation of the parameters blood volume, blood flow, and interstitial volume. Subsequently, the parameters were correlated with histologic mean vessel density (MVD), mean vessel area (MVA), and mean interstitial area (MIA), and it was found that the measured quantities of blood volume and interstitial volume did not reliably correlate with the histologic parameters[30]. Chen *et al*[31] performed both semi-quantitative and quantitaive analysis of DCE-MRI and correlated the parameters with Gleason score; they found that only the washout gradient correlated significantly with Gleason score. Another study using quantitaive analysis of DCE-MRI was also unable to identify any significant correlations with Gleason score or vascular endothelial growth factor (VEGF) expression, although k_{ep} was found to correlate moderately with microvessel density[32]. Recently, a study at 3 Tesla found that both semi-quantitative and quantitative parameters (mean and 75th percentile values of wash-in, mean wash-out, and 75th percentile of K^{trans}), differed significantly between low-grade (Gleason grades 2 and 3 present) and high-grade prostate cancer (primary Gleason grade of 4 and/or any 5 component) in the peripheral zone[33]. Two factors which were identified as being important in acquisition of data for optimal modeling were: (1) the use of high temporal resolution imaging (temporal resolution = 3 s), which allowed the investigators to more accurately probe the early phase of enhancement; and (2) the use of patient-specific AIF rather than population-based AIF.

ASSESSMENT OF TREATMENT RESPONSE

Androgen deprivation therapy

VEGF also called vascular permeability factor, is a stimulus of tumor neo-angiogenesis[34]. It has been shown that androgens induce the simulation of vascular endothelial growth factor production in human prostate cancer[35]. A study of 56 patients measured the effects of androgen deprivation therapy (ADT) on prostatic morphology and vascular permeability[36] and found a significant reduction in tumor permeability surface area product in the peripheral zone, central gland and tumor, as well as changes in washout patterns[36]. The authors also reported significant reductions in K^{trans} in the peripheral zone and central gland as well as a weak correlation between tumor K^{trans} and tumor volume change.

Another study examined the effect of ADT on prostate tumor blood flow by comparing quantitative parametric maps of the prostate for blood flow, blood volume, and blood oxygenation [intrinsic relaxivity (R_2*)], measured using a DSC-MRI acquisition and analysis, and K^{trans} and v_e, measured using a DCE-MRI acquisition and analysis; values acquired before ADT was administered were compared to those acquired after 1 mo and 3 mo of therapy[37]. The study found significant decreases in tumor blood volume and flow in the first month after treatment, and significant increases in R_2* of the prostate tumor by three months; the study also found significant reductions in tumor K^{trans} from baseline at both 1 and 3 mo. Another study looking at monitoring response with both DCE and DWI found that DCE-MRI parameters (K^{trans}, v_e, v_p, IAUGC-90) measured in tumor after 3 mo of therapy were significantly reduced as compared to those

measured before treatment, whereas normal-appearing peripheral zone tissue showed no significant change[38].

External-beam radiation therapy

When local recurrence is suspected after radiation treatment, MRI may be used to identify a target for biopsy and estimate the location and extent of the tumor. In an early study by Rouvière *et al*[39] assessing the value of DCE-MRI in patients with suspected recurrent prostate cancer after external beam radiotherapy (EBRT), readers interpreted contrast-enhanced images during the early phases, when prostatic tissue showed some degree of enhancement (the images were referred to as arterial phase images). They found that as compared to T2-weighted imaging, contrast-enhanced MRI localized recurrent cancer after EBRT more accurately and with less inter-observer variability. A later study found that in the localization of recurrent prostate cancer by sextant in patients with suspected relapse after EBRT, the sensitivity, positive predictive value and negative predictive value of DCE-MRI were significantly higher than those of T2-weighted imaging[40]. Although the investigators found that DCE-MRI had excellent sensitivity, negative predictive value (both of 100%), and good accuracy (82%) for the detection of prostate cancer recurrence after EBRT, the positive predictive value was not very high (46%), even though it was higher than that of T2-weighted imaging. Multi-parametric approaches have also been investigated[41,42]. One recent study found multi-parametric methods to be superior to T2-weighted imaging in the detection of recurrent prostate cancer after image-guided radiation therapy; however, there was no additional benefit when DCE-MRI was added to combined T2-weighed imaging and diffusion-weighted MRI (DW-MRI)[42].

High-dose-rate brachytherapy

A recent article retrospectively evaluated the ability of multiphase (specifically, 5-phase) dynamic contrast-enhanced MRI obtained every 30 s (as well as DW-MRI) to detect local recurrence after high-dose-rate brachytherapy[43]. Whereas the sensitivity, specificity, and accuracy of T2-weighted imaging were 27%, 99%, and 87%, respectively, those of DCE-MRI were 50%, 98%, and 90%, respectively. The authors found that a multi-parametric approach combining T2-weighted MRI, DW-MRI and DCE-MRI achieved the highest sensitivity (77%) with a slight reduction in specificity (92%) as compared to DW-MRI.

High-intensity focused ultrasound

For the treatment of patients with localized prostate cancer, a nonsurgical, noninvasive treatment referred to as transrectal high-intensity focused ultrasound (HIFU) can be considered[44,45]. DCE-MRI (combined with T2-weighted imaging) can have a role in detecting local cancer recurrences after HIFU. It can assist in distinguishing residual or recurrent cancers within 2-5 d after HIFU treatment[46] which are typically hypervascular from post-HIFU fibrosis which are often homogeneous and hypovascular[47] and can guide post-HIFU biopsy towards areas of recurrent cancer. One study found that although Gadolinium-enhanced MRI can accurately determine the extend of tissue damage following HIFU, it cannot predict histological results[46].

Surgery

A study by Casciani *et al*[48] to determine the ability of endorectal MRI (T1- and T2-weighted imaging) combined with DCE-MRI to detect local recurrence after radical prostatectomy found that all recurrences showed signal enhancement after gadolinium administration. In most cases of recurrence (22/24), tumors display rapid and early signal enhancement. The study found a significant improvement in the detection of recurrence with combined MRI and DCE-MRI as compared to MRI alone. Similarly, Sciarra *et al*[49] found that the use of DCE-MRI alone or in combination with spectroscopic imaging was accurate for identifying local prostate cancer recurrence in patients with biochemical progression after radical prostatectomy.

CHALLENGES AND FUTURE DIRECTIONS

Limitations in DCE-MRI specific to prostate cancer include motion artifact, specifically from rectal and colonic peristalsis. Further, hyperintense findings on MRI may correlate not only with abnormal tumor tissue but any changes in vascularity including BPH nodules, post-biopsy changes, and prostatitis. At present, an additional limitation of DCE-MRI of the prostate, which also applies to the imaging of all other organ systems, is the lack of standardization of sequences and analysis parameters[5]. With the availability of a wide range of imaging sequences on most MR units, a defining objective of many studies today is to identify the role of DCE-MRI as part of a multi-parametric examination[50].

CONCLUSION

We have reviewed DCE-MRI acquisition and data analysis methods for the detection and monitoring of cancer in the prostate. Potential clinical applications of DCE-MRI for prostate cancer include detection, localization and staging, assessment of tumor aggressiveness, and assessment of treatment response. Limitations include lack of standardized acquisition and analysis methods which can results in variability in the results. We expect that with the standardization of these methods will encourage more wide spread use of DCE-MRI in prostate cancer imaging.

REFERENCES

1 **Padhani AR**, Husband JE. Dynamic contrast-enhanced MRI studies in oncology with an emphasis on quantification, validation and human studies. *Clin Radiol* 2001; **56**: 607-620 [PMID: 11467863 DOI: 10.1053/crad.2001.0762]

2 **Knopp MV**, Giesel FL, Marcos H, von Tengg-Kobligk H, Choyke P. Dynamic contrast-enhanced magnetic resonance imaging in oncology.

Top Magn Reson Imaging 2001; **12**: 301-308 [PMID: 11687716]
3 **Tofts PS**, Brix G, Buckley DL, Evelhoch JL, Henderson E, Knopp MV, Larsson HB, Lee TY, Mayr NA, Parker GJ, Port RE, Taylor J, Weisskoff RM. Estimating kinetic parameters from dynamic contrast-enhanced T(1)-weighted MRI of a diffusable tracer: standardized quantities and symbols. *J Magn Reson Imaging* 1999; **10**: 223-232 [PMID: 10508281]
4 **Sourbron SP**, Buckley DL. Classic models for dynamic contrast-enhanced MRI. *NMR Biomed* 2013; **26**: 1004-1027 [PMID: 23674304 DOI: 10.1002/nbm.2940]
5 **Verma S**, Turkbey B, Muradyan N, Rajesh A, Cornud F, Haider MA, Choyke PL, Harisinghani M. Overview of dynamic contrast-enhanced MRI in prostate cancer diagnosis and management. *AJR Am J Roentgenol* 2012; **198**: 1277-1288 [PMID: 22623539 DOI: 10.2214/AJR.12.8510]
6 **Ferl GZ**, Port RE. Quantification of antiangiogenic and antivascular drug activity by kinetic analysis of DCE-MRI data. *Clin Pharmacol Ther* 2012; **92**: 118-124 [PMID: 22588603 DOI: 10.1038/clpt.2012.63]
7 **Donahue KM**, Burstein D, Manning WJ, Gray ML. Studies of Gd-DTPA relaxivity and proton exchange rates in tissue. *Magn Reson Med* 1994; **32**: 66-76 [PMID: 8084239]
8 **Tofts PS**. Modeling tracer kinetics in dynamic Gd-DTPA MR imaging. *J Magn Reson Imaging* 1997; **7**: 91-101 [PMID: 9039598]
9 **Brix G**, Bahner ML, Hoffmann U, Horvath A, Schreiber W. Regional blood flow, capillary permeability, and compartmental volumes: measurement with dynamic CT--initial experience. *Radiology* 1999; **210**: 269-276 [PMID: 9885619 DOI: 10.1148/radiology.210.1.r99ja46269]
10 **Weinmann HJ**, Laniado M, Mützel W. Pharmacokinetics of GdDTPA/dimeglumine after intravenous injection into healthy volunteers. *Physiol Chem Phys Med NMR* 1984; **16**: 167-172 [PMID: 6505043]
11 **Meng R**, Chang SD, Jones EC, Goldenberg SL, Kozlowski P. Comparison between population average and experimentally measured arterial input function in predicting biopsy results in prostate cancer. *Acad Radiol* 2010; **17**: 520-525 [PMID: 20074982 DOI: 10.1016/j.acra.2009.11.006]
12 **Fedorov A**, Fluckiger J, Ayers GD, Li X, Gupta SN, Tempany C, Mulkern R, Yankeelov TE, Fennessy FM. A comparison of two methods for estimating DCE-MRI parameters via individual and cohort based AIFs in prostate cancer: a step towards practical implementation. *Magn Reson Imaging* 2014; **32**: 321-329 [PMID: 24560287 DOI: 10.1016/j.mri.2014.01.004]
13 **Fennessy FM**, Fedorov A, Gupta SN, Schmidt EJ, Tempany CM, Mulkern RV. Practical considerations in T1 mapping of prostate for dynamic contrast enhancement pharmacokinetic analyses. *Magn Reson Imaging* 2012; **30**: 1224-1233 [PMID: 22898681 DOI: 10.1016/j.mri.2012.06.011]
14 **Fütterer JJ**, Heijmink SW, Scheenen TW, Veltman J, Huisman HJ, Vos P, Hulsbergen-Van de Kaa CA, Witjes JA, Krabbe PF, Heerschap A, Barentsz JO. Prostate cancer localization with dynamic contrast-enhanced MR imaging and proton MR spectroscopic imaging. *Radiology* 2006; **241**: 449-458 [PMID: 16966484 DOI: 10.1148/radiol.2412051866]
15 **Fütterer JJ**, Heijmink SW, Scheenen TW, Jager GJ, Hulsbergen-Van de Kaa CA, Witjes JA, Barentsz JO. Prostate cancer: local staging at 3-T endorectal MR imaging--early experience. *Radiology* 2006; **238**: 184-191 [PMID: 16304091 DOI: 10.1148/radiol.2381041832]
16 **Kim CK**, Park BK, Kim B. Localization of prostate cancer using 3T MRI: comparison of T2-weighted and dynamic contrast-enhanced imaging. *J Comput Assist Tomogr* 2006; **30**: 7-11 [PMID: 16365565]
17 **Villers A**, Puech P, Mouton D, Leroy X, Ballereau C, Lemaitre L. Dynamic contrast enhanced, pelvic phased array magnetic resonance imaging of localized prostate cancer for predicting tumor volume: correlation with radical prostatectomy findings. *J Urol* 2006; **176**: 2432-2437 [PMID: 17085122 DOI: 10.1016/j.juro.2006.08.007]
18 **Ocak I**, Bernardo M, Metzger G, Barrett T, Pinto P, Albert PS, Choyke PL. Dynamic contrast-enhanced MRI of prostate cancer at 3 T: a study of pharmacokinetic parameters. *AJR Am J Roentgenol* 2007; **189**: 849 [PMID: 17885055 DOI: 10.2214/AJR.06.1329]
19 **Engelbrecht MR**, Huisman HJ, Laheij RJ, Jager GJ, van Leenders GJ, Hulsbergen-Van De Kaa CA, de la Rosette JJ, Blickman JG, Barentsz JO. Discrimination of prostate cancer from normal peripheral zone and central gland tissue by using dynamic contrast-enhanced MR imaging. *Radiology* 2003; **229**: 248-254 [PMID: 12944607 DOI: 10.1148/radiol.2291020200]
20 **Alonzi R**, Padhani AR, Allen C. Dynamic contrast enhanced MRI in prostate cancer. *Eur J Radiol* 2007; **63**: 335-350 [PMID: 17689907 DOI: 10.1016/j.ejrad.2007.06.028]
21 **Fütterer JJ**, Engelbrecht MR, Huisman HJ, Jager GJ, Hulsbergen-van De Kaa CA, Witjes JA, Barentsz JO. Staging prostate cancer with dynamic contrast-enhanced endorectal MR imaging prior to radical prostatectomy: experienced versus less experienced readers. *Radiology* 2005; **237**: 541-549 [PMID: 16244263 DOI: 10.1148/radiol.2372041724]
22 **Bloch BN**, Furman-Haran E, Helbich TH, Lenkinski RE, Degani H, Kratzik C, Susani M, Haitel A, Jaromi S, Ngo L, Rofsky NM. Prostate cancer: accurate determination of extracapsular extension with high-spatial-resolution dynamic contrast-enhanced and T2-weighted MR imaging--initial results. *Radiology* 2007; **245**: 176-185 [PMID: 17717328 DOI: 10.1148/radiol.2451061502]
23 **Barentsz JO**, Richenberg J, Clements R, Choyke P, Verma S, Villeirs G, Rouviere O, Logager V, Fütterer JJ; European Society of Urogenital Radiology. ESUR prostate MR guidelines 2012. *Eur Radiol* 2012; **22**: 746-757 [PMID: 22322308 DOI: 10.1007/s00330-011-2377-y]
24 **Röthke M**, Blondin D, Schlemmer HP, Franiel T. [PI-RADS classification: structured reporting for MRI of the prostate]. *Rofo* 2013; **185**: 253-261 [PMID: 23404430]
25 **Gleason DF**, Mellinger GT. Prediction of prognosis for prostatic adenocarcinoma by combined histological grading and clinical staging. *J Urol* 1974; **111**: 58-64 [PMID: 4813554]
26 **Epstein JI**, Allsbrook WC Jr, Amin MB, Egevad LL. Update on the Gleason grading system for prostate cancer: results of an international consensus conference of urologic pathologists. *Adv Anat Pathol* 2006; **13**: 57-59 [PMID: 16462155 DOI: 10.1097/01.pap.0000202017.78917.18]
27 **Epstein JI**. What's new in prostate cancer disease assessment in 2006? *Curr Opin Urol* 2006; **16**: 146-151 [PMID: 16679850 DOI: 10.1097/01.mou.0000193389.31727.9b]
28 **Bak JB**, Landas SK, Haas GP. Characterization of prostate cancer missed by sextant biopsy. *Clin Prostate Cancer* 2003; **2**: 115-118 [PMID: 15040873]
29 **Padhani AR**, Gapinski CJ, Macvicar DA, Parker GJ, Suckling J, Revell PB, Leach MO, Dearnaley DP, Husband JE. Dynamic contrast enhanced MRI of prostate cancer: correlation with morphology and tumour stage, histological grade and PSA. *Clin Radiol* 2000; **55**: 99-109 [PMID: 10657154 DOI: 10.1053/crad.1999.0327]
30 **Franiel T**, Lüdemann L, Rudolph B, Rehbein H, Stephan C, Taupitz M, Beyersdorff D. Prostate MR imaging: tissue characterization with pharmacokinetic volume and blood flow parameters and correlation with histologic parameters. *Radiology* 2009; **252**: 101-108 [PMID: 19561252 DOI: 10.1148/radiol.2521081400]
31 **Chen M**, Dang HD, Wang JY, Zhou C, Li SY, Wang WC, Zhao WF, Yang ZH, Zhong CY, Li GZ. Prostate cancer detection: comparison of T2-weighted imaging, diffusion-weighted imaging, proton magnetic resonance spectroscopic imaging, and the three techniques combined. *Acta Radiol* 2008; **49**: 602-610 [PMID: 18568549 DOI: 10.1080/02841850802004983]
32 **Oto A**, Kayhan A, Jiang Y, Tretiakova M, Yang C, Antic T, Dahi F, Shalhav AL, Karczmar G, Stadler WM. Prostate cancer: differentiation of central gland cancer from benign prostatic hyperplasia by using diffusion-weighted and dynamic contrast-enhanced MR imaging. *Radiology* 2010; **257**: 715-723 [PMID: 20843992 DOI: 10.1148/radiol.10100021]
33 **Vos EK**, Litjens GJ, Kobus T, Hambrock T, Hulsbergen-van de Kaa CA, Barentsz JO, Huisman HJ, Scheenen TW. Assessment of prostate cancer aggressiveness using dynamic contrast-enhanced magnetic resonance imaging at 3 T. *Eur Urol* 2013; **64**: 448-455 [PMID: 23751135 DOI: 10.1016/j.eururo.2013.05.045]

34 **Dvorak HF**, Brown LF, Detmar M, Dvorak AM. Vascular permeability factor/vascular endothelial growth factor, microvascular hyperpermeability, and angiogenesis. *Am J Pathol* 1995; **146**: 1029-1039 [PMID: 7538264]

35 **Häggström S**, Lissbrant IF, Bergh A, Damber JE. Testosterone induces vascular endothelial growth factor synthesis in the ventral prostate in castrated rats. *J Urol* 1999; **161**: 1620-1625 [PMID: 10210429]

36 **Padhani AR**, MacVicar AD, Gapinski CJ, Dearnaley DP, Parker GJ, Suckling J, Leach MO, Husband JE. Effects of androgen deprivation on prostatic morphology and vascular permeability evaluated with mr imaging. *Radiology* 2001; **218**: 365-374 [PMID: 11161148 DOI: 10.1148/radiology.218.2.r01ja04365]

37 **Alonzi R**, Padhani AR, Taylor NJ, Collins DJ, D'Arcy JA, Stirling JJ, Saunders MI, Hoskin PJ. Antivascular effects of neoadjuvant androgen deprivation for prostate cancer: an in vivo human study using susceptibility and relaxivity dynamic MRI. *Int J Radiat Oncol Biol Phys* 2011; **80**: 721-727 [PMID: 20630668 DOI: 10.1016/j.ijrobp.2010.02.060]

38 **Barrett T**, Gill AB, Kataoka MY, Priest AN, Joubert I, McLean MA, Graves MJ, Stearn S, Lomas DJ, Griffiths JR, Neal D, Gnanapragasam VJ, Sala E. DCE and DW MRI in monitoring response to androgen deprivation therapy in patients with prostate cancer: a feasibility study. *Magn Reson Med* 2012; **67**: 778-785 [PMID: 22135228]

39 **Rouvière O**, Valette O, Grivolat S, Colin-Pangaud C, Bouvier R, Chapelon JY, Gelet A, Lyonnet D. Recurrent prostate cancer after external beam radiotherapy: value of contrast-enhanced dynamic MRI in localizing intraprostatic tumor--correlation with biopsy findings. *Urology* 2004; **63**: 922-927 [PMID: 15134982 DOI: 10.1016/j.urology.2003.12.017]

40 **Haider MA**, Chung P, Sweet J, Toi A, Jhaveri K, Ménard C, Warde P, Trachtenberg J, Lockwood G, Milosevic M. Dynamic contrast-enhanced magnetic resonance imaging for localization of recurrent prostate cancer after external beam radiotherapy. *Int J Radiat Oncol Biol Phys* 2008; **70**: 425-430 [PMID: 17881141 DOI: 10.1016/j.ijrobp.2007.06.029]

41 **Akin O**, Gultekin DH, Vargas HA, Zheng J, Moskowitz C, Pei X, Sperling D, Schwartz LH, Hricak H, Zelefsky MJ. Incremental value of diffusion weighted and dynamic contrast enhanced MRI in the detection of locally recurrent prostate cancer after radiation treatment: preliminary results. *Eur Radiol* 2011; **21**: 1970-1978 [PMID: 21533634]

42 **Donati OF**, Jung SI, Vargas HA, Gultekin DH, Zheng J, Moskowitz CS, Hricak H, Zelefsky MJ, Akin O. Multiparametric prostate MR imaging with T2-weighted, diffusion-weighted, and dynamic contrast-enhanced sequences: are all pulse sequences necessary to detect locally recurrent prostate cancer after radiation therapy? *Radiology* 2013; **268**: 440-450 [PMID: 23481164 DOI: 10.1148/radiol.13122149]

43 **Tamada T**, Sone T, Higashi H, Jo Y, Yamamoto A, Kanki A, Ito K. Prostate cancer detection in patients with total serum prostate-specific antigen levels of 4-10 ng/mL: diagnostic efficacy of diffusion-weighted imaging, dynamic contrast-enhanced MRI, and T2-weighted imaging. *AJR Am J Roentgenol* 2011; **197**: 664-670 [PMID: 21862809 DOI: 10.2214/AJR.10.5923]

44 **Uchida T**, Ohkusa H, Yamashita H, Shoji S, Nagata Y, Hyodo T, Satoh T. Five years experience of transrectal high-intensity focused ultrasound using the Sonablate device in the treatment of localized prostate cancer. *Int J Urol* 2006; **13**: 228-233 [PMID: 16643614]

45 **Poissonnier L**, Chapelon JY, Rouvière O, Curiel L, Bouvier R, Martin X, Dubernard JM, Gelet A. Control of prostate cancer by transrectal HIFU in 227 patients. *Eur Urol* 2007; **51**: 381-387 [PMID: 16857310 DOI: 10.1016/j.eururo.2006.04.012]

46 **Rouvière O**, Lyonnet D, Raudrant A, Colin-Pangaud C, Chapelon JY, Bouvier R, Dubernard JM, Gelet A. MRI appearance of prostate following transrectal HIFU ablation of localized cancer. *Eur Urol* 2001; **40**: 265-274 [PMID: 11684842]

47 **Rouvière O**, Girouin N, Glas L, Ben Cheikh A, Gelet A, Mège-Lechevallier F, Rabilloud M, Chapelon JY, Lyonnet D. Prostate cancer transrectal HIFU ablation: detection of local recurrences using T2-weighted and dynamic contrast-enhanced MRI. *Eur Radiol* 2010; **20**: 48-55 [PMID: 19690866 DOI: 10.1007/s00330-009-1520-5]

48 **Casciani E**, Polettini E, Carmenini E, Floriani I, Masselli G, Bertini L, Gualdi GF. Endorectal and dynamic contrast-enhanced MRI for detection of local recurrence after radical prostatectomy. *AJR Am J Roentgenol* 2008; **190**: 1187-1192 [PMID: 18430830 DOI: 10.2214/AJR.07.3032]

49 **Sciarra A**, Panebianco V, Salciccia S, Osimani M, Lisi D, Ciccariello M, Passariello R, Di Silverio F, Gentile V. Role of dynamic contrast-enhanced magnetic resonance (MR) imaging and proton MR spectroscopic imaging in the detection of local recurrence after radical prostatectomy for prostate cancer. *Eur Urol* 2008; **54**: 589-600 [PMID: 18226441 DOI: 10.1016/j.eururo.2007.12.034]

50 **Puech P**, Sufana-Iancu A, Renard B, Lemaitre L. Prostate MRI: can we do without DCE sequences in 2013? *Diagn Interv Imaging* 2013; **94**: 1299-1311 [PMID: 24211261 DOI: 10.1016/j.diii.2013.09.010]

P- Reviewer: Arcangeli S, Shoji S **S- Editor**: Cui LJ **L- Editor**: A **E- Editor**: Lu YJ

World Journal of Radiology

Submit a Manuscript: http://www.f6publishing.com

World J Radiol 2017 December 28; 9(12): 426-437

DOI: 10.4329/wjr.v9.i12.426

ISSN 1949-8470 (online)

REVIEW

Endovascular treatment of pulmonary embolism: Selective review of available techniques

John L Nosher, Arjun Patel, Sugeet Jagpal, Christopher Gribbin, Vyacheslav Gendel

John L Nosher, Arjun Patel, Christopher Gribbin, Vyacheslav Gendel, Division of Interventional Radiology, Department of Radiology, Rutgers Robert Wood Johnson Medical School, New Brunswick, NJ 08901, United States

Sugeet Jagpal, Division of Pulmonary and Critical Care Medicine, Department of Medicine, Rutgers Robert Wood Johnson Medical School, New Brunswick, NJ 08901, United States

ORCID number: John L Nosher (0000-0002-9358-5057); Arjun Patel (0000-0003-1088-6880); Sugeet Jagpal (0000-0002-8076-7652); Christopher Gribbin (0000-0002-6952-7252); Vyacheslav Gendel (0000-0002-8765-4626).

Author contributions: All authors equally contributed to this paper with conception and design of the study, literature review and analysis, drafting, critical revision and editing, and final approval of the final version.

Conflict-of-interest statement: No potential conflicts of interest. No financial support.

Manuscript source: Unsolicited manuscript

Correspondence to: John L Nosher, MD, Division of Interventional Radiology, Department of Radiology, Rutgers Robert Wood Johnson Medical School, 1 Robert Wood Johnson Place, MEB404, New Brunswick, NJ 08901, United States. nosher@rwjms.rutgers.edu
Telephone: +1-732-2357721

Received: July 18, 2017
Peer-review started: July 20, 2017
First decision: August 4, 2017
Revised: August 11, 2017
Accepted: September 3, 2017

Article in press: September 3, 2017
Published online: December 28, 2017

Abstract

Acute pulmonary embolism (PE) is the third most common cause of death in hospitalized patients. The development of sophisticated diagnostic and therapeutic modalities for PE, including endovascular therapy, affords a certain level of complexity to the treatment of patients with this important clinical entity. Furthermore, the lack of level I evidence for the safety and effectiveness of catheter directed therapy brings controversy to a promising treatment approach. In this review paper, we discuss the pathophysiology and clinical presentation of PE, review the medical and surgical treatment of the condition, and describe in detail the tools that are available for the endovascular therapy of PE, including mechanical thrombectomy, suction thrombectomy, and fibrinolytic therapy. We also review the literature available to date on these methods, and describe the function of the Pulmonary Embolism Response Team.

Key words: Pulmonary embolism; Thrombolysis; Endovascular; Interventional radiology; Thrombectomy; Fibrinolysis

Core tip: Endovascular treatment of pulmonary embolism (PE) represents several methods of minimally invasive therapy of this important clinical entity, including mechanical thrombectomy, suction thrombectomy, and fibrinolytic therapy. With this paper, we hope to provide a detailed review of these methods, which is critical to understanding the tools that are available to the clinician for the treatment of PE.

Nosher JL, Patel A, Jagpal S, Gribbin C, Gendel V. Endovascular

treatment of pulmonary embolism: Selective review of available techniques. *World J Radiol* 2017; 9(12): 426-437 Available from: URL: http://www.wjgnet.com/1949-8470/full/v9/i12/426.htm DOI: http://dx.doi.org/10.4329/wjr.v9.i12.426

INTRODUCTION

Acute pulmonary embolism (PE) is the third most common cause of death in hospitalized patients[1]. The development of sophisticated diagnostic and therapeutic modalities for PE, including medical and surgical treatment as well as newly developed endovascular therapy, affords a certain level of complexity to the treatment of patients with this important clinical entity.

Pathophysiology

PE, by definition, involves emboli to the pulmonary arterial circulation, which can induce acute pulmonary arterial hypertension, right heart strain, and in some patients, right ventricular infarction[2]. Angiographic studies have demonstrated that pulmonary artery pressures increase when the embolic load occludes more than 30%-50% of the cross sectional area of the pulmonary arterial bed[3]. Clot burden alone does not determine the degree of pulmonary hypertension. The disruption of the alveolar capillary membrane by thrombus results in disruption of the diffusion of oxygen, with subsequent decreased oxygen binding to hemoglobin. Both hypoxia and the release of vasoconstrictors precipitate vasoconstriction of the pulmonary circulation, which contributes to the acute development of pulmonary hypertension[4]. This pulmonary hypertension leads to right ventricular dilatation and subsequent right ventricular failure. Underlying cardiopulmonary disease influences the ability of the right heart to adapt to increased pulmonary artery pressure.

Clinical presentation

The majority of pulmonary emboli are clinically silent. This is due to the dual blood supply of the lung through the bronchial and pulmonary arteries, as well as the fact that most emboli to the lung are small and resolve before the manifestation of any physical signs and symptoms. The clinical presentation of PE depends upon its severity, which tends to vary widely. Patients with PE can range from being completely asymptomatic to presenting with cardiovascular collapse[5]. According to the Prospective Investigation of Pulmonary Embolism Diagnosis Ⅱ (PIOPED Ⅱ) study, the most commonly occurring complaints in patients with PE were sudden onset dyspnea, pleuritic chest pain, cough, orthopnea, calf/thigh pain with associated swelling, erythema, edema, tenderness and palpable cords, wheezing, and hemoptysis[6]. On physical exam, the most common presenting signs were tachypnea and tachycardia. Less commonly seen, but still significant, were rales, decreased breath sounds, an accentuated pulmonic component of the second heart sound, jugular venous distension, and fever. Patients with massive PE may present with acute right ventricular failure leading to increased jugular venous pressure, a right-sided third heart sound, parasternal lift, cyanosis, hypotension, and shock[7,8].

Cardiovascular collapse is the product of a large sized or saddle embolus, and therefore an uncommon presenting sign, given that most pulmonary emboli are small. It should still be noted, however, that in patients with comorbid severe pulmonary hypertension who suffer a small PE, entry into shock is still a strong possibility[7,8]. Syncope is a less common but clinically significant initial presenting sign of PE that occurs in approximately 10% of patients[9]. As PE causes a ventilation/perfusion (V/Q) mismatch, patients present with hypoxemia that results in hyperventilation, and ultimately hypocapnia, which leads to respiratory alkalosis. These findings, along with a widened alveolar-arterial oxygen gradient, are the most common findings on arterial blood gas analysis. Electrocardiographic abnormalities include nonspecific ST segment or T wave changes[10]. On chest radiography, parenchymal abnormality may be found[10]; however, cardiomegaly is the most common radiographic abnormality associated with acute PE[11]. Myocardial stretching, a marker of increased pulmonary pressures can be detected in the serum *via* elevated troponin and pro-BNP levels and are markers for increased risk of right heart failure and potentially right ventricular infarct[12].

Of the 80% of patients with PE who are normotensive, it is estimated that 27%-55% have echocardiographic evidence of RV dysfunction[13,14]. Normotensive patients with RV dysfunction have an increased risk of death from PE and recurrent PE[14]. The impact of RV dysfunction on mortality has been demonstrated in two multi-center registries. In the International Cooperative Pulmonary Embolism registry of 2454 patients with PE in the normotensive group with RV hypokinesis, the all-cause mortality was doubled at 3 mo[15]. In the Management Strategy and Prognosis of Pulmonary Embolism Registry, normotensive patients with RV dysfunction had an in-hospital mortality of 7.1% and a rate of recurrent PE of 14%[16].

The current mainstays in the imaging diagnosis of PE are computed tomographic pulmonary angiography (CTPA) and echocardiography, which aid in determining the significance of PE on right ventricular function. Historically, the diagnosis was often made by ventilation/perfusion nuclear medicine scans, which is still employed for patients who cannot receive iodinated contrast material. Catheter based pulmonary angiography, the "gold standard" for the diagnosis of PE, has been supplanted by CTPA and is now performed almost exclusively only prior to a catheter based intervention. Depending on the institution, patients with suspected PE who present in shock or are severely ill may be first evaluated with echocardiography in the emergency room. Evidence of right ventricular dysfunction, such as paradoxical septal bowing or an elevated right ventricle to left ventricle ratio (RV/LV) may then be triaged rapidly

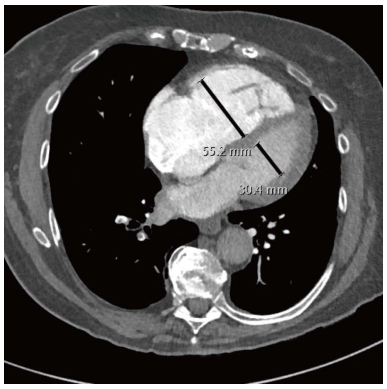

Figure 1 Right/left ventricular ratio greater than 0.9, measured in the basal portion of the ventricles at the level of the atrioventricular valve.

for CTPA or, if the diagnosis is sufficiently strong clinically and the patient is unstable, straight for angiography and intervention. In these patients, echocardiography may also disclose the presence of free floating clot in the right heart which, if available, may indicate surgical or large bore catheter intervention. More commonly, patients who are more stable will first be evaluated with CTPA. This, along with troponin and pro-BNP assays, permits assignment of patients to massive, submassive or low risk categories of PE. In addition to demonstrating the extent and distribution of PE, the CTPA can provide a sufficient indication of RV dysfunction, in the absence of echocardiography. Signs of RV dysfunction on CTPA include an elevated RV/LV ratio (generally shown to be > 0.9), septal bowing and reflux of contrast into the hepatic veins (Figure 1).

MEDICAL TREATMENT

The American Heart Association (AHA) divides PE into three categories: Massive PE, submassive PE, and low risk PE[12]. Massive PE is defined as acute PE with sustained hypotension (systolic BP < 90 mmHg for at least 15 min or requiring inotropic support), pulselessness, or persistent profound bradycardia (heart rate < 40 beats per minute with signs or symptoms of shock). Submassive PE presents with signs of right ventricular dysfunction including right ventricular dilatation on chest CTA (Figure 1), echocardiographic signs of right ventricular (RV) dysfunction, and/or serum markers consistent with myocardial stretching such as troponin and pro-BNP. Low risk PE shows no signs of RV dysfunction or biomarker evidence of strain[12]. Current treatment recommendations are for full anticoagulation for all three categories of PE, with thrombolysis for massive PE and to be considered in submassive PE[12]. Class III, Level B evidence recommends against fibrinolysis for low risk PE[12]. Cathether embolectomy and fragmentation or surgical embolectomy are alternatives for patients with massive PE with a contraindication for fibrinolysis[12]. In general, mechanical embolectomy should be reserved for main and lobar pulmonary arterial branches[12].

Organization of pulmonary emboli begins with adherence of clot to the vessel wall and the formation of a thin lining of endothelial cells over its surface, followed by ingrowth of cells from the intima media and capillary buds into the thrombus[17]. Serial imaging has demonstrated that reduction in amount of thrombus is 10% after 24 h, 40% after 7 d, and 50% after 2 to 4 wk[18]. Complete resolution is likely achieved in 70%-85% of patients at 6 to 12 mo after initial PE diagnosis[19]. The resolution of thrombi appears to plateau after 3 mo of adequate treatment, and only small amounts of improvement are seen after that time[20]. This forms the basis of recommendations for anticoagulation for 6 mo.

Unresolved thrombi can result in persistent perfusion defects and subsequently lead to chronic thromboembolic pulmonary hypertension (CTEPH). CTEPH following 3 mo of effective anticoagulatioin is defined by: (1) invasively measured mean pulmonary artery pressure > 25 mmHg with a pulmonary capillary wedge pressure < 15 mmHg; and (2) at least one segmental perfusion defect[21]. Patients with PE can have residual symptoms of reduced functional status, persistent thrombi, limitations of cardiopulmonary function, and CTEPH. The incidence of CTEPH is low, seen in 3.1% of patients at 1 year and in 3.8% of patients at 2 years in a cohort of 223 patients with confirmed PE, as reported by Pengo *et al*[22]. Although patients with CTEPH are a very small component of the total PE population, they unfortunately have the most functional impairment, and pulmonary endarterectomy and PAH Group 1 therapies are often discussed in this population[12].

SURGICAL TREATMENT

Several surgical treatment options are available for the management of PE. Historically, surgical pulmonary embolectomy has been indicated in patients who are hemodynamically unstable secondary to acute massive PE. Candidates for surgical embolectomy have failed or are not candidates for thrombolytic therapy. Surgical pulmonary embolectomy is also recommended for patients with persistent hemodynamic instability, or in patients with RV dysfunction that persists despite the use of fibrinolytic therapy[23]. There are reports in which surgical embolectomy is shown to be superior in the long term compared to thrombolysis in hemodynamically comparable patients. In a 2006 study by Meneveau *et al*[24], 488 patients with PE underwent thrombolysis, 40 of whom did not respond to the therapy. Of these 40 patients failing thrombolytic therapy, 14 patients were treated by rescue surgical embolectomy, and 26 were treated by repeat thrombolysis. Ultimately, rescue surgical embolectomy led to a better in-hospital course when compared with repeat thrombolysis in patients with massive PE who did not respond to thrombolysis[24]. In experienced centers, surgical embolectomy is considered to be a safe procedure with low mortality, providing improved postoperative right ventricular function and

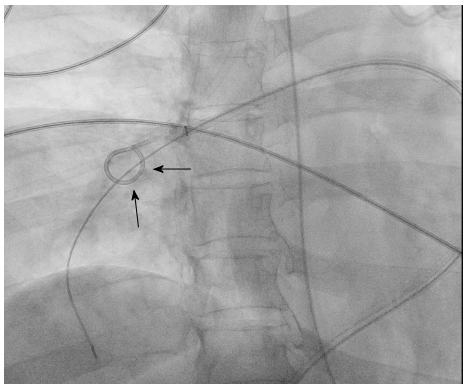

Figure 2 A pigtail catheter in the right pulmonary artery is rotated to fragment and then disperse clot into the larger volume peripheral circulation.

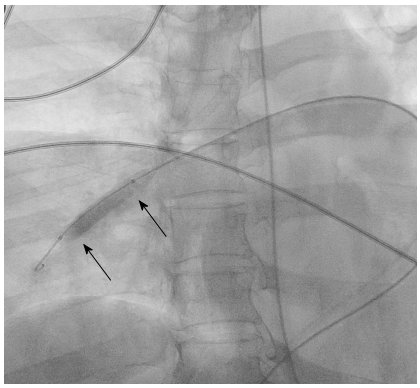

Figure 3 An angioplasty balloon catheter in the right pulmonary artery being used to fragment and disperse clot into the larger volume peripheral circulation.

pulmonary pressure as well as improved long-term outcome[25]. In a study of 37 consecutive cases, Edelman *et al*[25] demonstrated that elimination of a large portion of the clot burden could be life-saving. They concluded that pulmonary embolectomy should be considered as an initial treatment strategy in patients with massive or submassive pulmonary embolus with a large burden of proximal clot[25].

CATHETER DIRECTED THERAPY

Catheter directed therapy of PE includes mechanical thrombectomy/fragmentation, mechanical thrombectomy plus thrombolytic therapy, and catheter delivered thrombolytic therapy. The goal of catheter directed therapy is to decrease afterload on the right ventricle while reducing clot burden and long-term sequelae of CTEPH. Displacement of centrally occlusive thrombus to a more peripheral distribution in pulmonary arterial branches may decrease afterload in the right ventricle but may not address clot burden. We will not attempt to discuss all devices but limit discussion to the devices most reported for use in the pulmonary arteries. Given the large number of existing devices, it is clear that an ideal device is not currently available.

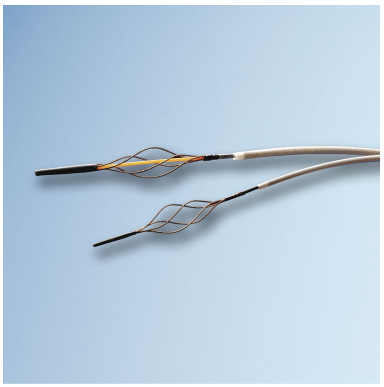

Figure 4 Trerotola thrombolytic device (Permission to use image granted by Teleflex Inc., Wayne, PA, United States).

Mechanical thrombectomy

Purely mechanical approaches to central pulmonary emboli include clot fragmentation, fragmentation with aspiration, and rheolytic thrombectomy[26,27]. Clot fragmentation has been achieved with procedures as simple as rotation of a pigtail catheter within the thrombus either manually or with mechanical assistance (Figure 2). Angioplasty balloons inflated within clot provide an alternative approach to fragmentation (Figure 3). Other mechanical devices such as the Trerotola Mechanical Thrombectomy Device (Teleflex Inc., Wayne, PA, United States) designed for use in thrombosed dialysis grafts have been used in the pulmonary arteries with mixed results (Figure 4).

There are several rheolytic thrombectomy devices, which have been used off label in the pulmonary arteries. The Amplatz thrombectomy device (Microvena, White Bear Lake, MN) is a 6-French catheter that incorporates a high-pressure air-driven high-speed impeller, creating a vacuum vortex-pulling clot into the distal tip of the catheter, fragmenting the thrombus, then expelling particles, most of which measure 50 μm or less[26,27].

The Angiojet catheter (Boston Scientific, Marlborough, MA, United States) is one of the most frequently used devices, which provides both clot fragmentation and aspiration of clot fragments. Saline jets directed into the clot at the distal end of the catheter result in clot fragmentation. These jets may also be used to distribute thrombolytic agents into the clot in the "power pulse mode". At the same time, aspiration of clot fragments is achieved at catheter sideports from high velocity saline looping back into a second lumen creating a Venturi effect (Figure 5). These procedures displace obstructive emboli from a central location into the larger volume peripheral pulmonary arterial vasculature, resulting in reduction of pulmonary artery pressure and afterload on the right heart[28]. Frequently, mechanical approaches are combined with infusion systems delivering low dose thrombolytics into residual thrombus.

Suction thrombectomy

Suction thrombectomy was one of the earliest ap-

Figure 5 Angiojet rheolytic thrombectomy device (Boston Scientific, Marlborough, MA, United States). Distal Saline jets fragment clots and high velocity saline loops into a second lumen, aspirating fragments of clot into the sideports through the Venturi effect (Image provided courtesy of Boston Scientific. ©2017 Boston Scientific Corporation or its affiliates. All rights reserved.

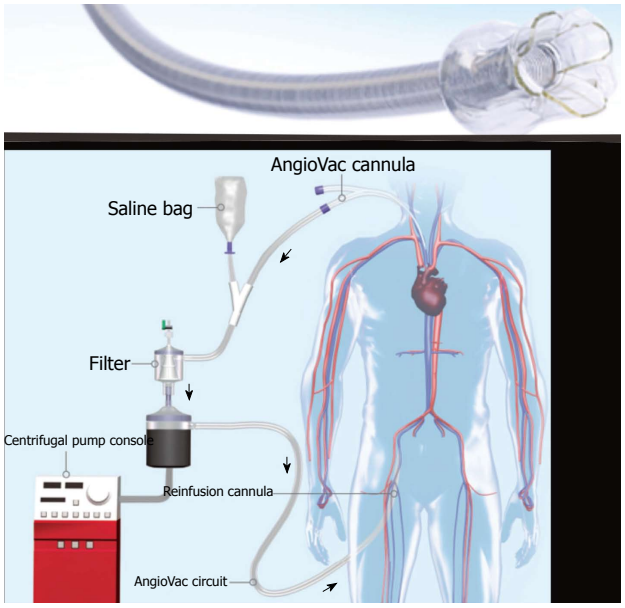

Figure 6 Angiovac catheter (Angiodynamics, Inc., Latham, NY, United States) and reperfusion circuit, in which aspirated clot is filtered from aspirated blood, which is subsequently returned to the patient (permission to use image granted by Angiodynamics, Inc.).

proaches to transcatheter treatment of pulmonary emboli, introduced by Greenfield, using a 12-French catheter with a cup on its distal end. Suction was applied to the catheter hub with a large volume syringe. A portion of thrombus was engaged in the cup and removed along with trailing adherent thrombus through a large diameter vascular sheath in either the femoral or jugular veins.

More recent approaches involve aspiration of thrombus into the lumen of an aspiration catheter of varying diameters with discharge into an aspiration container. The Angiovac system (Angiodynamics Inc., Latham, NY) consists of a 22-French coil reinforced cannula with a balloon actuated expandable funnel-shaped distal tip. The catheter is part of a veno-venous recirculation system with aspirated thrombus and blood separated and returned to the patient through a large central venous return cannula (Figure 6). The system requires a perfusionist to be present during the procedure and the added time required to assemble this team.

An alternative large lumen suction device is the FlowTriever system (Inari Medical, Irvine, CA, United States), in which a large bore (20-French) sheath is introduced for placement of suction catheter, which is connected to a retraction aspirator, providing a vacuum for clot aspiration. Blood admixed with clot does not have a means to return to the circulation (Figure 7). The advantage of the large bore catheters is the ability to remove large volumes of thrombus rapidly; however, their size and rigidity makes access to pulmonary artery branches more difficult. In addition, stiffness increases the possibility of injury to the heart or to the pulmonary artery.

The Penumbra system (Penumbra Inc., Alameda, CA, United States) is a suction aspiration system first used in the endovascular treatment of stroke. The Penumbra INDIGO CAT 8 system is a flexible 8-French aspiration catheter, which is connected to a continuous suction vacuum system. A wire separator in the catheter lumen facilitates clot retrieval (Figure 8). As with the FlowTriever device, the Penumbra lacks a means to return blood to the patient and can lead to significant blood loss if not embedded in clot. None of the suction systems is FDA approved in the United States for the treatment of PE, and their use is considered "off label". The FlowTriever system has received approval from the FDA for the FLARE IDE clinical trial for patients with submassive pulmonary emboli and is currently recruiting.

Fibrinolytic therapy

Fibrinolysis is most effective when the agent is delivered directly into the thrombus. There are several catheter systems available for delivery of fibrinolytic agents directly into the thrombus. The Unifuse infusion system (Angiodynamics, Latham, NY, United States) consists of a multi-hole catheter with an end hole and side holes distributed in variable lengths along the distal catheter. Their distribution is defined by radiopaque markers. The catheter is introduced over a standard guidewire. Following desired placement in the clot, an occluding ball guide wire is introduced to obstruct the end hole, thereby forcing the infusate out the side holes. This catheter can be used to simply infuse or pulse spray fibrinolytics by forcible injection at the catheter hub (Figure 9).

Ultrasound assisted infusion of thrombolytics through the Ekos system (Ekos Corp., Bothel, WA, United States) utilizes an ultrasonic core to generate an acoustic field dispersing the fibrinolytic agent into the clot. In addition, this acoustic field is felt to disaggregate thrombus with separation of fibrin crosslinks, accelerating clot lysis. The system consists of a 5.4-French infusion catheter with markers delineating the active area, an ultrasound core

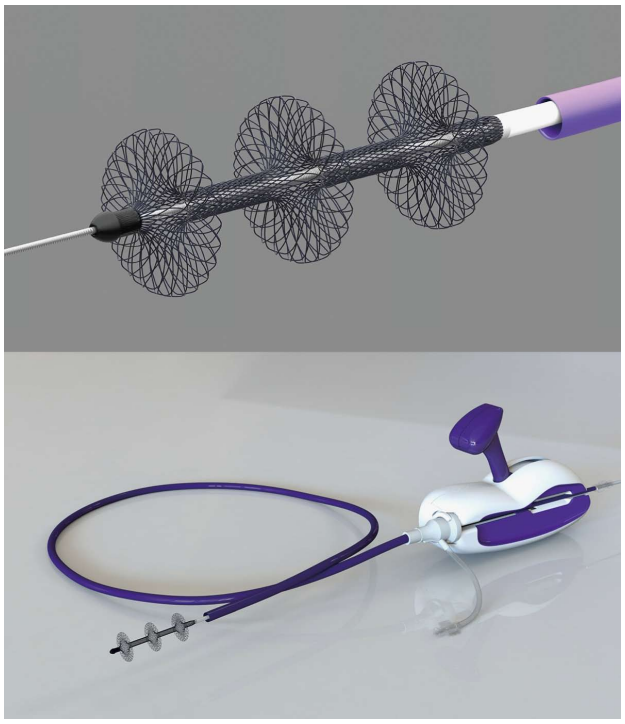

Figure 7 Flowtriever device (Inari Medical, Irvine, CA, United States) with three braided nitinol disks to engage clot and pull it into the aspiration guide catheter for evacuation by the retraction aspirator (Permission to use image granted by Inari Medical).

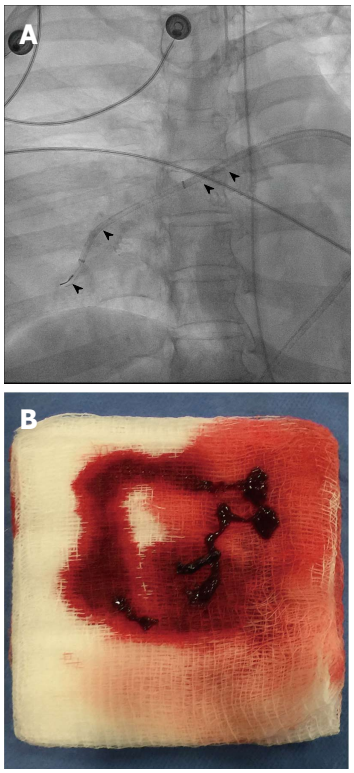

Figure 8 Penumbra device. A: Penumbra Indigo CAT-8 (Penumbra, Inc., Alameda, CA, United States) in the right pulmonary artery. The guiding catheter (arrowheads) is in the right main pulmonary artery and the aspiration catheter (arrows) is in the right lower lobe pulmonary artery. The separator wire used to promote aspiration is exiting the aspiration catheter; B: Small volume clot aspirated with the Penumbra Indigo CAT-8 system.

transducer, and a control unit. The catheter has both a drug delivery lumen and a central coolant channel (Figure 10).

REVIEW OF RESULTS

In spite of greater than 30 years of experience with catheter directed therapy for acute PE, controversy still exists as to its precise role. This is primarily related to the lack of level I evidence of its safety and effectiveness. Most evidence is based on small non-controlled cohort studies with non-consecutive recruitment and varying criteria for success (Table 1).

Any review of results of studies dealing with PE treatment should begin with a brief explanation of the Miller score, which is one of several scoring systems that attempt to objectively quantify the magnitude of PE (Figure 11). Described in 1975[29] and based on pulmonary arteriography it is the sum of obstruction and perfusion scores. The obstruction index divides the lung into nine segments on the right and seven on the left. Thrombus in any segment is given a score of 1. Thrombus proximal to segmental branches is given a score of the number of branches peripheral to the thrombus (*i.e.*, right lower lobe pulmonary artery = 4, saddle embolus = 16). The perfusion index divides each lung into upper, middle and lower zones scored as no perfusion (3), severely reduced perfusion (2), mildly reduced perfusion (1), and normal perfusion (0). Therefore the worst Miller index combining obstruction and perfusion is 34.

Suction thrombectomy

The earliest reports were those describing suction embolectomy with the Greenfield suction embolectomy catheter. Greenfield reported 46 patients treated with the 12-French suction catheter[30]. Of these patients, 33 had sustained massive pulmonary emboli, 4 submassive, and 9 chronic. Mean pulmonary arterial pressure was reduced from 32 to 24 mmHg in 31 patients, in whom it was measured with clinical success in 36/46 patients. After the adoption of prophylactic inferior vena cava (IVC) filters following the procedure, the 30 d survival increased from 50% in the first 10 patients to 70% in the subsequent 36 patients. Because of the size and difficulty of placement of the Greenfield suction embolectomy catheter, the device fell out of favor.

Currently, two large bore aspiration catheters are available. The Angiovac system, approved for use in treating thrombi in the venous system, is being used off-label in the pulmonary arteries. There have been case reports and small series reporting the use of this device with mixed results[31]. A retrospective review of five consecutive patients in whom the Angiovac was used included four patients with massive PE and one with submassive PE[32]. Technical success, defined as

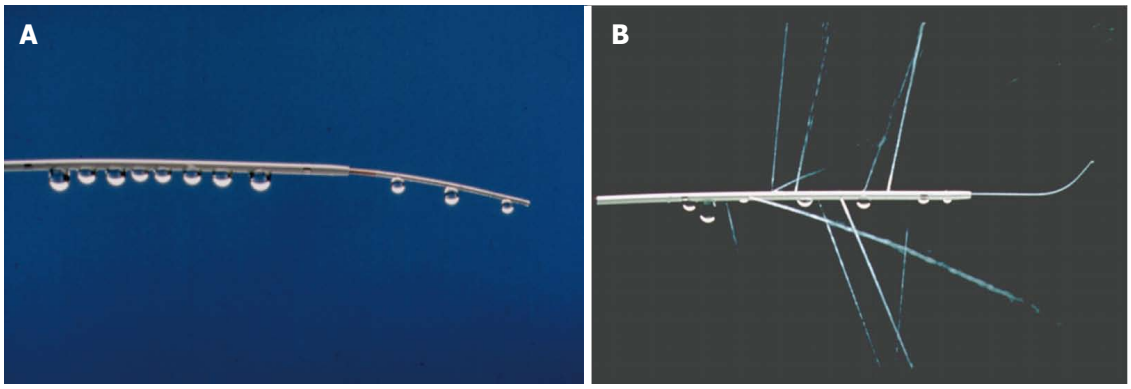

Figure 9 Multiholed infusion catheter. A: A multiholed infusion catheter with sideholes dispersing infusate within clot and infusion wire further distributing the infusate while also occluding the endhole of the infusion catheter, forcing flow out of the sideholes of the catheter (Permission to use image granted by Angiodynamics, Inc.); B: A multiholed infusion catheter with sideholes dispersing infusate within clot and infusion wire further distributing the infusate while also occluding the endhole of the infusion catheter, forcing flow out the sideholes of the catheter (Permission to use image granted by Angiodynamics, Inc.).

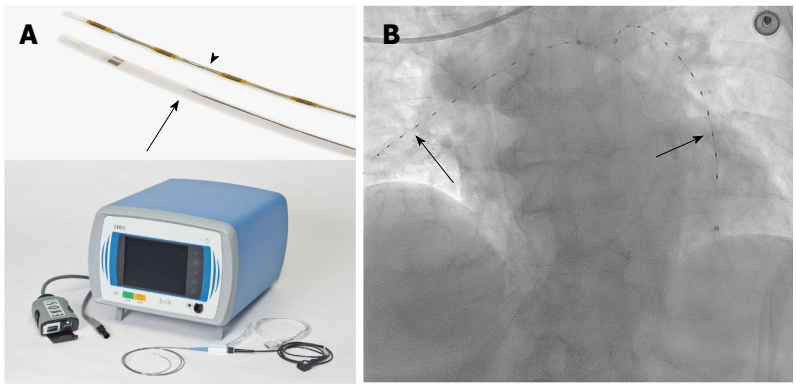

Figure 10 Ekos system. A: Ekos system with multiholed infusion catheter (arrow), ultrasonic core transducer (arrowhead) and control unit (Permission to use image granted by Ekos Corp., Bothel, WA, United States); B: Ekos catheters (arrows) with ultrasonic core transducers in place in the right and left pulmonary arteries.

successful removal of some thrombus combined with reduction of the Miller score by greater than or equal to 5 was achieved in two of the four patients with massive PE. Four patients died at a mean of 7.3 d, all having presented with massive PE. One death was related to catheter perforation of the right ventricular free wall. In another small series of three patients in whom thrombectomy of the pulmonary arteries was attempted, the procedure was unsuccessful in two of the three patients. Lack of success was attributed to size, stiffness and lack of maneuverability of the device.

There is even less information on the use of the FlowTriever device in the pulmonary arteries. A single case of success in a saddle embolus in the pulmonary artery was recently reported[33]. It is uncertain if similar problems with stiffness and lack of maneuverability are encountered with this device. The FlowTriever FLARE trial will help clarify these issues in a larger cohort of patients. Unfortunately this trial excludes patients with massive PE - a group of patients in whom suction embolectomy is most appropriate.

The Penumbra device is another suction device currently available in an 8-French system, providing the flexibility for placement in segmental branches of the pulmonary artery. However, luminal diameter limits the volume of clot aspirated. There is no evidence available at the current time to support its use.

Mechanical thrombectomy

The Amplatz thrombectomy device has been used in the pulmonary arteries and reported about in small series. A report by Muller-Hulsbeck included 9 patients, out of which, 5 were treated with additional tPA[34]. Miller index was reduced from 18 to 11. Of interest, the mean pulmonary arterial pressure was reduced from 57 to 55 mmHg after mechanical thrombectomy. The addition of fibrinolytic therapy achieved further reduction of mean pulmonary arterial pressure to 39 mmHg, raising question of the value of the mechanical component of the procedure.

The Angiojet device is the most studied rheolytic thrombectomy device. A study by Nassiri *et al*[35] reviewed experience with 15 consecutive patients, one with massive and 14 with submassive pulmonary emboli. Adjunctive tPA was administered in 10 patients. Completion angiography was used to assess success. Significant clot resolution (> 75%) was observed in 9 patients, moderate (50%-75%) in 5 patients, and minimal (< 50%) in 1 patient. All patients receiving adjunctive tPA had significant or moderate clot resolution.

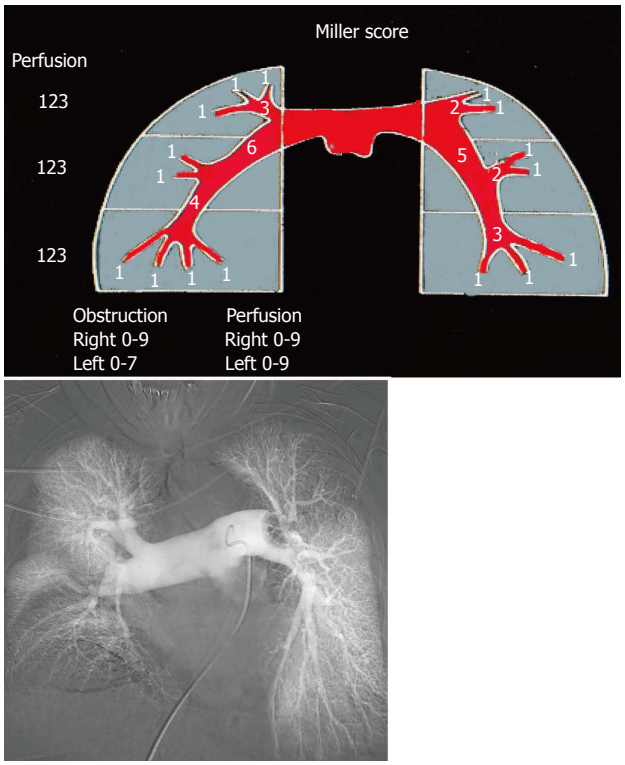

Figure 11 Miller Score. Pulmonary arteriogram demonstrating left main pulmonary artery embolus (obstruction score 7) and severely reduced perfusion of the upper and middle zones of the left lung (perfusion index 2 + 2). There is occlusion of the left lower lobe pulmonary and middle lobe pulmonary artery (obstructive score 4 + 2) with perfusion severely reduced in the lower lobe and mildly reduced in the middle lobe (perfusion index 2 + 1). This patients combined Miller score is therefore 20.

There were no in-hospital deaths or recurrent pulmonary emboli. Two patients had post procedural renal failure and there was one case of cardiopulmonary arrest.

Chechi retrospectively reviewed 51 patients presenting with massive (in 22 patients) or submassive (in 29 patients) pulmonary emboli[36]. Technical success determined by angiography was achieved in 92% of cases, with mean reduction of the Miller index by 51%. Adjunctive fibrinolytic therapy was performed in 21% of patients. The in-hospital mortality was 42% in patients presenting with shock, 12% in patients with hypotension, and 3.4% in patients with submassive pulmonary emboli. Renal failure was reported in 24% of patients, while bradycardia requiring transvenous pacing was reported in 8%.

Systemic complications of renal insufficiency, bradycardia, and asystole are frequently reported with the Angiojet device. Both complications stem from red blood cell destruction leading to the release of adenosine, causing bradycardia and asystole. Some operators limit activation of the device to five-second intervals, separating the intervals to limit the amount of adenosine in the circulation. Renal insufficiency is felt to result from hemoglobinuria and resultant acute tubular necrosis. Aggressive hydration and administration of bicarbonate to raise urine pH to above 6.5 may diminish the tubular toxicity of hemoglobin[37].

Fibrinolytic therapy

Patients with massive PE who have failed systemic thrombolysis, have absolute contraindications to thrombolysis, or cannot await the two hour time interval for administration of systemic thrombolytics are clearly candidates for either catheter directed therapy or surgical thrombo-embolectomy. Unfortunately few centers are equipped for urgent surgical thrombo-embolectomy and few will achieve the survival outcomes of centers with expertise in pulmonary thrombo-embolectomy.

A meta-analysis of catheter directed treatment of PE by Tafur[38] included 24 studies, enrolling 700 patients, of who 653 received endovascular treatment. Pooled data estimated risk of death in non-ultrasound assisted thrombolysis (USAT) studies at 9% and 4% in the USAT group. In studies using risk stratification, the Miller index decreased from 19.4 to 9.9 following intervention. In studies including pulmonary artery pressures, mean pressures were reduced from 57 to 36 mmHg. The main safety outcome of major bleeding was 4% in the USAT studies and 10% in the non-USAT group.

A review of data of a nationwide inpatient sample of 72230 patients with PE who were considered unstable reported a case fatality rate of 47% in patients not receiving thrombolytic therapy and 15% in patients receiving thrombolytics. However 70% of these patients were denied thrombolytics for various reasons[39]. Given this data randomization of patients with massive PE and contraindications to systemic thrombolysis to catheter directed intervention *vs* no therapy raises both ethical concerns and recruitment challenges and is unlikely to occur.

Catheter directed therapy in massive PE

There is evidence supporting the use of catheter directed therapy in patients with massive PE. A meta-analysis of catheter directed therapy in 2009[40] identified a subset 594 patients from 35 uncontrolled studies treated for massive PE defined by hypotension. Clinical success was determined by stabilization of hemodynamics, resolution of hypoxia, and survival. Ninety six percent of patients did not receive thrombolytics before catheter directed therapy. Thirty three percent of patients received mechanical thrombectomy alone, while 60%-67% received both mechanical thrombectomy and pharmacologic thrombolysis. Mechanical technique most often used was pigtail catheter fragmentation in 69% of patients; used alone in 53%. Clinical success was achieved in 86.5% of patients. Clinical success was higher in studies in which patients received catheter directed thrombolytic therapy compared to those in which thrombolytic was less frequently given. The pooled risk of minor complications was 7.9% and major complication 2.4%. Of interest, five procedural related deaths were all associated with use of the Angiojet device.

Given the fatality rate that approaches 50%, as reported for untreated patients with massive PE, and subset analysis of catheter directed therapy in patients with massive PE reporting mortality rates as low as

Table 1 Comparison of pulmonary embolism treatment devices based on currently available evidence

Treatment method	Type of device	No. of patients	Outcomes
Suction thrombectomy	Greenfield suction embolectomy catheter	n = 46[32] 33 with massive PE 4 with submassive PE 9 with chronic PE	Mean PAP reduction from 32 to 24 mmHg in 31 patients
	Angiovac	n = 5[34] 4 with massive PE 1 with submassive PE	Technical success in 2 of the 4 patients with massive PE
	Flowtriever	n = 1[35]	Procedure successful
	Flowtriever	FLARE trial - ongoing	pending
	Penumbra	None	None
Mechanical thrombectomy	Amplatz thrombectomy device	n = 9[36] (5 were treated with tPA)	Reduction of Miller index from 18 to 11 Mean PAP reduction from 57 to 55 mmHg Addition of tPA achieved further mean PAP reduction to 39 mmHg
	Angiojet	n = 15[37] 10 were treated with tPA	9 patients - significant clot resolution 5 patients - moderate clot resolution 1 patient - minimal clot resolution
	Angiojet	n = 51[38] 22 patients - massive PE 29 patients - submassive PE	92% technical success Mean reduction of Miller index by 51%
Catheter directed fibrinolysis	USAT	n = 59[47] (ULTIMA trial) 29 patients - UFH alone 30 patients - unfractionated heparin + USAT	Greater mean decrease of RV/LV ratio in the UFH + USAT group *vs* UFH alone (0.30 *vs* 0.03)

PE: Pulmonary embolism; USAT: Ultrasound-assisted thrombolysis; PAP: Pulmonary arterial pressure; RV/LV: Right ventricle to left ventricle ratio; UFH: Unfractionated heparin.

15%, this therapy appears to be appropriate. Since many if not most of these patients had received both mechanical as well as pharmaco-mechanical treatment, it is therefore difficult to predict the effectiveness of mechanical thrombo-dispersion-thrombectomy alone. Certainly the next generation of thrombectomy devices will facilitate access to the main pulmonary arteries and segmental branches, improving the efficacy of mechanical thrombectomy. Currently, there is no data supporting the addition of catheter directed therapy to systemic therapy for patients who have responded to systemic therapy in spite of its ability to further decrease clot burden and the sequelae of CTEPH.

Catheter directed therapy in submassive PE

For patients with submassive PE, there is controversy as to the role of both systemic or catheter directed therapy. A meta-analysis of randomized controlled trials comparing systemic thrombolytic therapy with heparin alone in patients with PE showed a benefit only in patients with massive PE[41]. In contrast, the MAPPET-3 trial[42] randomized 256 patients with sub-massive PE into heparin plus tPA (118 patients) *vs* heparin plus placebo (138 patients). The primary endpoint of in hospital mortality or clinical deterioration requiring an escalation of treatment was significantly higher in the heparin plus placebo group primarily due to the need for treatment escalation (26% *vs* 10%). Mortality in both groups was low: 3.4% in the heparin plus tPA group and 2.2% in the heparin plus placebo group. No fatal or intracranial hemorrhage was observed.

The PEITHO trial[43] randomized 1006 patients with submassive PE to systemic tenecteplase (30-50 mg) as a single bolus or placebo with both groups receiving intravenous heparin. The primary endpoints were death, hemodynamic decompensation, confirmed recurrent PE within 7 d, death within 30 d, and major adverse events within 30 d. Death or hemodynamic decompensation occurred in 2.6% of patients in the tenecteplase group and in 5.6% in the placebo group (P = 0.02). Extracranial bleeding occurred in 6.3% of the tenecteplase group and in 1.2% of the placebo group ($P \leqslant 0.001$). Stroke occurred in 2.4% of the tenecteplase group and in 0.2% of the placebo group. At 30 d, the mortality was 2.4% and 3.2% in the tenecteplase and placebo groups, respectively. Thrombolytic therapy decreased the need for escalation of care with no difference in mortality but at the expense of increased bleeding complications including hemorrhagic stroke.

The MOPETT trial[44] randomized 121 patients with moderate PE to receive a "safe dose" of systemic thrombolytic (50 mg tPA) in 61 patients or anticoagulation alone in 60 patients. The primary end point was pulmonary hypertension and composite endpoints of pulmonary hypertension and recurrent PE at 28 mo. Secondary endpoints included total mortality, duration of hospital stay, and bleeding during hospitalization. Pulmonary hypertension and the composite endpoint of pulmonary hypertension and recurrent PE occurred in 16% of the thrombolytic group and in 57% of the control group ($P \leqslant 0.001$). Death and recurrent PE occurred in 1.6% and 10% of the tPA and control groups respectively.

There was no major bleeding in either group. When death or recurrent PE were assessed independently there was no difference between the groups. There have been numerous papers published on the delivery of fibrinolytic agents through infusion catheters placed directly into pulmonary artery thrombus. The most compelling evidence for the effectiveness of catheter directed treatment of PE comes from the ULTIMA trial[45]. In this prospective randomized trial, USAT was compared to heparin alone in patients with submassive PE. A dose of 10-20 mg recombinant tissue plasminogen activator (rtPA) was infused over 15 h (approximately 0.75 to 1.5 mg/h) in the USAT group. RV/LV ratio showed a mean decrease at 24 h of 0.30 *vs* 0.03 in the heparin alone group ($P < 0.001$). At 90 d, there was one death from pancreatic cancer in the heparin group. There was no major bleeding and 4 episodes of minor bleeding: 3 in the USAT group, 1 in the heparin alone group ($P = 0.61$). Criticism of this trial includes failure to randomize patients with perhaps the greatest need for catheter directed therapy, the elderly and those with cancer; a low recruitment rate; and failure to follow patients to 6 mo when the heparin alone group may have additionally benefited from physiologic thrombolysis.

There is conflicting evidence as to whether ultrasound assisted delivery of fibrinolytic agents is more effective than infusion alone. In the PREFECT registry[46], 101 consecutive patients were enrolled at 7 sites. Twenty-eight patients had massive PE (28%) and 73 had submassive PE (73%). Patients with massive PE were treated with mechanical thrombectomy or pharmaco-mechanical thrombectomy with clinical success in 24/28 patients and 14% mortality. Clinical success in the submassive group was 97% with 3% mortality. While the device choices for mechanical thrombectomy are not mentioned in the study, the Angiojet device was not used because of reported complications. In a subgroup analysis, comparing USAT with CDT there was no difference in post treatment pulmonary artery pressures, average pressure change, thrombolytic dose, raising the question of the added expense of USAT.

Looking at the evidence of systemic and catheter directed therapy in patients with submassive PE, it appears that patients receiving lytic therapy have a decreased need for escalation of care compared to those with heparin administration alone, a more rapid resolution of afterload on the right heart, but no significant survival advantage. However, there may be greater improvement in pulmonary artery pressures in the long term. The advantages of catheter directed therapies over systemic administration are thrombolytic delivery directly into the clot and the requirement of a lower dose of thrombolytics, which may decrease hemorrhagic complications. In light of the effectiveness of thrombolytics alone, one questions the need for mechanical thrombectomy in submassive PE, unless there is a contraindication to thrombolysis.

Pulmonary embolism response teams

As treatment options for patients with PE have evolved, the concept of bringing together experts from different disciplines in an urgent manner to create the best treatment plan for patients presenting with PE has led to the creation of Pulmonary Embolism Response Teams (PERT)[47]. Similar multidisciplinary collaborations have been employed to facilitate patients presenting with stroke (the "Stroke Team")[48] or cardiac events (the "Heart Team").

The manner in which clinicians are summoned to make decisions about treatment varies considerably from institution to institution. It may involve alerting the members of the team through a beeper system that a patient has presented, or it may involve protocols which dictate how triage should be accomplished, with the necessary members alerted as needed[49]. Members involved typically include pulmonary/critical care, cardiology, vascular/cardiothoracic surgery and interventional radiology or cardiology. Additional members who may be involved include anesthesiologists, perfusionists, diagnostic radiologists, and pharmacists. Activation may involve several or all of the members converging at the patient's bedside. In some instances, this may be done *via* videoconference with subsequent in-person activation of the physicians relevant to the particular patient's situation[50].

An important function of the PERT process is data collection and the refinement of treatment protocols. By examining outcomes and correlating them with initial data collected, such as high and low heart rates, blood pressure, oxygen saturation, number of segments with thrombus, RV/LV ratio, *etc*., triage of patients to different treatment arms may be optimized. Ideally, patients may subsequently be seen in follow up in a dedicated PERT clinic. Long term follow up can then be introduced to the PERT database. Centers with PERT programs have the opportunity to share data with each other allowing for more rapid determination of critical treatment parameters. Collaboration regarding data sharing is evolving through multicenter affiliations such as the PERT Consortium[51].

In addition to streamlined treatment, another function of the PERT process is data collection, which will lead to the refinement of treatment protocols. Members of the national PERT Consortium will have the opportunity to share data advancing the understanding of PE and its treatment. The success of a PERT program requires extensive education of referring physicians, house staff, nursing staff, ED and ICU staff, pharmacy, and the community.

CONCLUSION

Currently, the precise role of catheter directed therapy in the treatment of both massive and submassive PE remains to be established through well-designed prospective controlled trials. For patients with massive PE in whom there is an absolute contraindication for systemic thrombolysis, a failure of systemic thrombolysis or no time for the 2 h of administration of systemic

thrombolytic agents, mechanical thrombectomy provides the primary alternative to surgical thrombectomy. With respect to submassive PE, catheter directed therapy decreases the need for treatment escalation, decreases the time for clinical improvement, but does not increase overall survival. An overall reduction in clot burden may decrease the incidence of CETPH and improve quality of life.

REFERENCES

1 **Pulido T**, Aranda A, Zevallos MA, Bautista E, Martínez-Guerra ML, Santos LE, Sandoval J. Pulmonary embolism as a cause of death in patients with heart disease: an autopsy study. *Chest* 2006; **129**: 1282-1287 [PMID: 16685020 DOI: 10.1378/chest.129.5.1282]

2 **McIntyre KM**, Sasahara AA. The hemodynamic response to pulmonary embolism in patients without prior cardiopulmonary disease. *Am J Cardiol* 1971; **28**: 288-294 [PMID: 5155756 DOI: 10.1016/0002-9149(71)90116-0]

3 **McIntyre KM**, Sasahara AA. Determinants of right ventricular function and hemodynamics after pulmonary embolism. *Chest* 1974; **65**: 534-543 [PMID: 4826027 DOI: 10.1378/chest.65.5.534]

4 **Stratmann G**, Gregory GA. Neurogenic and humoral vasoconstriction in acute pulmonary thromboembolism. *Anesth Analg* 2003; **97**: 341-354 [PMID: 12873915 DOI: 10.1213/01.ANE.0000068983.18131.F0]

5 **Corrigan D**, Prucnal C, Kabrhel C. Pulmonary embolism: the diagnosis, risk-stratification, treatment and disposition of emergency department patients. *Clin Exp Emerg Med* 2016; **3**: 117-125 [PMID: 27752629 DOI: 10.15441/ceem.16.146]

6 **Stein PD**, Beemath A, Matta F, Weg JG, Yusen RD, Hales CA, Hull RD, Leeper KV Jr, Sostman HD, Tapson VF, Buckley JD, Gottschalk A, Goodman LR, Wakefied TW, Woodard PK. Clinical characteristics of patients with acute pulmonary embolism: data from PIOPED II. *Am J Med* 2007; **120**: 871-879 [PMID: 17904458 DOI: 10.1016/j.amjmed.2007.03.024]

7 Guidelines on diagnosis and management of acute pulmonary embolism. Task Force on Pulmonary Embolism, European Society of Cardiology. *Eur Heart J* 2000; **21**: 1301-1336 [PMID: 10952823 DOI: 10.1053/euhj.2000.2250]

8 **Kucher N**, Goldhaber SZ. Management of massive pulmonary embolism. *Circulation* 2005; **112**: e28-e32 [PMID: 16009801 DOI: 10.1161/CIRCULATIONAHA.105.55.551374]

9 **Castelli R**, Tarsia P, Tantardini C, Pantaleo G, Guariglia A, Porro F. Syncope in patients with pulmonary embolism: comparison between patients with syncope as the presenting symptom of pulmonary embolism and patients with pulmonary embolism without syncope. *Vasc Med* 2003; **8**: 257-261 [PMID: 15125486 DOI: 10.1191/1358863x03vm510oa]

10 **Stein PD**, Terrin ML, Hales CA, Palevsky HI, Saltzman HA, Thompson BT, Weg JG. Clinical, laboratory, roentgenographic, and electrocardiographic findings in patients with acute pulmonary embolism and no pre-existing cardiac or pulmonary disease. *Chest* 1991; **100**: 598-603 [PMID: 1909617 DOI: 10.1378/chest.100.3.604]

11 **Elliott CG**, Goldhaber SZ, Visani L, DeRosa M. Chest radiographs in acute pulmonary embolism. Results from the International Cooperative Pulmonary Embolism Registry. *Chest* 2000; **118**: 33-38 [PMID: 10893356 DOI: 10.1378/chest.118.1.33]

12 **Jaff MR**, McMurtry MS, Archer SL, Cushman M, Goldenberg N, Goldhaber SZ, Jenkins JS, Kline JA, Michaels AD, Thistlethwaite P, Vedantham S, White RJ, Zierler BK; American Heart Association Council on Cardiopulmonary, Critical Care, Perioperative and Resuscitation; American Heart Association Council on Peripheral Vascular Disease; American Heart Association Council on Arteriosclerosis, Thrombosis and Vascular Biology. Management of massive and submassive pulmonary embolism, iliofemoral deep vein thrombosis, and chronic thromboembolic pulmonary hypertension: a scientific statement from the American Heart Association. *Circulation* 2011; **123**: 1788-1830 [PMID: 21422387 DOI: 10.1161/CIR.0b013e318214914f]

13 **Grifoni S**, Olivotto I, Cecchini P, Pieralli F, Camaiti A, Santoro G, Conti A, Agnelli G, Berni G. Short-term clinical outcome of patients with acute pulmonary embolism, normal blood pressure, and echocardiographic right ventricular dysfunction. *Circulation* 2000; **101**: 2817-2822 [PMID: 10859287 DOI: 10.1161/01.CIR.101.24.2817]

14 **Kreit JW**. The impact of right ventricular dysfunction on the prognosis and therapy of normotensive patients with pulmonary embolism. *Chest* 2004; **125**: 1539-1545 [PMID: 15078772 DOI: 10.1378/chest.125.4.1539]

15 **Goldhaber SZ**, Visani L, De Rosa M. Acute pulmonary embolism: clinical outcomes in the International Cooperative Pulmonary Embolism Registry (ICOPER). *Lancet* 1999; **353**: 1386-1389 [PMID: 10227218 DOI: 10.1016/S0140-6736(98)07534-5]

16 **Kasper W**, Konstantinides S, Geibel A, Olschewski M, Heinrich F, Grosser KD, Rauber K, Iversen S, Redecker M, Kienast J. Management strategies and determinants of outcome in acute major pulmonary embolism: results of a multicenter registry. *J Am Coll Cardiol* 1997; **30**: 1165-1171 [PMID: 9350909 DOI: 10.1016/S0735-1097(97)00319-7]

17 **Wagenvoort CA**. Pathology of pulmonary thromboembolism. *Chest* 1995; **107**: 10S-17S [PMID: 7813322 DOI: 10.1378/chest.107.1_Supplement.10S]

18 **Dong BR**, Hao Q, Yue J, Wu T, Liu GJ. Thrombolytic therapy for pulmonary embolism. *Cochrane Database Syst Rev* 2009; **8**: CD004437 [PMID: 19588357 DOI: 10.1002/14651858.CD004437.pub3]

19 **Alonso-Martínez JL**, Anniccherico-Sánchez FJ, Urbieta-Echezarreta MA, García-Sanchotena JL, Herrero HG. Residual pulmonary thromboemboli after acute pulmonary embolism. *Eur J Intern Med* 2012; **23**: 379-383 [PMID: 22560390 DOI: 10.1016/j.ejim.2011.08.018]

20 **Stein PD**, Yaekoub AY, Matta F, Janjua M, Patel RM, Goodman LR, Gross ML, Denier JE. Resolution of pulmonary embolism on CT pulmonary angiography. *AJR Am J Roentgenol* 2010; **194**: 1263-1268 [PMID: 20410413 DOI: 10.2214/AJR.09.3410]

21 **Lang IM**, Pesavento R, Bonderman D, Yuan JX. Risk factors and basic mechanisms of chronic thromboembolic pulmonary hypertension: a current understanding. *Eur Respir J* 2013; **41**: 462-468 [PMID: 22700839 DOI: 10.1183/09031936.00049312]

22 **Pengo V**, Lensing AW, Prins MH, Marchiori A, Davidson BL, Tiozzo F, Albanese P, Biasiolo A, Pegoraro C, Iliceto S, Prandoni P; Thromboembolic Pulmonary Hypertension Study Group. Incidence of chronic thromboembolic pulmonary hypertension after pulmonary embolism. *N Engl J Med* 2004; **350**: 2257-2264 [PMID: 15163775 DOI: 10.1056/NEJMoa032274]

23 **Moorjani N**, Price S. Massive pulmonary embolism. *Cardiol Clin* 2013; **31**: 503-518, vii [PMID: 24188217 DOI: 10.1016/j.ccl.2013.07.005]

24 **Meneveau N**, Séronde MF, Blonde MC, Legalery P, Didier-Petit K, Briand F, Caulfield F, Schiele F, Bernard Y, Bassand JP. Management of unsuccessful thrombolysis in acute massive pulmonary embolism. *Chest* 2006; **129**: 1043-1050 [PMID: 16608956 DOI: 10.1378/chest.129.4.1043]

25 **Edelman JJ**, Okiwelu N, Anvardeen K, Joshi P, Murphy B, Sanders LH, Newman MA, Passage J. Surgical Pulmonary Embolectomy: Experience in a Series of 37 Consecutive Cases. *Heart Lung Circ* 2016; **25**: 1240-1244 [PMID: 27423976 DOI: 10.1016/j.hlc.2016.03.010]

26 **Sharafuddin MJ**, Hicks ME. Current status of percutaneous mechanical thrombectomy. Part I. General principles. *J Vasc Interv Radiol* 1997; **8**: 911-921 [PMID: 9399459 DOI: 10.1016/S1051-0443(97)70687-0]

27 **Sharafuddin MJ**, Hicks ME. Current status of percutaneous mechanical thrombectomy. Part II. Devices and mechanisms of action. *J Vasc Interv Radiol* 1998; **9**: 15-31 [PMID: 9468392 DOI: 10.1016/S1051-0443(98)70477-4]

28 **Dawson CA**, Rickaby DA, Linehan JH, Bronikowski TA. Distributions of vascular volume and compliance in the lung. *J Appl Physiol* (1985) 1988; **64**: 266-273 [PMID: 3356646]

29 **Tibbutt DA**, Fletcher EW, Thomas L, Sutton GC, Miller GA. Evaluation of a method for quantifying the angiographic severity of major pulmonary embolism. *Am J Roentgenol Radium Ther Nucl Med* 1975; **125**: 895-899 [PMID: 1211520 DOI: 10.2214/ajr.125.4.895]

30 **Greenfield LJ**, Proctor MC, Williams DM, Wakefield TW. Long-term experience with transvenous catheter pulmonary embolectomy. *J Vasc Surg* 1993; **18**: 450-457; discussion 457-458 [PMID: 8377239 DOI: 10.1067/mva.1993.48033]

31 **Donaldson CW**, Baker JN, Narayan RL, Provias TS, Rassi AN, Giri JS, Sakhuja R, Weinberg I, Jaff MR, Rosenfield K. Thrombectomy using suction filtration and veno-venous bypass: single center experience with a novel device. *Catheter Cardiovasc Interv* 2015; **86**: E81-E87 [PMID: 24975395 DOI: 10.1002/ccd.25583]

32 **Al-Hakim R**, Park J, Bansal A, Genshaft S, Moriarty JM. Early Experience with AngioVac Aspiration in the Pulmonary Arteries. *J Vasc Interv Radiol* 2016; **27**: 730-734 [PMID: 27106647 DOI: 10.1016/j.jvir.2016.01.012]

33 **Weinberg AS**, Dohad S, Ramzy D, Madyoon H, Tapson VF. Clot Extraction With the FlowTriever Device in Acute Massive Pulmonary Embolism. *J Intensive Care Med* 2016; **3**: 676-679 [PMID: 27601482 DOI: 10.1177/0885066616666031]

34 **Müller-Hülsbeck S**, Brossmann J, Jahnke T, Grimm J, Reuter M, Bewig B, Heller M. Mechanical thrombectomy of major and massive pulmonary embolism with use of the Amplatz thrombectomy device. *Invest Radiol* 2001; **36**: 317-322 [PMID: 11410751 DOI: 10.1097/00004424-200106000-00003]

35 **Nassiri N**, Jain A, McPhee D, Mina B, Rosen RJ, Giangola G, Carroccio A, Green RM. Massive and submassive pulmonary embolism: experience with an algorithm for catheter-directed mechanical thrombectomy. *Ann Vasc Surg* 2012; **26**: 18-24 [PMID: 21885244 DOI: 10.1016/j.avsg.2011.05.026]

36 **Chechi T**, Vecchio S, Spaziani G, Giuliani G, Giannotti F, Arcangeli C, Rubboli A, Margheri M. Rheolytic thrombectomy in patients with massive and submassive acute pulmonary embolism. *Catheter Cardiovasc Interv* 2009; **73**: 506-513 [PMID: 19235240 DOI: 10.1002/ccd.21858]

37 **Dukkipati R**, Yang EH, Adler S, Vintch J. Acute kidney injury caused by intravascular hemolysis after mechanical thrombectomy. *Nat Clin Pract Nephrol* 2009; **5**: 112-116 [PMID: 19092794 DOI: 10.1038/ncpneph1019]

38 **Tafur AJ**, Shamoun FE, Patel SI, Tafur D, Donna F, Murad MH. Catheter-Directed Treatment of Pulmonary Embolism. *Clin Appl Thromb Hemost* 2016; **1**: 1076029616661414 [PMID: 27481877 DOI: 10.1177/1076029616661414]

39 **Stein PD**, Matta F. Thrombolytic therapy in unstable patients with acute pulmonary embolism: saves lives but underused. *Am J Med* 2012; **125**: 465-470 [PMID: 22325236 DOI: 10.1016/j.amjmed.2011.10.015]

40 **Kuo WT**, Gould MK, Louie JD, Rosenberg JK, Sze DY, Hofmann LV. Catheter-directed therapy for the treatment of massive pulmonary embolism: systematic review and meta-analysis of modern techniques. *J Vasc Interv Radiol* 2009; **20**: 1431-1440 [PMID: 19875060 DOI: 10.1016/j.jvir.2009.08.002]

41 **Wan S**, Quinlan DJ, Agnelli G, Eikelboom JW. Thrombolysis compared with heparin for the initial treatment of pulmonary embolism: a meta-analysis of the randomized controlled trials. *Circulation* 2004; **110**: 744-749 [PMID: 15262836 DOI: 10.1161/01.CIR.0000137826.09715.9C]

42 **Konstantinides S**, Geibel A, Heusel G, Heinrich F, Kasper W; Management Strategies and Prognosis of Pulmonary Embolism-3 Trial Investigators. Heparin plus alteplase compared with heparin alone in patients with submassive pulmonary embolism. *N Engl J Med* 2002; **347**: 1143-1150 [PMID: 12374874 DOI: 10.1056/NEJMoa021274]

43 **Meyer G**, Vicaut E, Danays T, Agnelli G, Becattini C, Beyer-Westendorf J, Bluhmki E, Bouvaist H, Brenner B, Couturaud F, Dellas C, Empen K, Franca A, Galiè N, Geibel A, Goldhaber SZ, Jimenez D, Kozak M, Kupatt C, Kucher N, Lang IM, Lankeit M, Meneveau N, Pacouret G, Palazzini M, Petris A, Pruszczyk P, Rugolotto M, Salvi A, Schellong S, Sebbane M, Sobkowicz B, Stefanovic BS, Thiele H, Torbicki A, Verschuren F, Konstantinides SV; PEITHO Investigators. Fibrinolysis for patients with intermediate-risk pulmonary embolism. *N Engl J Med* 2014; **370**: 1402-1411 [PMID: 24716681 DOI: 10.1056/NEJMoa1302097]

44 **Sharifi M**, Bay C, Skrocki L, Rahimi F, Mehdipour M; "MOPETT" Investigators. Moderate pulmonary embolism treated with thrombolysis (from the "MOPETT" Trial). *Am J Cardiol* 2013; **111**: 273-277 [PMID: 23102885 DOI: 10.1016/j.amjcard.2012.09.027]

45 **Kucher N**, Boekstegers P, Müller OJ, Kupatt C, Beyer-Westendorf J, Heitzer T, Tebbe U, Horstkotte J, Müller R, Blessing E, Greif M, Lange P, Hoffmann RT, Werth S, Barmeyer A, Härtel D, Grünwald H, Empen K, Baumgartner I. Randomized, controlled trial of ultrasound-assisted catheter-directed thrombolysis for acute intermediate-risk pulmonary embolism. *Circulation* 2014; **129**: 479-486 [PMID: 24226805 DOI: 10.1161/CIRCULATIONAHA.113.005544]

46 **Kuo WT**, Banerjee A, Kim PS, DeMarco FJ Jr, Levy JR, Facchini FR, Unver K, Bertini MJ, Sista AK, Hall MJ, Rosenberg JK, De Gregorio MA. Pulmonary Embolism Response to Fragmentation, Embolectomy, and Catheter Thrombolysis (PERFECT): Initial Results From a Prospective Multicenter Registry. *Chest* 2015; **148**: 667-673 [PMID: 25856269 DOI: 10.1378/chest.15-0119]

47 **Dudzinski DM**, Piazza G. Multidisciplinary Pulmonary Embolism Response Teams. *Circulation* 2016; **133**: 98-103 [PMID: 26719388 DOI: 10.1161/CIRCULATIONAHA.115.015086]

48 **Jauch EC**, Saver JL, Adams HP Jr, Bruno A, Connors JJ, Demaerschalk BM, Khatri P, McMullan PW Jr, Qureshi AI, Rosenfield K, Scott PA, Summers DR, Wang DZ, Wintermark M, Yonas H; American Heart Association Stroke Council; Council on Cardiovascular Nursing; Council on Peripheral Vascular Disease; Council on Clinical Cardiology. Guidelines for the early management of patients with acute ischemic stroke: a guideline for healthcare professionals from the American Heart Association/American Stroke Association. *Stroke* 2013; **44**: 870-947 [PMID: 23370205 DOI: 10.1161/STR.0b013e318284056a]

49 **Provias T**, Dudzinski DM, Jaff MR, Rosenfield K, Channick R, Baker J, Weinberg I, Donaldson C, Narayan R, Rassi AN, Kabrhel C. The Massachusetts General Hospital Pulmonary Embolism Response Team (MGH PERT): creation of a multidisciplinary program to improve care of patients with massive and submassive pulmonary embolism. *Hosp Pract* (1995) 2014; **42**: 31-37 [PMID: 24566594 DOI: 10.3810/hp.2014.02.1089]

50 **Kabrhel C**, Jaff MR, Channick RN, Baker JN, Rosenfield K. A multidisciplinary pulmonary embolism response team. *Chest* 2013; **144**: 1738-1739 [PMID: 24189880 DOI: 10.1378/chest.13-1562]

51 **PERT**. The National Consortium of Pulmonary Embolism Response Teams: Developing effective solutions to a devastating illness. Available from: URL: http://pertconsortium.org

P- Reviewer: Gao BL, Gumustas OG, Shen J, van Beek EJR, Yazdi HR
S- Editor: Ji FF **L- Editor**: A **E- Editor**: Lu YJ

World Journal of Radiology

Submit a Manuscript: http://www.f6publishing.com

World J Radiol 2017 December 28; 9(12): 438-447

DOI: 10.4329/wjr.v9.i12.438

ISSN 1949-8470 (online)

MINIREVIEWS

Imaging features of intrathoracic complications of lung transplantation: What the radiologists need to know

Elisa Chia, Simeon Niyi Babawale

Elisa Chia, Simeon Niyi Babawale, Department of Radiology, Royal Perth Hospital, Wellington Street Campus, Perth, WA 6001, Australia

ORCID number: Elisa Chia (0000-0003-1110-6524); Simeon Niyi Babawale (0000-0002-3482-3158).

Author contributions: Chia E collated imaging used in the manuscript after obtaining consent from the patients and contributed to the drafting and editing of the manuscript; Babawale SN contributed to the writing of the manuscript, manuscript editing and review of the imaging.

Conflict-of-interest statement: No conflicts of interest were noted in the making of this manuscript. There is no financial support or relationships associated with the authors of this work that may pose a conflict of interest.

Manuscript source: Unsolicited manuscript

Correspondence to: Elisa Chia, MBBS, Department of Radiology, Royal Perth Hospital, Wellington Street Campus, GPO Box X2213, Perth, WA 6001, Australia. elisa.chia@health.wa.gov.au
Telephone: +61-08-92242244
Fax: +61-08-92242912

Received: July 2, 2017
Peer-review started: July 3, 2017
First decision: August 7, 2017
Revised: October 20, 2017
Accepted: November 8, 2017
Article in press: November 8, 2017
Published online: December 28, 2017

Abstract

Lung transplantation has been a method for treating end stage lung disease for decades. Despite improvements in the preoperative assessment of recipients and donors as well as improved surgical techniques, lung transplant recipients are still at a high risk of developing post-operative complications which tend to impact negatively the patients' outcome if not recognised early. The recognised complications post lung transplantation can be broadly categorised into acute and chronic complications. Recognising the radiological features of these complications has a significant positive impact on patients' survival post transplantation. This manuscript provides a comprehensive review of the radiological features of post lung transplantations complications over a time continuum.

Key words: Lung transplantation; Post-surgical features of lung transplantation; Complication of lung transplantation; Imaging features; Early and late complications

Core tip: Lung transplantation is a common method of treating end stage lung disease. However, despite advances in surgical techniques, complications are still common and can occur years after lung transplantation. Radiological imaging plays an essential role in characterising many post-transplantation complications. It is crucial for radiologists to identify early signs of common complications on imaging to ensure that appropriate treatments are instituted early.

Chia E, Babawale SN. Imaging features of intrathoracic complications of lung transplantation: What the radiologists need to know. *World J Radiol* 2017; 9(12): 438-447 Available from: URL: http://www.wjgnet.com/1949-8470/full/v9/i12/438.htm DOI: http://

dx.doi.org/10.4329/wjr.v9.i12.438

INTRODUCTION

Lung transplantation is an accepted treatment modality for end stage lung disease with over 3614 transplantations performed worldwide between July 2013 and June 2014[1]. In Australia alone, over 163 of lung transplantations were performed in 2014[2]. During the early 1960s when human lung transplantation was explored, multiple attempts at the procedure often failed rapidly due to rejection and issues with bronchial and vessel anastomoses. However, over years, this measure of treatment has achieved remarkable outcomes.

Given the inherent risks associated with lung transplantation, patients are carefully selected for their suitability for treatment. Improved outcomes have been associated with advancing surgical techniques, appropriate patient selection, cautious harvesting and preservation of organs, and improved immunosuppressive therapy[3]. Despite the pre-transplant strict selection criteria, complications are still frequent.

Postoperative complications can be categorised broadly into: Early complications; including but not limited to reperfusion oedema and acute rejection; and late complications including infections, anastomotic complications and chronic graft rejection. Understanding the timeline of post-operative complications is a key to making accurate diagnosis for early intervention.

EARLY COMPLICATIONS

Early complications of lung transplantation generally occur within few weeks post- operatively. These account for the significant proportion of mortality in patients who undergo lung transplantation.

Donor lung and recipient thorax mismatch

Donor lung and recipient thoracic cage mismatch is a potential underlying cause of some of the early complications of lung transplantation. Therefore, meticulous attention to details in selecting appropriate donor lung is a crucial initial step in obviating the likelihood of complications relating to donor-recipient mismatch. These complications include pleural effusion and pneumothorax, which have been shown to develop especially if the donor lung is too small for the recipient thorax. These complications may, in certain cases require interventions such as thoracocentesis and antibiotic therapy. This contributes to a prolonged hospitalisation and increased overall cost of lung transplantation.

However, deliberately mismatching the donor lung and the recipient's thorax may have some potential benefits. Moderately oversized donor lung has been shown to reduce the risk of early primary graft dysfunction[4]. However, in cases where the donor lung is too large in size, atelectasis and impaired ventilation may ensue[4].

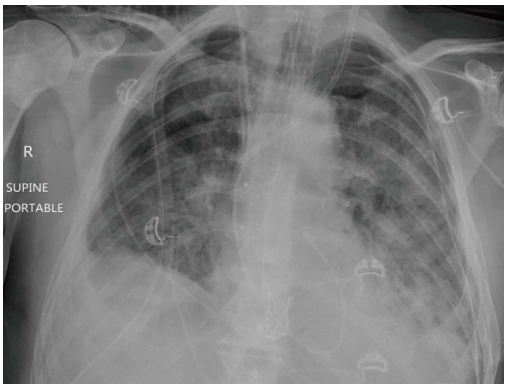

Figure 1 Chest X-ray of a 64-year-old male 3 d post transplantation showing reperfusion oedema. Bilateral airspace opacity predominantly in the mid to lower zones with associated bilateral pleural effusions.

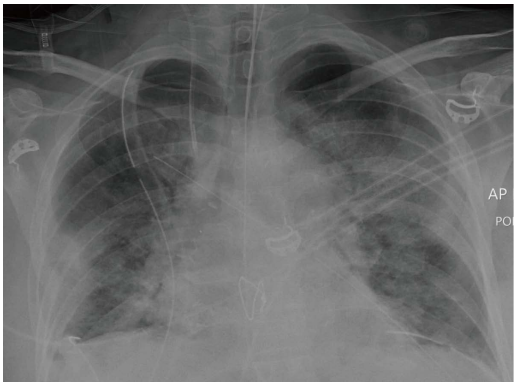

Figure 2 Chest X-ray 3 d post transplantation shows reperfusion oedema. Bilateral airspace opacity in the mid to lower zones and sub-pleural consolidation in the lower zone of the right lower lobe.

Ischaemia-reperfusion injury

Ischaemic-reperfusion injury, also known as primary graft dysfunction is a frequent complication following lung transplantation. It is one of the leading causes of early post-transplant morbidity and mortality. It is a severe acute lung injury syndrome that develops within the first 48-72 h post lung transplantation[5].

Reperfusion oedema has variable imaging features. On chest X-ray, it may present with hazy peri-hilar airspace opacity in milder cases, and dense peri-hilar consolidations with air bronchograms in more severe cases[6] (Figures 1 and 2).

High resolution computerised tomography (HRCT) will demonstrate the above features in greater details, even though these are not specific only to pulmonary oedema. Perihilar ground-glass opacities, peribronchovascular thickening and reticulations with predilection for the middle and lower lobes are elegantly demonstrable on HRCT[7,8].

Acute rejection

Acute cellular rejection occurs generally within the first

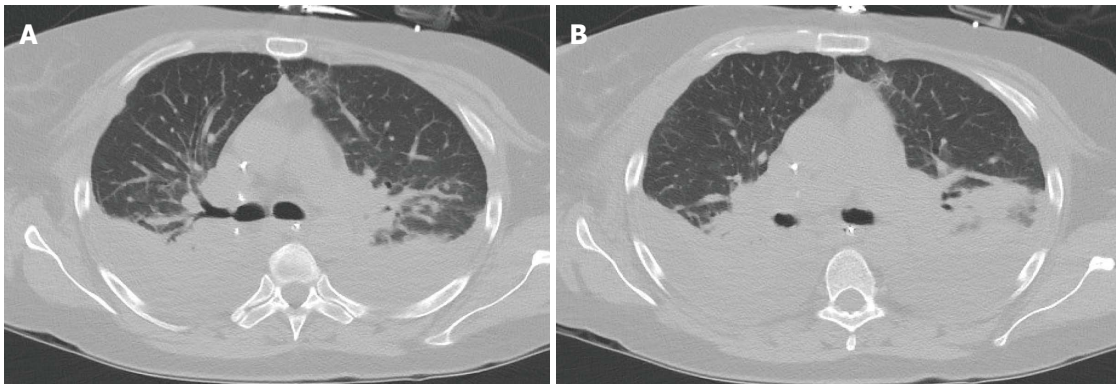

Figure 3 Computerised tomography images of the chest 4 wk post-transplantation showing acute rejection. Bilateral basal predominant consolidation, diffuse ground glass opacity and atelectasis with large bilateral pleural effusions. A: Axial slice of CT chest image showing bilateral basal consolidations; B: Axial slice of CT chest image illustrating extensive bilateral pleural effusions with pulmonary atelectasis. CT: Computerised tomography.

Figure 4 Acute rejection in a 50-year-old female 3 wk post-transplantation. CT scan of the chest shows bilateral diffuse ground glass opacity, linear atelectases, bilateral pleural effusion and bilateral peribronchial thickening. A: Coronal slice of CT chest image showing bilateral ground glass opacities and linear atelectasis; B: Axial slice of CT chest image highlighting bilateral pleural effusions; C: Axial slice of CT chest image highlighting peribronchial thickening. CT: Computerised tomography.

Figure 5 Chest X-ray shows increased lucency of the costophrenic angles on both sides (deep sulcus sign) in keeping with bilateral supine pneumothoraces.

2 wk post-lung transplantation. This complication is a potential cause of significant morbidity. Acute cellular rejection is a cell-mediated immune response to human leukocyte antigen (HLA) complex expressed in the donor lung. This immune response leads to perivascular lymphocytic infiltrate[9-11].

Imaging findings in the mild acute rejection may be very subtle and, hence, trans-bronchial lung biopsy is the gold standard for diagnosis in this setting. Normal findings on chest X-rays, therefore, does not exclude the diagnosis of acute rejection, especially in the mild form[10]. Radiological findings, demonstrable on HRCT, include lower lobe predominant peri-hilar ground glass opacities, peri-bronchial cuffing, interlobular septal thickening, and new or increasing pleural effusions[9,11] (Figures 3 and 4). Notably, the absence of ground glass opacities in HRCT within the first few weeks post lung transplantation virtually excludes the diagnosis of severe acute rejection[7].

Pleural complications

The spectrums of acute pleural complications include minor air leaks, haemothorax, pneumothorax, chylothorax and pleural effusions. Air leaks may occur transiently following lung transplantation or persist for quite a while. Pleural leaks (Figure 5) are considered transient if spontaneous resolution occurs within 7 d post-transplantation. Air leaks that are unresolved after 7 d post-transplantation are dubbed persistent and may signify more serious complications such as significant bronchial dehiscence or airway ischaemia. This may eventually lead to pneumomediastinum, persistent pneumothorax or subcutaneous emphysema[9].

Pleural effusion may persist for few months. At 3 mo, approximately 59% of patients may have some pleural

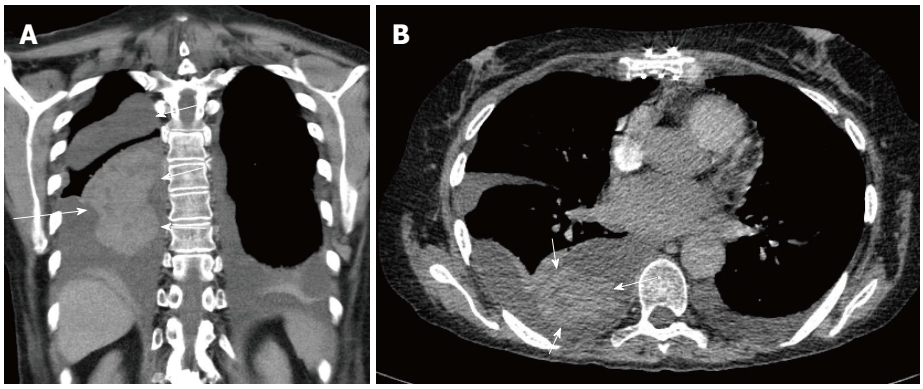

Figure 6 Computerised tomography scan of the chest in a 63-year-old female performed 16 d post bilateral lung transplant showing a coronal slice and an axial slice of a left pleural effusion and right haemothorax with clotted blood component (arrow). A: Coronal slice; B: Axial slice.

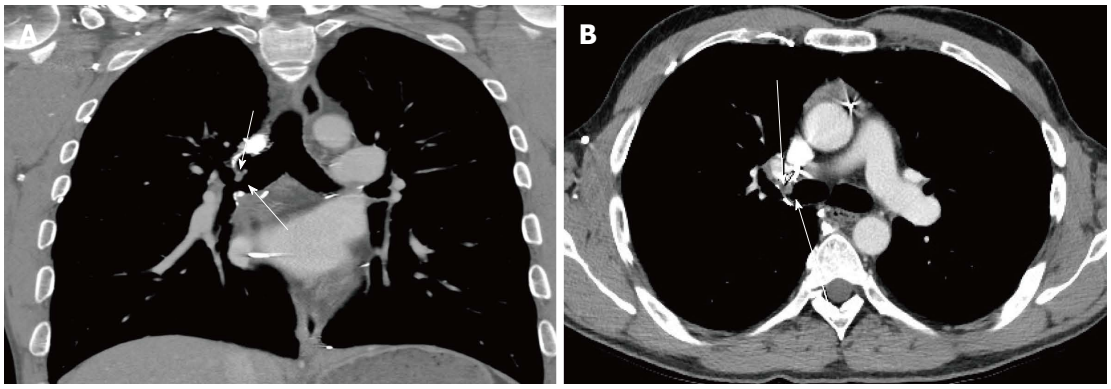

Figure 7 Computerised tomography scan images of a 37-year-old man performed 18 mo post-transplantation showing a coronal slice and an axial slice of a stenosis of the right main stem bronchus (arrow). A: Coronal slice; B: Axial slice.

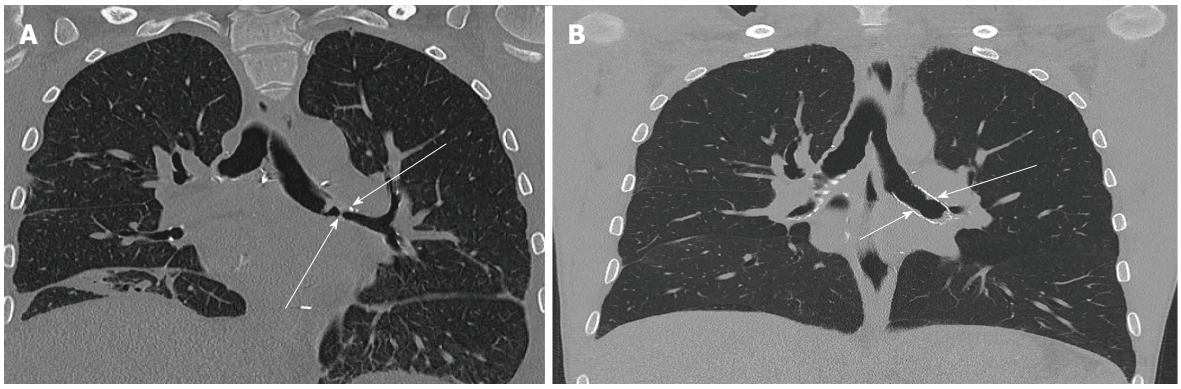

Figure 8 Computerised tomography scan of the chest showing a left main stem bronchial stenosis (arrow) in a 36-year-old male 2 mo post lung transplantation. A: Coronal slice of CT chest image before insertion of bronchial stent; B: Coronal slice of CT chest image after insertion of bronchial stent. CT: Computerised tomography.

effusions detectable on imaging study, especially on computerised tomography (CT) scan. However, majority of pleural effusion resolve completely by 12 mo (8%)[12]. Pleural thickening and calcification may manifest as a long-term complication. Figure 6 illustrates some of the more common pleural complications.

Bronchial anastomotic complications

Bronchial dehiscence, bronchial stenosis, bronchomalacia and bronchopleural fistulas are some of the airway anastomotic complications that can occur. The most frequent of these complications is bronchial stenosis. There are two patterns of bronchial stenosis: Surgical site anastomotic stenosis and segmental non-anastomotic bronchial stenosis.

Bronchial stenosis is easily demonstrable in chest X-ray. Bronchial stenosis may be severe enough to cause the atelectasis of the affected lobe[13]. As demonstrated in Figures 7 and 8, helical CT with multiplanar reconstruction will demonstrate this and

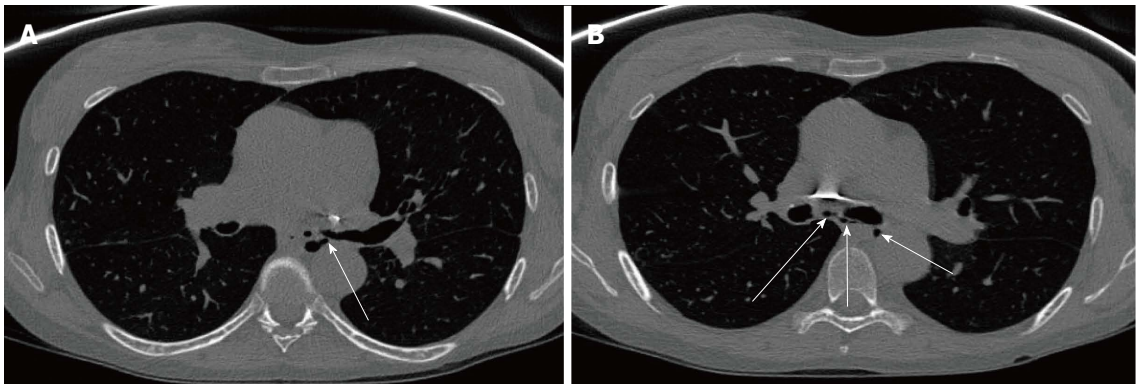

Figure 9 Computerised tomography scan of the chest in a 51-year-old female performed nearly 3 years post bilateral lung transplantation shows left main bronchial dehiscence resulting in gas locules tracking from the left main stem bronchus to the mediastinum causing pneumomediastinum. A: Axial slice of CT chest image showing gas leaks (arrow) from the left main stem bronchus; B: Axial slice of CT chest image showing multiple gas locules (arrow) causing pneumomediastinum. CT: Computerised tomography.

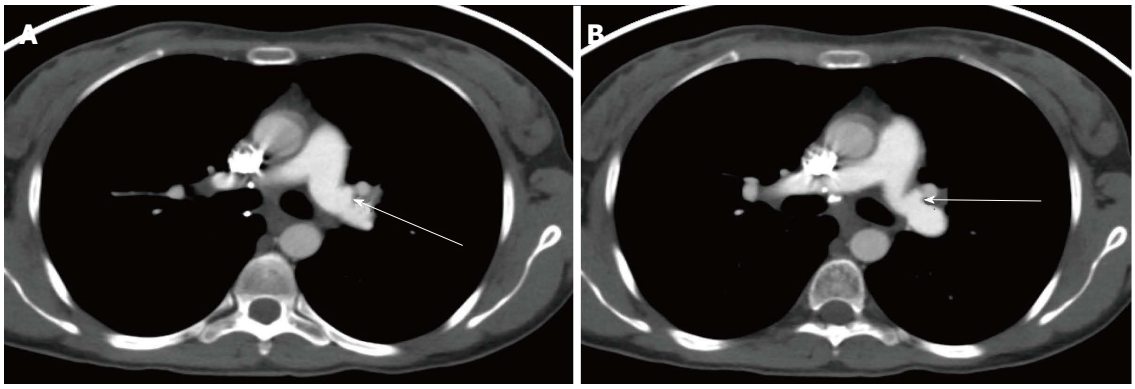

Figure 10 Computerised tomography scan of the chest in a 31-year-old female 3 mo post bilateral lung transplantation showing peri-anastomotic left pulmonary artery saccular aneurysm. A: Axial slice of CT chest image showing a left pulmonary artery saccular aneurysm (arrow); B: Axial slice of CT chest image showing a left pulmonary artery saccular aneurysm (arrow). CT: Computerised tomography.

other associated features more elegantly and is said to have an accuracy of 94% for detecting bronchial stenosis[13].

Bronchial dehiscence results from ongoing mucosal necrosis of the donor bronchus secondary to disruption of the bronchial circulation[7]. Chest radiography is unreliable for the diagnosis of bronchial dehiscence due to the presence of peri-bronchial air that may obscure the major airways.

CT scan is more sensitive and readily able to identify the features of bronchial dehiscence including bronchial wall defects, fixed or dynamic bronchial narrowing, and peribronchial air around the anastomosis[13] (Figure 9).

Bronchopleural fistula manifests as progressive increase in the intrapleural air, new or progressing hydro-pneumothorax and changes in the already present air-fluid levels. In severe cases, tension pneumothorax may occur with imaging demonstrating contralateral mediastinal shift, flattening of the ipsilateral diaphragm, ipsilateral widening of intercostal spaces and atelectasis of the contralateral lung.

Vascular anastomotic complications

Complications involving the vasculature anastomotic sites post lung transplantation are much less frequent compared to airway anastomotic complications. Vascular complications include pulmonary artery stenosis, kinking of the pulmonary artery and pulmonary vein thrombosis. Peri-anastomotic pulmonary artery aneurysm is an unusual complication (Figure 10).

Pulmonary artery stenosis can occur early or late after lung transplantation and is generally a result of incongruent lengths of the donor and recipient segments, technical narrowing or twisting of the anastomosis[14].

CT angiogram is the acceptable imaging modality for investigating these complications. Narrowing or occlusion of the affected artery is readily demonstrable with CT angiogram. Diminished opacification of the corresponding pulmonary segment may indicate atelectasis or evolving pulmonary infarction[15].

Infections

Pulmonary infection after lung transplantation remains an important complication that is associated with high rates of morbidity and mortality. The incidence of infection is far more frequent in the lung transplant recipients than any other organ transplant recipients[9]. This is due to the higher level of immunosuppression and loss of local pulmonary host defences characterised by the reduction in lymphatic drainage, and reduced mucociliary

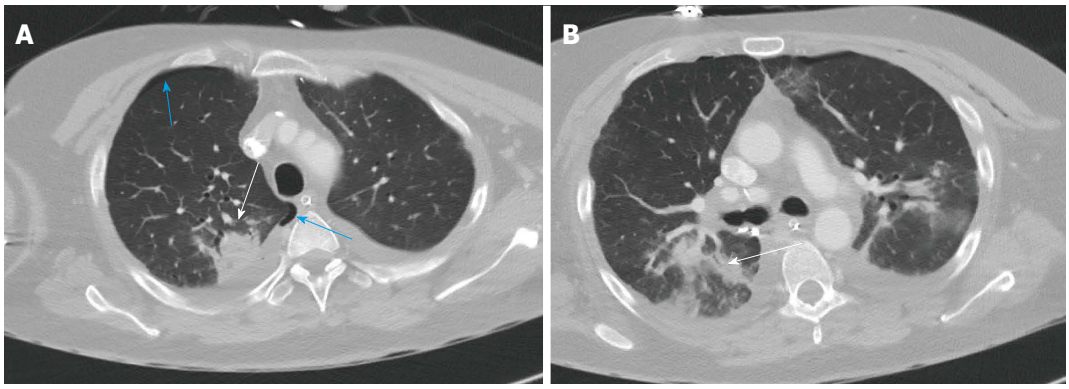

Figure 11 Computerised tomography scan of the chest 2 wk post-transplantation shows consolidation in the right upper lobe posteriorly with air bronchogram in keeping with pneumonia. Associated right sided pneumothorax. A: Axial slice of CT chest showing right upper lobe consolidation (white arrow), and right sided pneumothorax (blue arrows); B: Axial slice showing consolidation on the right upper lobe with air bronchogram (arrow). CT: Computerised tomography.

Figure 12 Chest computerised tomography scan of a 57-year-old male performed 2 years post-transplantation shows pseudomonas lung infection. Geographic area of ground glass opacity with associated diffuse centrilobular ground glass opacities and bronchiolar thickening mainly in the basal segment of the left upper lobe. A: Axial slice of CT chest image showing ground glass opacity (arrow); B: Axial slice of CT chest image highlighting diffuse centrilobar ground glass opacities on the left; C: Axial slice of CT chest image showing bronchiolar wall thickening in the left upper lobe (arrow). CT: Computerised tomography.

clearance.

Bacterial pneumonia accounts for approximately 36% of pneumonias[16] occurring post lung transplantation. *Staphylococcus aureus, pseudomonas aeruginosa* and *Enterobacteriaceae* are the most common bacterial culprits.

Radiographic manifestation of bacterial pneumonia (Figures 11 and 12) may be nonspecific with the occurrence of patchy or confluent consolidation, ground-glass opacity, septal thickening and pleural effusions[16]. These features and the presence of tree-in-bud opacity on chest radiograph, in conjunction with the appropriate clinical picture, makes the radiographic diagnosis of pneumonia fairly obvious. Pleural effusion is nonspecific. It may be indicative of haemorrhage, rejection or empyema[17].

LATE COMPLICATIONS

Late complications post lung transplantation can occur anytime from months to years. It is vitally important to have a high index of suspicion in recognising the signs of late complications as these largely contribute to the patients' morbidity and mortality.

Chronic rejection

Chronic allograft rejection is one of the causes attributed to the increased rate of mortality and morbidity post lung transplantation, whether single lung transplantation or bilateral. Chronic allograft rejection is described clinically as bronchiolitis obliterans syndrome. Cryptogenic organising pneumonia may also be seen. Patho-physiologically, chronic rejection is typified by inflammatory and fibrotic processes. Eosinophilic hyaline fibrosis of the small airways leads to progressive concentric bronchiolar luminal narrowing and eventually bronchiolar occlusion[7].

Plain radiograph is of limited diagnostic value in chronic graft rejection. Non-specific features in plain radiograph that can suggest chronic rejection include pulmonary hyperinflation, decreased vascular markings, regional volume loss, subsegmental atelectasis, linear opacities and bronchiectasis[7].

Chest CT is the imaging of choice for demonstrating the features of small airway and interstitial lung parenchymal changes that occur in chronic graft rejection (Figure 13). Some of these features, which are readily demonstrable on chest CT, include bronchial wall thickening, interlobular septal thickening, reticulo-nodular opacity, ground-glass opacity with mosaic attenuation, air trapping and peripherally predominant bronchiectasis[7,9,18].

Atypical infections

Iatrogenic immunosuppression post lung transplantation

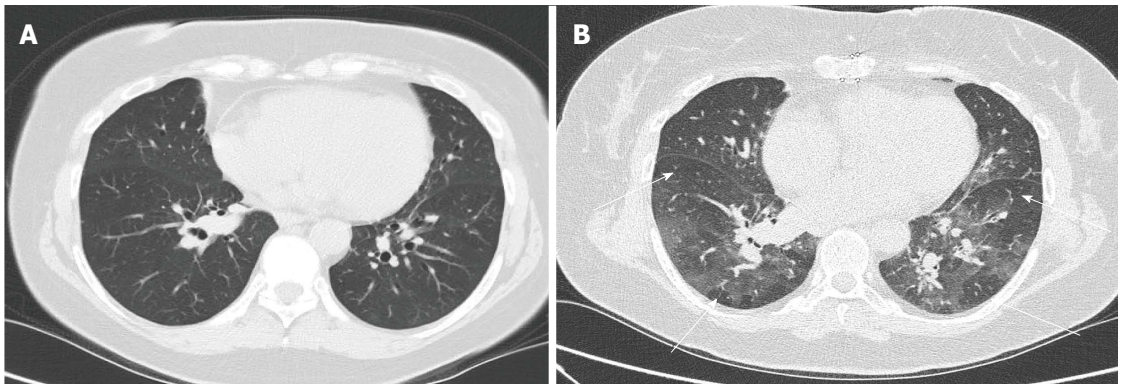

Figure 13 Bronchiolitis/small airway disease. CT scan of the chest performed 8 years post-transplantation shows patchy multifocal air trapping with bronchiolar thickening. A: Axial slice of CT chest image showing bronchiolar thickening; B: Axial slice of CT chest image showing multifocal areas of patchy air trapping. CT: Computerised tomography.

Figure 14 Chest computerised tomography scan of a 30-year-old male performed 2 mo after lung transplantation shows fungal infection. Two partly solid nodules in the right lung (one in the basal segment of the right upper lobe and the other in the right lower lobe. A: Axial slice of CT chest image showing right lower lobe nodule (arrow); B: Coronal slice of CT chest image showing 2 nodules on the lower segment of the right upper lobe (blue arrow) and right lower lobe (white arrow); C: Axial slice of CT chest image showing partially solid nodule (arrow). CT: Computerised tomography.

is an important predisposing factor for infection with atypical organisms such as viruses, fungi and mycobacterium.

Viruses, particularly cytomegalovirus (CMV), are largely opportunistic infections and are a risk factor for the development of transplant rejection. Lung transplant recipients are particularly susceptible to CMV infection and the rate of infection in these patients can be as high as 50%[7]. Other viral culprits include parainfluenza virus, respiratory syncytia virus and adenovirus.

Features of viral chest infections are nonspecific. It is usually patchy with no particular lobar predilection. Nodular opacities, patchy consolidation, diffuse ground-glass opacity and bronchiolar thickening can be seen in viral chest infections. Adenoviral pneumonia imaging findings typically are more extensive compared to those caused by other viral infections[19].

Fungal infection post lung transplantation is less frequent than bacterial and viral infections, however they are associated with high mortality rates. *Aspergillus* and *Candida* species are the most common causes of fungal infections in lung transplant recipients (Figure 14). Colonisation of the airways by aspergillus species is a common occurrence in lung transplant recipients, particularly those with underlying cystic fibrosis. Colonisation with these organisms increase the risk of developing invasive aspergillosis which could be fatal and may result in as high as 55% mortality in lung transplant recipients if not aggressively treated[20].

Fungal chest infections have various chest CT features including consolidation, lung nodules and cavitating nodules or masses. Ground glass opacity surrounding a lung nodule or mass (Figures 15 and 16) dubbed as a halo sign is highly suggestive, although not specific, of fungal infection in appropriate clinical settings[7].

Rate of tuberculosis infections usually vary by geographic location. However, tuberculosis infection has been shown to be significantly higher in transplant recipients compared to the general population irrespective of geographic location[21]. It presents commonly as a reactivation of the latent infection in the transplant recipients, but can also be acquired from unrecognised infected donor lung. Pulmonary tuberculosis is commonly seen radiologically as focal infiltrates or in a miliary pattern[22].

Thromboembolism

Thromboembolism (including pulmonary embolism and deep vein thrombosis) is a common complication that tends to occur within few months post-transplantation. It is important to recognise this since up to 27% of lung transplant recipients are prone to this complication[23]. This

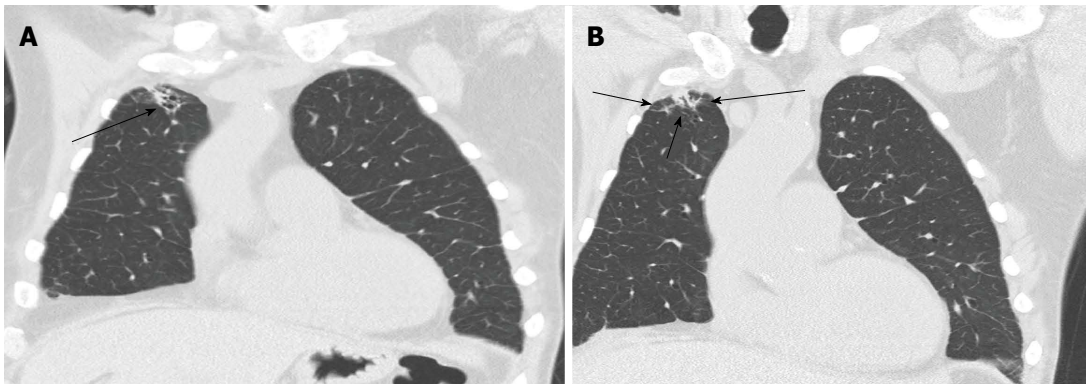

Figure 15 Broncho-alveolar lavage proven aspergillosis. CT scan of the chest shows right lung apex sub-pleural nodule with surrounding ground glass opacity and focal bronchiectasis. A: Coronal slice of CT chest showing right apical sub-pleural nodule (arrow); B: Coronal slice of CT chest showing surrounding ground glass opacity and focal bronchiectasis (arrow) around a sub-pleural nodule. CT: Computerised tomography.

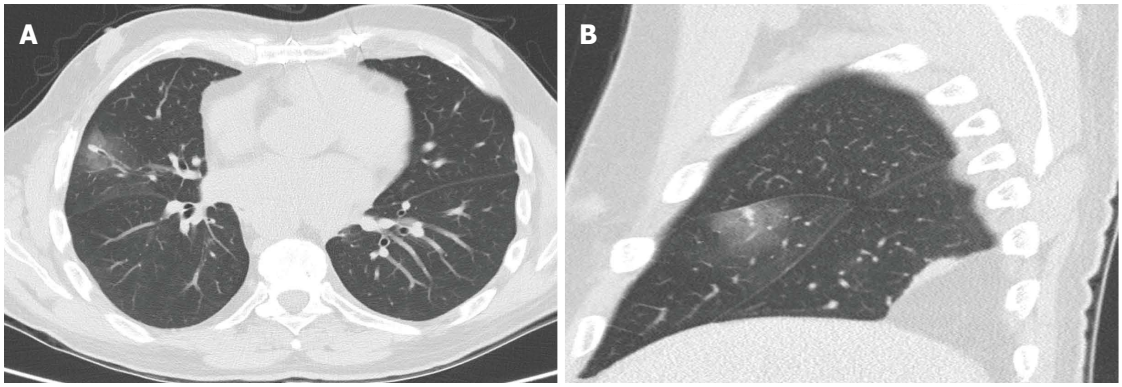

Figure 16 Computerised tomography scan of the chest performed 1 year post bilateral lung transplant shows pulmonary aspergillosis. An axial slice (A) and sagittal slice (B) showing a middle lobe small solid nodule with relatively large peripheral halo of ground glass opacity known as a "halo sign" (arrow). Bronchoscopy confirmed aspergillosis. A: Axial slice; B: Sagittal slice.

has been suggested to be due to the hypercoagulable state caused by the inflammatory response to the donor organ[11]. Potential thrombogenic surfaces, such as the pulmonary artery anastomotic site and central lines, also act as sources of venous thromboembolisms[23].

Lung transplant recipients are more susceptible to thromboembolic induced pulmonary infarcts due to a deficient dual blood supply (bronchial and pulmonary arterial supply) in the early post-operative period. Clues suggesting pulmonary thromboembolism on chest radiography include segmental oligaemia, pleural effusion, dilated central pulmonary arteries and cardiomegaly[7]. Wedge shaped sub-pleural opacity representing lung infarct is readily demonstrable on chest radiograph.

CT pulmonary angiogram is the gold standard for diagnosing pulmonary embolism. Filling defects with segmental partial or total occlusion in the central or segmental branches of the pulmonary arteries are the most reliable direct signs of thromboembolism[7,10]. Indirect features include consolidation in specific vascular territories, mosaic perfusion, atelectasis and pleural effusions[7,10]. Ventilation perfusion scans is a viable alternative in patients who have contraindications to CT pulmonary angiogram.

Transplant related lymphoproliferative disorder

A diverse number of lymphoproliferative diseases may develop post lung transplantation. These are collectively termed post-transplantation lymphoproliferative disorders (PTLD) and occur in approximately 5% of lung transplant recipients[24]. Patho-physiologically, transplant recipients are predisposed to Epstein-Barr virus (EBV) which induces B-cell proliferative responses leading to PTLD, usually within a year after transplantation.

CT features of PTLD are variable, and may be seen as a single or multiple pulmonary nodules or masses with or without mediastinal, hilar and extra-thoracic adenopathy[25].

Primary lung carcinoma

Primary lung carcinomas occurring in the lung allograft are rare[26]. This is attributable in part to the comprehensive screening process prior to transplantation aiming at excluding donors with underlying parenchymal lung disease and those with significant smoking history. The risk of developing primary pulmonary carcinoma in transplant recipients is therefore the same as the general population.

Nevertheless, in cases where primary lung allograft

carcinomas arise, tumours tend to be more aggressive[26]. This is likely due to immunosuppression, and can be challenging radiologically to distinguish from an infectious process.

Recurrence of primary disease

Despite lung transplantation being the only available therapy for end-stage lung disease, a number of diseases have been reported to recur in the lung allograft. Sarcoidosis has been demonstrated to have a high recurrence rate[27]. Lymphangioleiomyomatosis and diffuse panbronchiolitis and pulmonary alveolar proteinosis have also been reported to recur post lung transplantation. Radiological findings of these diseases, however, have slight morphological differences at recurrence compared with pre-transplantation[27].

CONCLUSION

Lung transplantation is essentially the only viable option for treating end stage lung disease. Despite this advanced procedure, it poses a diverse list of complications that are associated with morbidity and mortality for transplant recipients. Although radiological manifestations of post-lung transplant complications may be non-specific, understanding the main features of post-transplant complications over a time continuum is the key to improving patients' survival. By recognising these radiological features, early treatment can be instituted.

REFERENCES

1 **International Society for Heart and Lung Transplantation**. The registry of the international society for heart and lung transplantation: Thirty-second annual report. Available from: URL: https://www.ishlt.org/downloadables/slides/2015/introduction.pptx

2 **ANZOD Committee**. ANZOD Registry Annual Report 2015. Australia and New Zealand Organ Donation Registry. Available from: URL: http://www.anzdata.org.au/anzod/ANZODReport/2015/2015ANZOD_annrpt.pdf

3 **O'Donovan PB**. Imaging of complications of lung transplantation. *Radiographics* 1993; **13**: 787-796 [PMID: 8356268 DOI: 10.1148/radiographics.13.4.8356268]

4 **Eberlein M**, Permutt S, Chahla MF, Bolukbas S, Nathan SD, Shlobin OA, Shelhamer JH, Reed RM, Pearse DB, Orens JB, Brower RG. Lung size mismatch in bilateral lung transplantation is associated with allograft function and bronchiolitis obliterans syndrome. *Chest* 2012; **141**: 451-460 [PMID: 21799025 DOI: 10.1378/chest.11-0767]

5 **Kundu S**, Herman SJ, Winton TL. Reperfusion edema after lung transplantation: radiographic manifestations. *Radiology* 1998; **206**: 75-80 [PMID: 9423654 DOI: 10.1148/radiology.206.1.9423654]

6 **Herman SJ**, Rappaport DC, Weisbrod GL, Olscamp GC, Patterson GA, Cooper JD. Single-lung transplantation: imaging features. *Radiology* 1989; **170**: 89-93 [PMID: 2642351 DOI: 10.1148/radiology.170.1.2642351]

7 **Krishnam MS**, Suh RD, Tomasian A, Goldin JG, Lai C, Brown K, Batra P, Aberle DR. Postoperative complications of lung transplantation: radiologic findings along a time continuum. *Radiographics* 2007; **27**: 957-974 [PMID: 17620461 DOI: 10.1148/rg.274065141]

8 **Belmaati EO**, Steffensen I, Jensen C, Kofoed KF, Mortensen J, Nielsen MB, Iversen M. Radiological patterns of primary graft dysfunction after lung transplantation evaluated by 64-multi-slice computed tomography: a descriptive study. *Interact Cardiovasc Thorac Surg* 2012; **14**: 785-791 [PMID: 22378316 DOI: 10.1093/icvts/ivs065]

9 **Diez Martinez P**, Pakkal M, Prenovault J, Chevrier MC, Chalaoui J, Gorgos A, Ferraro P, Poirier C, Chartrand-Lefebvre C. Postoperative imaging after lung transplantation. *Clin Imaging* 2013; **37**: 617-623 [PMID: 23557663 DOI: 10.1016/j.clinimag. 2013. 02.008]

10 **Hochhegger B**, Irion KL, Marchiori E, Bello R, Moreira J, Camargo JJ. Computed tomography findings of postoperative complications in lung transplantation. *J Bras Pneumol* 2009; **35**: 266-274 [PMID: 19390726 DOI: 10.1590/S1806-37132009000300012]

11 **Ahmad S**, Shlobin OA, Nathan SD. Pulmonary complications of lung transplantation. *Chest* 2011; **139**: 402-411 [PMID: 21285054 DOI: 10.1378/chest.10-1048]

12 **Ferrer J**, Roldan J, Roman A, Bravo C, Monforte V, Pallissa E, Gic I, Sole J, Morell F. Acute and chronic pleural complications in lung transplantation. *J Heart Lung Transplant* 2003; **22**: 1217-1225 [PMID: 14585383 DOI: 10.1016/S1053-2498(02)01230-5]

13 **Santacruz JF**, Mehta AC. Airway complications and management after lung transplantation: ischemia, dehiscence, and stenosis. *Proc Am Thorac Soc* 2009; **6**: 79-93 [PMID: 19131533 DOI: 10.1513/pats.200808-094GO]

14 **Anaya-Ayala JE**, Loebe M, Davies MG. Endovascular management of early lung transplant-related anastomotic pulmonary artery stenosis. *J Vasc Interv Radiol* 2015; **26**: 878-882 [PMID: 25851200 DOI: 10.1016/j.jvir.2015.02.017]

15 **Madan R**, Chansakul T, Goldberg HJ. Imaging in lung transplants: Checklist for the radiologist. *Indian J Radiol Imaging* 2014; **24**: 318-326 [PMID: 25489125 DOI: 10.4103/0971-3026.143894]

16 **Collins J**, Müller NL, Kazerooni EA, Paciocco G. CT findings of pneumonia after lung transplantation. *AJR Am J Roentgenol* 2000; **175**: 811-818 [PMID: 10954472 DOI: 10.2214/ajr.175.3.1750811]

17 **Judson MA**, Handy JR, Sahn SA. Pleural effusions following lung transplantation. Time course, characteristics, and clinical implications. *Chest* 1996; **109**: 1190-1194 [PMID: 8625665 DOI: 10.1378/chest.109.5.1190]

18 **Bankier AA**, Van Muylem A, Scillia P, De Maertelaer V, Estenne M, Gevenois PA. Air trapping in heart-lung transplant recipients: variability of anatomic distribution and extent at sequential expiratory thin-section CT. *Radiology* 2003; **229**: 737-742 [PMID: 14657310 DOI: 10.1148/radiol.2293020827]

19 **Matar LD**, McAdams HP, Palmer SM, Howell DN, Henshaw NG, Davis RD, Tapson VF. Respiratory viral infections in lung transplant recipients: radiologic findings with clinical correlation. *Radiology* 1999; **213**: 735-742 [PMID: 10580947 DOI: 10.1148/radiology.213.3.r99dc25735]

20 **Singh N**, Husain S. Aspergillus infections after lung transplantation: clinical differences in type of transplant and implications for management. *J Heart Lung Transplant* 2003; **22**: 258-266 [PMID: 12633692 DOI: 10.1016/S1053-2498(02)00477-1]

21 **Morales P**, Briones A, Torres JJ, Solé A, Pérez D, Pastor A. Pulmonary tuberculosis in lung and heart-lung transplantation: fifteen years of experience in a single center in Spain. *Transplant Proc* 2005; **37**: 4050-4055 [PMID: 16386624 DOI: 10.1016/j.transproceed.2005.09.144]

22 **Singh N**, Paterson DL. Mycobacterium tuberculosis infection in solid-organ transplant recipients: impact and implications for management. *Clin Infect Dis* 1998; **27**: 1266-1277 [PMID: 9827281 DOI: 10.1086/514993]

23 **Krivokuca I**, van de Graaf EA, van Kessel DA, van den Bosch JM, Grutters JC, Kwakkel-van Erp JM. Pulmonary embolism and pulmonary infarction after lung transplantation. *Clin Appl Thromb Hemost* 2011; **17**: 421-424 [PMID: 20547546 DOI: 10.1177/1076029610371474]

24 **Kremer BE**, Reshef R, Misleh JG, Christie JD, Ahya VN, Blumenthal NP, Kotloff RM, Hadjiliadis D, Stadtmauer EA, Schuster SJ, Tsai DE. Post-transplant lymphoproliferative disorder after lung transplantation: a review of 35 cases. *J Heart Lung Transplant* 2012; **31**: 296-304 [PMID: 22112992 DOI: 10.1016/j.healun.2011.10.013]

25 **Rappaport DC**, Chamberlain DW, Shepherd FA, Hutcheon MA. Lymphoproliferative disorders after lung transplantation: imaging

features. *Radiology* 1998; **206**: 519-524 [PMID: 9457207 DOI: 10.1148/radiology.206.2.9457207]
26 **Grewal AS**, Padera RF, Boukedes S, Divo M, Rosas IO, Camp PC, Fuhlbrigge A, Goldberg H, El-Chemaly S. Prevalence and outcome of lung cancer in lung transplant recipients. *Respir Med* 2015; **109**: 427-433 [PMID: 25616348 DOI: 10.1016/j.rmed.2014.12.013]
27 **Collins J**, Hartman MJ, Warner TF, Müller NL, Kazerooni EA, McAdams HP, Slone RM, Parker LA. Frequency and CT findings of recurrent disease after lung transplantation. *Radiology* 2001; **219**: 503-509 [PMID: 11323479 DOI: 10.1148/radiology.219.2.r01ma12503]

P- Reviewer: Cerwenka H, Li YZ **S- Editor**: Ji FF **L- Editor**: A
E- Editor: Lu YJ

World Journal of Radiology

Submit a Manuscript: http://www.f6publishing.com

World J Radiol 2017 December 28; 9(12): 448-453

DOI: 10.4329/wjr.v9.i12.448

ISSN 1949-8470 (online)

CASE REPORT

Aggressive blood pressure treatment of hypertensive intracerebral hemorrhage may lead to global cerebral hypoperfusion: Case report and imaging perspective

Jose Gavito-Higuera, Rakesh Khatri, Ihtesham A Qureshi, Alberto Maud, Gustavo J Rodriguez

Jose Gavito-Higuera, Rakesh Khatri, Ihtesham A Qureshi, Alberto Maud, Gustavo J Rodriguez, Department of Neurology, Paul L. Foster School of Medicine, Texas Tech University of Health Sciences Center, El Paso, TX 79905, United States

Author contributions: All authors contributed equally.

Informed consent statement: Informed consent was obtained from the family of the patient for the purpose of publication.

Conflict-of-interest statement: None.

Manuscript source: Invited manuscript

Correspondence to: Rakesh Khatri, MD, Assistant Professor, Department of Neurology, Paul L. Foster School of Medicine, Texas Tech University of Health Sciences Center, 5001 El Paso Drive, El Paso, TX 79905, United States. rakesh.khatri@ttuhsc.edu
Telephone: +1-915-2155900
Fax: +1-915-5456705

Received: February 8, 2017
Peer-review started: February 12, 2017
First decision: May 17, 2017
Revised: August 22, 2017
Accepted: November 29, 2017
Article in press: November 29, 2017
Published online: December 28, 2017

Abstract

Hypoperfusion injury related to blood pressure decrease in acute hypertensive intracerebral hemorrhage continues to be a controversial topic. Aggressive treatment is provided with the intent to stop the ongoing bleeding. However, there may be additional factors, including autoregulation and increased intracranial pressure, that may limit this approach. We present here a case of acute hypertensive intracerebral hemorrhage, in which aggressive blood pressure management to levels within the normal range led to global cerebral ischemia within multiple border zones. Global cerebral ischemia may be of concern in the management of hypertensive hemorrhage in the presence of premorbid poorly controlled blood pressure and increased intracranial pressure.

Key words: Intracranial hemorrhage; Neurocritial care; Stroke management; Perihematoma ischemia

Core tip: The current case report highlights the risk of aggressive management of acute hypertension in the setting of intracerebral hemorrhage causing global cerebral hypoperfusion, despite maintenance of cerebral perfusion pressure above the lower threshold of autoregulation. The authors suggest the use of accurate method to measure cerebral oxygenation, such as brain-tissue oxygen monitoring, which could help individualize aggressive blood pressure control in patients with acute hypertensive intracerebral hemorrhage.

Gavito-Higuera J, Khatri R, Qureshi IA, Maud A, Rodriguez GJ. Aggressive blood pressure treatment of hypertensive intracerebral hemorrhage may lead to global cerebral hypoperfusion: Case report and imaging perspective. *World J Radiol* 2017; 9(12): 448-453 Available from: URL: http://www.wjgnet.com/1949-8470/full/v9/i12/448.htm DOI: http://dx.doi.org/10.4329/wjr.v9.i12.448

INTRODUCTION

Up to one-third of spontaneous intracerebral hemorrhages (ICHs) expand, typically, within the first 6 h after the ictus. This expansion contributes to clinical deterioration and worse outcome[1-3]. Persistent high blood pressure may promote recurrent early bleeding[4-6]. Despite several reports that supported aggressive blood pressure control, reducing the risk of bleeding and improving the outcome, recent randomized larger trials have failed to prove it[7-9]. The safety of this approach has been questioned, mainly based on the concern that the perihematoma region may already be ischemic, due to local tissue pressure and have impaired autoregulation. But it may also be because autoregulation may be globally impaired after the ictus, or autoregulation may be retained but shifted substantially toward higher perfusion pressures. Based on these concerns, aggressive blood pressure reduction might lead to local or global ischemia.

There is evidence suggesting that autoregulation is retained locally in the perihematoma region. Blood flow decreases in areas adjacent to the hematoma; although, there is an accompanying decrease in metabolism without evidence of ischemia[10]. Cerebral autoregulation has been shown to be preserved in small- and medium-sized hematomas; however, it is variably shifted to higher levels in patients with chronic hypertension[11,12]. Determining whether blood pressure management prevents hematoma growth after ICH and how blood pressure reduction can be safely performed are key research priorities[13].

We present herein a case of spontaneous ICH, for which aggressive treatment of hypertension did not lead to infarction around the hematoma but globally in multiple border zone areas.

CASE REPORT

A 52-year-old black woman suddenly developed slurred speech and mild right hemiparesis. Medical history included poorly controlled chronic hypertension, and no known history of atrial fibrillation. In the emergency department, the initial blood pressure reading was 264/218 mmHg. The patient had right hemiparesis and dysarthria, and it was also noted that she was confused. After an episode of emesis she became lethargic, requiring emergent endotracheal intubation. A computerized tomography (CT) scan of the head showed a left thalamic hemorrhage (volume 36 mL, A × B × C/2) with intraventricular extension and developing hydrocephalus. Treatment to control blood pressure included intravenous labetalol boluses and nitroprusside infusion. External ventricular drainage was placed to manage hydrocephalus, and intracranial pressure and cerebral perfusion pressure were then monitored (Figure 1).

The patient underwent CT angiography of the head on arrival, which revealed no vessel occlusion. In addition, further work-up including continuous

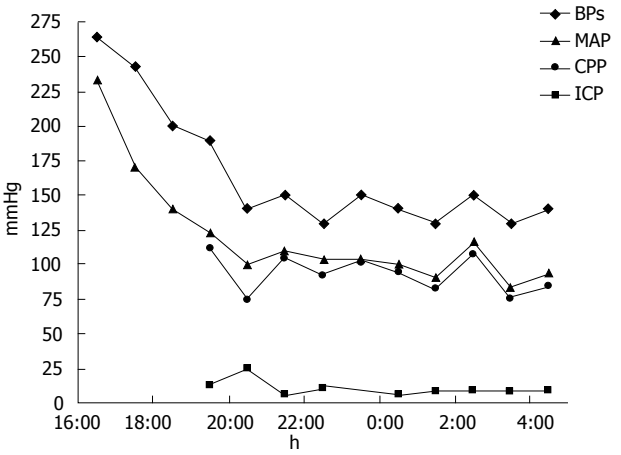

Figure 1 Diagram showing the evolution of systolic blood pressure, mean arterial blood pressure, cerebral perfusion pressure and intracranial pressure within the first 12 h. BP: Blood pressure; MAP: Mean arterial blood pressure; CPP: Cerebral perfusion pressure; ICP: Intracranial pressure.

cardiac monitoring in telemetry unit in the intensive care unit (ICU) for several days, electrocardiogram and echocardiogram did not reveal any cardioembolic etiology, except for left ventricular hypertrophy. For the following days, the patient remained comatose, although examination was limited due to sedation. A follow-up CT of the head at 96 h post-admission showed a cerebellar hypodensity. Magnetic resonance imaging (MRI) of the brain showed areas of restricted diffusion consistent with acute ischemia in multiple internal border zone areas of bilateral cerebral and cerebellar hemispheres (Figure 2). No significant stenosis was found in the magnetic angiography of the neck or brain. Cerebral perfusion pressure was above 70 mmHg, except for two measurements (68 mmHg on day 2 and 62 mmHg on day 4). On day 2, intraventricular thrombolytics were administered and the ventriculostomy was clamped. On day 4, blood pressure was 110/55 (the lowest recorded) and the nitroprusside drip was reduced with rapid improvement. The patient survived, but was aphasic and right hemiparetic at the time of discharge to a nursing home.

DISCUSSION

Two features in this case are to be discussed. First, global cerebral ischemia after aggressive blood pressure reduction seemed more a concern than the presence of ischemia around the hematoma; and, second, global ischemia developed despite maintenance of cerebral perfusion pressure above the lower threshold of autoregulation in normals.

The fact that the region around the hematoma was spared, with a mean arterial pressure reduction of about 50%, goes along with recent work by Powers *et al*[12] and Zazulia *et al*[14]. Although ischemia around the hematoma was initially thought to be present and to contribute to secondary brain injury based on experimental animal models[15-17], nowadays it is

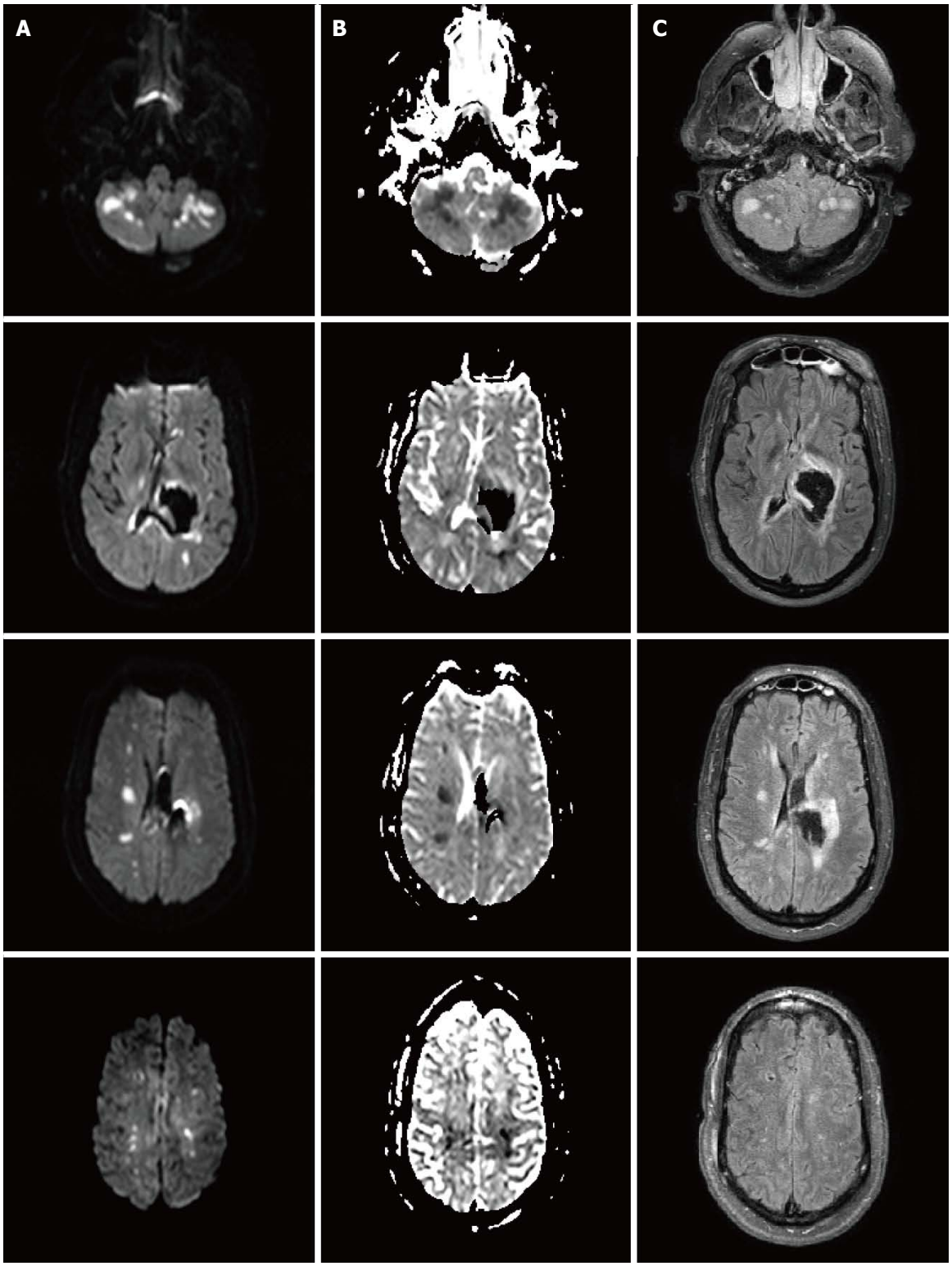

Figure 2 Brain magnetic resonance imaging with diffusion weighted imaging (A), apparent diffusion coefficient (B) and FLAIR sequences (C) showing multiple areas of infarction in the internal border zone areas of bilateral cerebral and cerebellar hemispheres. There is no evidence of perihematoma infarction. MRI: Magnetic resonance imaging.

more controversial and it is becoming more evident about its absence, based on human studies. Using MRI, no markers of ischemia were associated with the perihematomal region in acute ICH[18,19]. Positron emission tomography (PET) studies also reported perihematomal cerebral blood flow reductions, without evidence of ischemia[20]. Reduced perihematomal cerebral blood flow was associated with a decreased metabolic rate of oxygen and oxygen extraction fraction, suggesting that flow changes represent hypoactive

rather than ischemic tissue[14].

On the basis of evidence derived from laboratory and clinical studies, three phases have been identified[10]. The hibernation phase, an acute period of concomitant hypoperfusion and hypometabolism, predominantly involves the perihematoma region and occurs during the first 2 d. The reperfusion phase is observed between days 2 and 14, with a heterogeneous pattern of cerebral blood flow, consisting of areas of relatively normal flow, persistent hypoperfusion and hyperperfusion. And, the normalization phase is observed thereafter, with normal cerebral blood flow reestablished in all viable regions. In this case, hypometabolism in the area around the hematoma might have prevented the tissue from infarction.

The reduction of about 50% in the mean arterial pressure may seem unsafe; although, once the intracranial pressure was monitored, the cerebral perfusion pressure (CPP) could be calculated, and in fact it was kept above the lower range for normals. Nevertheless, strong evidence-based guidelines for the management of blood pressure in patients with spontaneous ICH with systolic blood pressure more than 220 mm Hg are not clearly established. The writing group of the stroke council for the American Heart Association encourages in their guidelines, aggressive treatment of high blood pressure to prevent ongoing bleeding with the caveat that aggressive treatment may decrease cerebral perfusion and worsen brain damage, especially[21-23]. Based on these two rationales, the recommendation is for patients presenting with a systolic blood pressure between 150 and 220 mmHg, acute lowering of systolic blood pressure to 140 mmHg is safe (Class Ⅰ; Level of Evidence A); however, if the systolic blood pressure at presentation is above 220 mmHg, the recommendation of aggressive reduction is less clear (Class Ⅱb; Level of Evidence C). Intracranial pressure monitoring is also considered in patients with significant intraventricular hemorrhage or hydrocephalus, with a reasonable goal CPP between 50-70 mmHg (Class Ⅱb; Level of Evidence C).

Cerebral autoregulation maintains cerebral blood flow by modifying the cerebrovascular resistance when cerebral perfusion pressure fluctuates, keeping cerebral blood flow constant in normal subjects at a CPP between 50-70 mmHg[24]. In chronic hypertension, cerebral autoregulation is shifted to higher levels and the degree correlates with the severity of hypertension. Thickening in the vascular wall increases the resistance, providing tissue protection if CPP is high; however, the ability to dilate when CPP lowers is lessened[25,26]. While perfusion pressure is calculable at bedside, quantitative tissue flow cannot be measured without employing a method such PET or a more invasive one using brain-tissue oxygen monitors[27]. Recently, it has been shown in traumatic brain injury that up to one-third of patients may demonstrate low brain tissue oxygen despite adequate CPP[28,29].

The patient presented herein developed multiple cerebral border zone infarcts after aggressive but carefully monitored treatment of blood pressure with labetalol and nitroprusside. Several modern imaging studies suggest that an internal watershed infarction is primarily caused by hypoperfusion as seen in our patient; this should not be confused with cortical watershed infarct, which is primarily caused by microembolism[30-33].

We hypothesize that the lower limit of autoregulation was shifted to higher levels secondary to chronic untreated hypertension. What is an adequate cerebral perfusion pressure in a normal subject was not so in her case, resulting in insufficient cerebral blood flow and ischemia. Alternatively, decreased cerebral perfusion pressure could have occurred during treatment of hypertension prior to intracranial pressure monitoring (Figure 2).

In conclusion, aggressive management of acute hypertension in ICH is controversial. Global but not perihematoma hypoperfusion may be of more concern in this approach, since cerebral autoregulation in chronic hypertensive patients is variably shifted to higher levels. An accurate method to measure cerebral oxygenation, such as brain-tissue oxygen monitoring, could help individualize aggressive blood pressure control in patients with acute hypertensive ICH.

ARTICLE HIGHLIGHTS

Case characteristics

This case illustrates diffuse border zone infarcts caused by rapid and dramatic reduction in blood pressure in a patient presenting with intracerebral hemorrhage and chronic uncontrolled hypertension.

Clinical diagnosis

Stroke, sudden onset of slurred speech, right-sided hemiparesis, dysarthria, lethargy, blood pressure of 264/218.

Differential diagnosis

Ischemic stroke, hemorrhagic stroke, transient ischemic attack, hypoglycemia, Todd's paralysis, intracerebral aneurysm rupture.

Laboratory diagnosis

No laboratory test was diagnostic; the patient, however, presented with very elevated blood pressure levels, and normal blood sugar levels.

Imaging diagnosis

Non-contrast computed tomography (CT) scan of the head showed left thalamic hemorrhage with intraventricular extension and developing hydrocephalus. Follow-up non-contrast CT scan of the head at 96 h showed a cerebellar hypodensity. Electrocardiogram revealed normal sinus rhythm. Echocardiogram did not reveal any cardioembolic etiology, except for left ventricular hypertrophy. Magnetic resonance imaging of the brain showed areas of restricted diffusion consistent with acute ischemia in multiple internal border zone areas of bilateral cerebral and cerebellar hemispheres; the location in the border zone areas makes embolic etiology of the ischemia unlikely. Magnetic resonance angiography of the brain and neck revealed no significant stenosis that could have contributed to the cerebral ischemia.

Treatment

Blood pressure control with intravenous labetalol boluses and nitroprusside infusion. For the management of hydrocephalus and monitoring of intracranial and cerebral perfusion pressures, external ventricular drain was placed.

Intraventricular thrombolytics were given to prevent clot formation in the ventricles and facilitate the cerebrospinal fluid drainage.

Related reports

There are several randomized controlled trials that have focused on blood pressure control in the setting of intracerebral hemorrhage; however, strong evidence-based guidelines for the management of blood pressure in patients with spontaneous intracerebral hemorrhage and systolic blood pressure more than 220 mmHg are not clearly established.

Term explanation

Hematoma expansion: An increase in size of the initial intracerebral hemorrhage that occurs in up to one-third of the patients, usually within the first 24 h. Borderline or watershed infarctions: Those that occur in areas shared by two vascular territories; those areas are more susceptible to perfusion reduction as it happens with blood pressure reduction and/or shifted cerebral autoregulation. Cerebral autoregulation: A physiological mechanism that maintains cerebral blood flow at different blood pressure levels. In patients with chronic hypertension, the curve shifts to the right ("right shifted"); autoregulation is used for higher blood pressure levels, and it is more protective to elevated blood pressure but fails to react in case of lower blood pressure levels.

Experiences and lessons

Caution should be advised when blood pressure reduction is considered in patients with intracerebral hemorrhage, especially if arriving with very elevated blood pressure and known to have untreated chronic hypertension. In addition, the presence of concomitant increased intracranial pressure due to the mass effect and/or hydrocephalus after intraventricular extension increases the intracranial pressure and thus decreases the cerebral perfusion pressure. Cerebral autoregulation shifts to the right in patients with chronic untreated hypertension and a reduction in blood pressure may not be tolerated leading to ischemia; therefore, such intervention in certain cases may be unsafe, as described in the article.

REFERENCES

1 **Brott T**, Broderick J, Kothari R, Barsan W, Tomsick T, Sauerbeck L, Spilker J, Duldner J, Khoury J. Early hemorrhage growth in patients with intracerebral hemorrhage. *Stroke* 1997; **28**: 1-5 [PMID: 8996478 DOI: 10.1161/01.STR.28.1.1]

2 **Kazui S**, Naritomi H, Yamamoto H, Sawada T, Yamaguchi T. Enlargement of spontaneous intracerebral hemorrhage. Incidence and time course. *Stroke* 1996; **27**: 1783-1787 [PMID: 8841330 DOI: 10.1161/01.STR.27.10.1783]

3 **Broderick JP**, Brott TG, Tomsick T, Barsan W, Spilker J. Ultra-early evaluation of intracerebral hemorrhage. *J Neurosurg* 1990; **72**: 195-199 [PMID: 2295917 DOI: 10.3171/jns.1990.72.2.0195]

4 **Kazui S**, Minematsu K, Yamamoto H, Sawada T, Yamaguchi T. Predisposing factors to enlargement of spontaneous intracerebral hematoma. *Stroke* 1997; **28**: 2370-2375 [PMID: 9412616 DOI: 10.1161/01.STR.28.12.2370]

5 **Becker KJ**, Baxter AB, Bybee HM, Tirschwell DL, Abouelsaad T, Cohen WA. Extravasation of radiographic contrast is an independent predictor of death in primary intracerebral hemorrhage. *Stroke* 1999; **30**: 2025-2032 [PMID: 10512902 DOI: 10.1161/01.STR.30.10.2025]

6 **Ohwaki K**, Yano E, Nagashima H, Hirata M, Nakagomi T, Tamura A. Blood pressure management in acute intracerebral hemorrhage: relationship between elevated blood pressure and hematoma enlargement. *Stroke* 2004; **35**: 1364-1367 [PMID: 15118169 DOI: 10.1161/01.STR.0000128795.38283.4b]

7 **Anderson CS**, Heeley E, Huang Y, Wang J, Stapf C, Delcourt C, Lindley R, Robinson T, Lavados P, Neal B, Hata J, Arima H, Parsons M, Li Y, Wang J, Heritier S, Li Q, Woodward M, Simes RJ, Davis SM, Chalmers J; INTERACT2 Investigators. Rapid blood-pressure lowering in patients with acute intracerebral hemorrhage. *N Engl J Med* 2013; **368**: 2355-2365 [PMID: 23713578 DOI: 10.1056/NEJMoa1214609]

8 **Qureshi AI**. Antihypertensive Treatment of Acute Cerebral Hemorrhage (ATACH): rationale and design. *Neurocrit Care* 2007; **6**: 56-66 [PMID: 17356194 DOI: 10.1385/NCC:6:1:56]

9 **Qureshi AI**, Palesch YY, Barsan WG, Hanley DF, Hsu CY, Martin RL, Moy CS, Silbergleit R, Steiner T, Suarez JI, Toyoda K, Wang Y, Yamamoto H, Yoon BW; ATACH-2 Trial Investigators and the Neurological Emergency Treatment Trials Network. Intensive Blood-Pressure Lowering in Patients with Acute Cerebral Hemorrhage. *N Engl J Med* 2016; **375**: 1033-1043 [PMID: 27276234 DOI: 10.1056/NEJMoa1603460]

10 **Qureshi AI**, Hanel RA, Kirmani JF, Yahia AM, Hopkins LN. Cerebral blood flow changes associated with intracerebral hemorrhage. *Neurosurg Clin N Am* 2002; **13**: 355-370 [PMID: 12486925 DOI: 10.1016/S1042-3680(02)00012-8]

11 **Strandgaard S**. Autoregulation of cerebral blood flow in hypertensive patients. The modifying influence of prolonged antihypertensive treatment on the tolerance to acute, drug-induced hypotension. *Circulation* 1976; **53**: 720-727 [PMID: 815061 DOI: 10.1161/01.CIR.53.4.720]

12 **Powers WJ**, Zazulia AR, Videen TO, Adams RE, Yundt KD, Aiyagari V, Grubb RL Jr, Diringer MN. Autoregulation of cerebral blood flow surrounding acute (6 to 22 hours) intracerebral hemorrhage. *Neurology* 2001; **57**: 18-24 [PMID: 11445622 DOI: 10.1212/WNL.57.1.18]

13 **NINDS ICH Workshop Participants**. Priorities for clinical research in intracerebral hemorrhage: report from a National Institute of Neurological Disorders and Stroke workshop. *Stroke* 2005; **36**: e23-e41 [PMID: 15692109 DOI: 10.1161/01.STR.0000155685.77775.4c]

14 **Zazulia AR**, Diringer MN, Videen TO, Adams RE, Yundt K, Aiyagari V, Grubb RL Jr, Powers WJ. Hypoperfusion without ischemia surrounding acute intracerebral hemorrhage. *J Cereb Blood Flow Metab* 2001; **21**: 804-810 [PMID: 11435792 DOI: 10.1097/00004647-200107000-00005]

15 **Kobari M**, Gotoh F, Tomita M, Tanahashi N, Shinohara T, Terayama Y, Mihara B. Bilateral hemispheric reduction of cerebral blood volume and blood flow immediately after experimental cerebral hemorrhage in cats. *Stroke* 1988; **19**: 991-996 [PMID: 3400110 DOI: 10.1161/01.STR.19.8.991]

16 **Bullock R**, Brock-Utne J, van Dellen J, Blake G. Intracerebral hemorrhage in a primate model: effect on regional cerebral blood flow. *Surg Neurol* 1988; **29**: 101-107 [PMID: 3336844 DOI: 10.1016/0090-3019(88)90065-1]

17 **Nehls DG**, Mendelow AD, Graham DI, Sinar EJ, Teasdale GM. Experimental intracerebral hemorrhage: progression of hemodynamic changes after production of a spontaneous mass lesion. *Neurosurgery* 1988; **23**: 439-444 [PMID: 3200374]

18 **Butcher KS**, Baird T, MacGregor L, Desmond P, Tress B, Davis S. Perihematomal edema in primary intracerebral hemorrhage is plasma derived. *Stroke* 2004; **35**: 1879-1885 [PMID: 15178826 DOI: 10.1161/01.STR.0000131807.54742.1a]

19 **Schellinger PD**, Fiebach JB, Hoffmann K, Becker K, Orakcioglu B, Kollmar R, Jüttler E, Schramm P, Schwab S, Sartor K, Hacke W. Stroke MRI in intracerebral hemorrhage: is there a perihemorrhagic penumbra? *Stroke* 2003; **34**: 1674-1679 [PMID: 12805502 DOI: 10.1161/01.STR.0000076010.10696.55]

20 **Hirano T**, Read SJ, Abbott DF, Sachinidis JI, Tochon-Danguy HJ, Egan GF, Bladin CF, Scott AM, McKay WJ, Donnan GA. No evidence of hypoxic tissue on 18F-fluoromisonidazole PET after intracerebral hemorrhage. *Neurology* 1999; **53**: 2179-2182 [PMID: 10599802 DOI: 10.1212/WNL.53.9.2179]

21 **Hemphill JC 3rd**, Greenberg SM, Anderson CS, Becker K, Bendok BR, Cushman M, Fung GL, Goldstein JN, Macdonald RL, Mitchell PH, Scott PA, Selim MH, Woo D; American Heart Association Stroke Council; Council on Cardiovascular and Stroke Nursing; Council on Clinical Cardiology. Guidelines for the Management of Spontaneous Intracerebral Hemorrhage: A Guideline for Healthcare Professionals From the American Heart Association/American Stroke Association. *Stroke* 2015; **46**: 2032-2060 [PMID: 26022637 DOI: 10.1161/STR.0000000000000069]

22 **D'Amore C**, Paciaroni M. Border-zone and watershed infarctions. *Front Neurol Neurosci* 2012; **30**: 181-184 [PMID: 22377891 DOI: 10.1159/000333638]

23 **Gerraty RP**, Gilford EJ, Gates PC. Watershed cerebral infarction associated with perioperative hypotension. *Clin Exp Neurol* 1993; **30**: 82-89 [PMID: 7712632]

24 **Aaslid R**, Lindegaard KF, Sorteberg W, Nornes H. Cerebral autoregulation dynamics in humans. *Stroke* 1989; **20**: 45-52 [PMID: 2492126 DOI: 10.1161/01.STR.20.1.45]

25 **Baumbach GL**, Heistad DD. Cerebral circulation in chronic arterial hypertension. *Hypertension* 1988; **12**: 89-95 [PMID: 3044994 DOI: 10.1161/01.HYP.12.2.89]

26 **Agnoli A**, Fieschi C, Bozzao L, Battistini N, Prencipe M. Autoregulation of cerebral blood flow. Studies during drug-induced hypertension in normal subjects and in patients with cerebral vascular diseases. *Circulation* 1968; **38**: 800-812 [PMID: 5677964 DOI: 10.1161/01.CIR.38.4.800]

27 **Powers WJ**, Zazulia AR. The use of positron emission tomography in cerebrovascular disease. *Neuroimaging Clin N Am* 2003; **13**: 741-758 [PMID: 15024958]

28 **Stiefel MF**, Udoetuk JD, Spiotta AM, Gracias VH, Goldberg A, Maloney-Wilensky E, Bloom S, Le Roux PD. Conventional neurocritical care and cerebral oxygenation after traumatic brain injury. *J Neurosurg* 2006; **105**: 568-575 [PMID: 17044560 DOI: 10.3171/jns.2006.105.4.568]

29 **Stocchetti N**, Chieregato A, De Marchi M, Croci M, Benti R, Grimoldi N. High cerebral perfusion pressure improves low values of local brain tissue O2 tension (PtiO2) in focal lesions. *Acta Neurochir Suppl* 1998; **71**: 162-165 [PMID: 9779173 DOI: 10.1007/978-3-7091-6475-4_47]

30 **Zheng M**, Sun A, Sun Q, Zhang H, Fan D. Clinical and Imaging Analysis of a Cerebellar Watershed Infarction. *Chinese Medicine* 2015; **6**: 54-60 [DOI: 10.4236/cm.2015.61006]

31 **Moriwaki H**, Matsumoto M, Hashikawa K, Oku N, Ishida M, Seike Y, Watanabe Y, Hougaku H, Handa N, Nishimura T. Hemodynamic aspect of cerebral watershed infarction: assessment of perfusion reserve using iodine-123-iodoamphetamine SPECT. *J Nucl Med* 1997; **38**: 1556-1562 [PMID: 9379192]

32 **Lee PH**, Bang OY, Oh SH, Joo IS, Huh K. Subcortical white matter infarcts: comparison of superficial perforating artery and internal border-zone infarcts using diffusion-weighted magnetic resonance imaging. *Stroke* 2003; **34**: 2630-2635 [PMID: 14563962 DOI: 10.1161/01.STR.0000097609.66185.05]

33 **Gould B**, McCourt R, Gioia LC, Kate M, Hill MD, Asdaghi N, Dowlatshahi D, Jeerakathil T, Coutts SB, Demchuk AM, Emery D, Shuaib A, Butcher K; ICH ADAPT Investigators. Acute blood pressure reduction in patients with intracerebral hemorrhage does not result in borderzone region hypoperfusion. *Stroke* 2014; **45**: 2894-2899 [PMID: 25147326 DOI: 10.1161/STROKEAHA.114.005614]

P- Reviewer: Kim MS, Llompart-Pou JA, Shen J, Zavras N
S- Editor: Kong JX **L- Editor**: Filipodia **E- Editor**: Lu YJ

World Journal of Radiology

Submit a Manuscript: http://www.f6publishing.com

World J Radiol 2017 December 28; 9(12): 454-458

DOI: 10.4329/wjr.v9.i12.454

ISSN 1949-8470 (online)

CASE REPORT

Case of victims of modern imaging technology: Increased information noise concealing the diagnosis

Abhishek Mahajan, G V Santhoshkumar, Ameya Shirish Kawthalkar, Richa Vaish, Nilesh Sable, Supreeta Arya, Subhash Desai

Abhishek Mahajan, G V Santhoshkumar, Ameya Shirish Kawthalkar, Richa Vaish, Nilesh Sable, Supreeta Arya, Subhash Desai, Department of Radiodiagnosis and Imaging, Tata Memorial Hospital, Mumbai 400012, India

ORCID number: Abhishek Mahajan (0000-0001-6606-6537); G V Santhoshkumar (0000-0001-5426-5651); Ameya Shirish Kawthalkar (0000-0002-3248-325X); Richa Vaish (0000-0002-3384-9380); Nilesh Sable (0000-0002-3384-9380); Supreeta Arya (0000-0002-0483-9095); Subhash Desai (0000-0003-2525-0690).

Author contributions: All authors contributed to study concepts/study design, data acquisition or data analysis/interpretation, manuscript drafting or manuscript revision for important intellectual content, manuscript final version approval, literature research,manuscript editing and integrity of the data/ the accuracy of the data analysis.

Informed consent statement: Participant gave informed consent for data sharing.

Conflict-of-interest statement: I confirm that this manuscript is not published anywhere else and on behalf of all authors, I state that there is no conflict of interests (including none for related to commercial, personal, political, intellectual, or religious interests).

Manuscript source: Unsolicited manuscript

Correspondence to: Abhishek Mahajan, MRes, MD, Radiodiagnosis, Fellowship in Cancer Imaging, Associate professor, Department of Radiodiagnosis and Imaging, Tata Memorial Hospital, Room No. 127, Dr E Borges Road, Parel, Mumbai 400012, India. mahajana@tmc.gov.in
Telephone: +91-99-20210811

Received: September 13, 2017
Peer-review started: September 19, 2017
First decision: October 23, 2017
Revised: November 9, 2017
Accepted: November 27, 2017
Article in press: November 27, 2017
Published online: December 28, 2017

Abstract

We present a case of tubercular arthritis who underwent numerous unnecessary investigations what is known as "victims of modern imaging technology" or VOMIT. Today there is an exponential rise in the volume of the medical imaging, part of which is contributed by unnecessary and unjustified indications. We discuss about the untoward effects of the uninhibited and careless use of modern imaging modalities and possible ways to avoid. Skeletal manifestation of the tuberculosis is still common in the endemic countries like India. Although the final diagnosis of the skeletal tuberculosis like tubercular arthritis is made by bacteriological and histological studies, few demographic, clinical and radiological features might help making early diagnosis.

Key words: Radiology; Modern imaging; Patient care; Healthcare costs; Tubercular arthritis; Diagnostic imaging overuse

Core tip: The primary objective is to highlight the possible consequences of the irrational use of imaging investigations. In this case report, we want to explain about an anxious patient undergoing some myriad

investigations for an uncommon presentation of common presentations. It is important to optimally use available resources with improved communication with referring physicians and increasing the awareness regarding the utility and indications for various imaging.

Mahajan A, Santhoshkumar GV, Kawthalkar AS, Vaish R, Sable N, Arya S, Desai S. Case of victims of modern imaging technology: Increased information noise concealing the diagnosis. *World J Radiol* 2017; 9(12): 454-458 Available from: URL: http://www.wjgnet.com/1949-8470/full/v9/i12/454.htm DOI: http://dx.doi.org/10.4329/wjr.v9.i12.454

INTRODUCTION

With modern medical imaging boom and exponential rise of its volume as well as with increasing accuracy from these imaging, it is small wonder that the examples of victims of modern imaging technology or VOMIT are on the rise[1,2]. While radiology and imaging are influencing patient management and treatment decisions like never before, unscrupulous and careless use of newer imaging techniques is detrimental to the patient's as well as hospital's resources and, contributes significantly to patient's anxiety if a grave diagnosis is mistakenly made.

Skeletal tuberculosis is uncommon in third world countries with Appendicular joint affectation being uncommon than spinal tuberculosis[3]. The few cases of distal small joint affectations are all prior to 1980[4]. Two cases of tubercular arthritis mimicking neoplasm have been reported[5]. However, there is no case reported of carcinomatous arthropathy of the first metacarpophalangeal joint[6]. As an example of VOMIT in the modern era, we wish to highlight a rare case of tubercular arthritis of the first metacarpophalangeal joint masquerading as skeletal metastasis, which demonstrates the ill-effects of unwarranted excessive medical imaging.

CASE REPORT

A 40-year-old male presented with pain and swelling of the left thumb in the past 1 mo along with vague bone and joint pains and associated swelling in the neck. Clinical evaluation for the midline neck swelling revealed an indeterminate heteroechoic 15 mm thyroid lesion on sonography (Figure 1). His routine blood investigations and serum biochemistry were normal. The radiograph of his left thumb revealed destruction of the left first metacarpophalangeal joint. A Tc-99m pertechnate thyroid scan showed focal low-grade uptake in the thyroid in the same location. Assuming this thyroid lesion as a primary carcinoma and the thumb lesion as metastatic, the patient was advised a fluoride-18 bone scan for the multiple vague bone and joint pains that showed a focus of intense tracer uptake at the left first metacarpophalangeal joint accompanied by varying degrees of uptake at multiple sites in the appendicular and axial skeleton. The patient was thus referred to our tertiary cancer institute for further management.

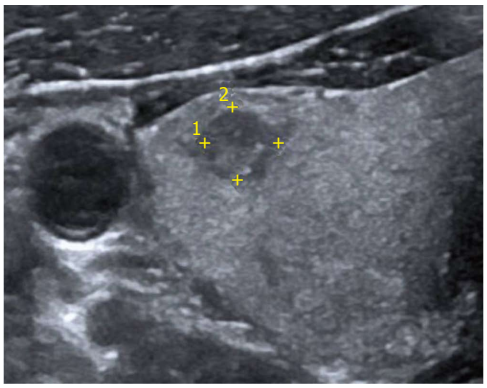

Figure 1 High resolution ultrasonography of the neck reveals a well-defined heteroechoic lesion in the right lobe of thyroid gland which appeared indeterminate on imaging (TIRADS 4B).

Our Head and Neck Surgical Oncology OPD advised sonography-guided thyroid FNAC that was reported as benign colloid goiter (Bethesda category Ⅱ). The CT-guided biopsy of hand lesion (Figure 2) reported necrotic tissue with calcification and reparative changes, along with few lymphoid cells and, suggested evaluation for any parathyroid pathology. On sonography, the parathyroids were normal and he had normal levels of rheumatoid factor, serum uric acid, and parathormone levels. ESR was marginally elevated (42 mm/h).

An FDG positron emission tomography- computed tomography (PET-CT) was performed to confirm/rule out malignancy, which revealed a lytic destructive lesion of the first metacarpophalangeal joint with a soft tissue component, having a maximum standardized uptake value (SUV) of 17.2. No uptake was noted elsewhere in the appendicular or axial skeleton. The lung images showed diffuse ground glass opacities with multiple subcentimeter sized soft tissue density nodules, fibrotic changes and calcified granulomas in both the lungs (Figure 3). Considering the patient's demographic and clinical background these were most likely suggestive of active pulmonary tuberculosis.

MR of the affected hand suggested by our orthopedic surgeons revealed altered marrow signal intensity involving the left first MCP joint with associated articular cortical destruction, synovitis, active enhancing pannus formation and rim-enhancing soft tissue component (abscesses) (Figure 4). A review of the previous radiograph showed joint destruction and peri-articular osteopenia (Figure 5). Malignancy being ruled out, the differentials narrowed down to an infective or traumatic arthropathy. Correlating the radiographic, PET-CT and MR findings, a provisional diagnosis of tubercular arthritis secondary to active pulmonary tuberculosis was made.

A pathology review of the CT guided biopsy sample was asked with real time polymerase chain reaction

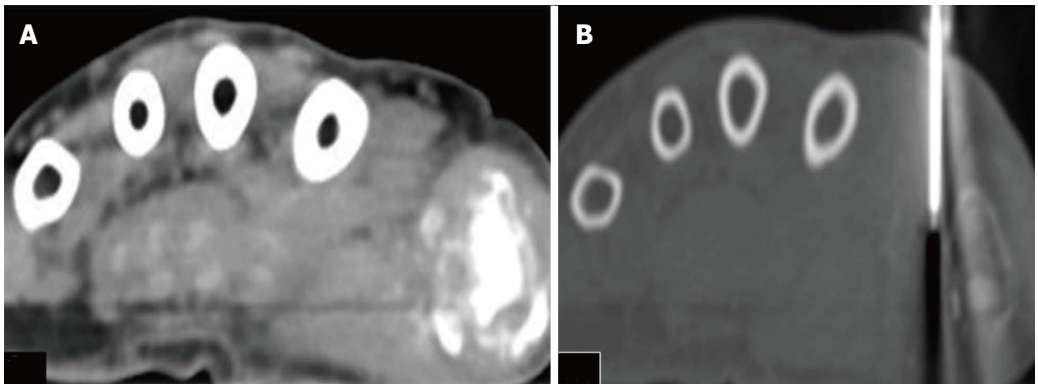

Figure 2 Axial computed tomography of the hand. The patient is positioned in prone position. A: Axial CT scan image in soft tissue window; B: Axial CT scan image in bone window is showing Trucut biopsy needle taking tissue sample from the soft tissue component surrounding the area of lytic destructive lesion at the first metacarpo-phalangeal joint. CT: Computed tomography.

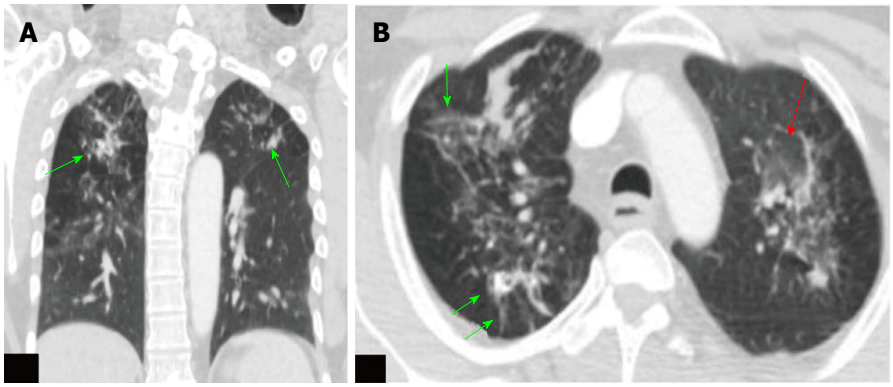

Figure 3 Computed tomography thorax images of the positron emission tomography-computed tomography scan. A: Coronal CT scan image of the thorax in lung window; B: Axial CT scan image of the thorax in lung window at upper thorax. These images show ground glass opacities (red arrow) with multiple soft tissue density nodules (green arrow), fibrotic changes and calcified granulomas in both the lungs. Features are suggestive of active tuberculosis. CT: Computed tomography.

(RT-PCR). This test revealed evidence of mycobacterium tuberculosis within the biopsy sample, thus establishing the diagnosis of tubercular arthritis of the left first metacarpophalangeal joint.

At the end of all these diagnostic investigations which included radiological, biochemical and histological tests, patient spent a significant amount of money and time. He also paid for travel expenses and registration and consultation charges in various hospitals. Added to this he must have underwent metal turmoil of anxiety and frustration. Not only these were costing him, there was waste of resources and time of hospitals/country which might have be used for patient in need.

DISCUSSION

It's been a while that the concept of VOMIT was put forth to prevent patients from needless diagnostic costs and mental anguish after being put through a battery of expensive and misdirected imaging tests[1,2]. Still cases such as these are routinely found in clinical practice; the primary reason is our inability to discern pertinent data from the flood of information provided by myriad new imaging studies.

In this century and in endemic countries like India, primary bone tuberculosis not as common; spine and large joint affectations are seen, but those of small joints infrequent[3,4]. The mean age of presentation is 20 to 40 years and presenting with pain and swelling of affected joint; mostly metacarpal of the little finger[7]. Radiologically, the key to diagnosis is the Phemister's triad that includes juxta-articular osteopenia, subarticular erosions and joint space narrowing, with or without soft tissue component[2]. Key magnetic resonance imaging (MRI) features include synovitis, joint effusion, subarticular erosions, active and chronic pannus, abscesses, hypo-intense synovium and bone chips[8].

The final diagnosis of tuberculous arthritis is based on bacteriology and histological studies. The differential diagnosis of tuberculous arthritis includes gout, sarcoidosis, osteomyelitis and tumors[9]. Inflammatory and infective lesions may show high grade FDG uptake, and every lesion which demonstrates high SUV should not be labeled as a malignancy[10]. Metastatic arthropathy is a rare occurrence with only a handful of cases reported in the literature[5,6]. For joint disease in patients with a known primary, other etiologies should always be considered first in the differential diagnosis.

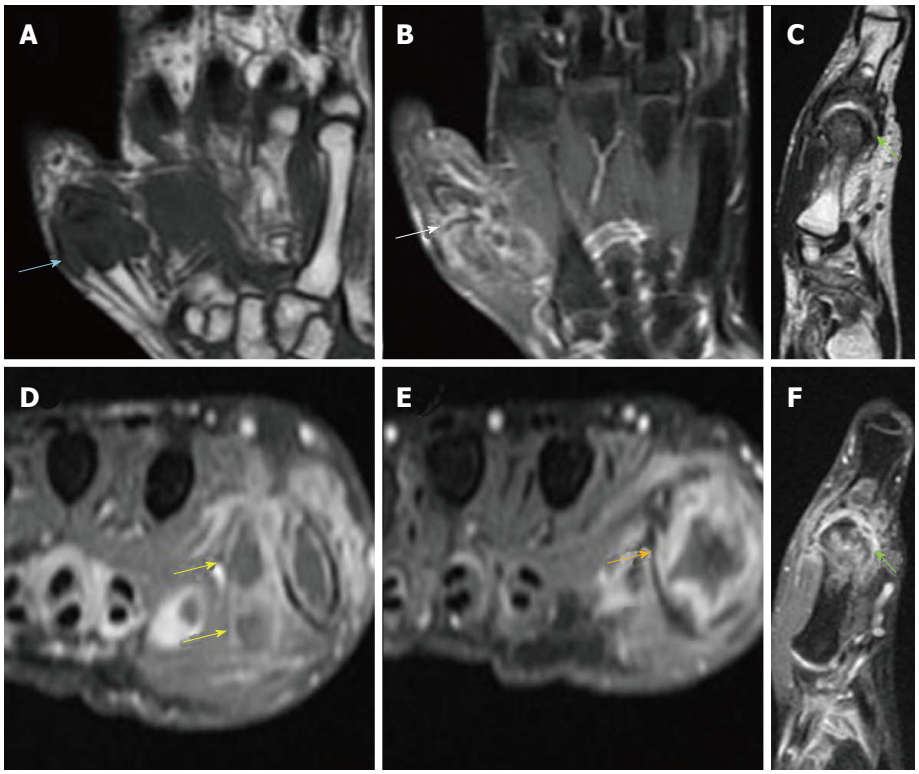

Figure 4 Plain and contrast enhanced magnetic resonance imaging images of proximal hand. A: Coronal T1W. Hypointense soft-tissue is noted surrounding the first MCP joint with hypointense marrow changes; B: Coronal STIR. Irregular hyperintensities are seen surrounding the first MCP joint along with hyperintensity within the peri-articular bone marrow; C: Sagittal T2W. Mild joint effusion is seen with hypertrophied T2 hypointense synovium and pannus formation; D-F: Axial and sagittal post-contrast Fat Sat T1W. Arrows indicate peripherally enhancing abscesses adjacent to the first MCP joint. Also noted in the vicinity is enhancing proliferative pannus. MCP: Metacarpophalangeal.

Figure 5 Radiograph of left thumb shows destruction of left first metacarpophalangeal joint with juxta-articular osteopenia and foci of calcification. In view of this appearance gout was also considered in the differential. However in view of normal serum uric acid levels, infective arthropathy was the most likely diagnosis.

To conclude, radiologists should improve communication with referring physicians and increase their awareness regarding the utility and indications for various imaging tests[11]. Radiologists should also themselves act as true imaging gatekeepers, preventing unnecessary overuse of imaging and striving to overcome commoditization of imaging modalities[12].

While making of provisional diagnosis, a radiologist should think of common disease over uncommon diseases. With high prevalence of common disease, a radiologist making a diagnosis of common disease, statistically will be correct in most of the cases. But it should be kept in mind that not to miss a grave or medico legally important condition even it might be uncommon.

It is always worth to follow protocol in certain conditions, which are made for standardization, streamlining the workflow, increase the accuracy as well better communication among clinicians and radiologist. A good example for a well-accepted protocol is Breast Imaging Reporting and Data System (BIRADS). At times a radiologist giving a BIRADS category of 3, he might be more than 98% accurate in diagnosis (BIRADS category 3 translates to "probably benign". The likelihood of malignancy is 0%-2%). To address this small portion of likelihood of malignancy, it is advised to have a short interval follow up, rather than further investigations to confirm the benignity.

A referring clinician needs to know what imaging study is suitable to ascertain a particular condition. An open and free discussion with the radiologist regarding patient disease condition, availability of imaging resources, benefits and limitation of diagnostic modality should be encouraged.

There is a need for setting objective benchmarks for missed diagnoses in the field of radiology. There must be greater knowledge sharing, targeted instruction and team-working among various clinical fields.

ARTICLE HIGHLIGHTS

Case characteristics

A case of tubercular arthritis who underwent a number of investigations in suspicion of malignancy, each one adding to the confusion rather than helping in arriving diagnosis.

Clinical diagnosis

Infective arthritis of hand.

Differential diagnosis

Rheumatoid arthritis; Septic arthritis; Primary or secondary malignancy.

Laboratory diagnosis

Demonstration of Mycobacterium tuberculosis on culture of bone tissue/positive Ziehl-Neelsen staining/rapid PCR DNA detection.

Imaging diagnosis

Radiography: Juxta-articular osteopenia, subarticular erosions and joint space narrowing, with or without soft tissue component. MRI: Synovitis, joint effusion, subarticular erosions, active and chronic pannus, abscesses, hypo-intense synovium and bone chips.

Pathological diagnosis

Features favoring tubercular infection as granulomas with caseous necrosis in synovial tissue and bone.

Treatment

Skeletal tuberculosis including arthritis are treated with 9-12 mo of anti-tubercular drug regimen.

Related reports

Several cases of tubercular involvement of small joints of hand are reported in literature. In most of the cases, septic and rheumatoid arthritis were considered as differential diagnosis. Two cases of tubercular arthritis mimicking neoplasm have been reported.

Term explanation

VOMIT: Victims of modern imaging technology; Phemister's triad: Juxta-articular osteopenia, subarticular erosions and joint space narrowing.

Experiences and lessons

Following standardized guidelines reduces the errors in diagnostic and treatment workflow. While making of provisional diagnosis, a radiologist should think of common disease over uncommon diseases. A free and open discussion among clinicians, radiologists and pathologists should be encouraged.

REFERENCES

1 **Hayward R**. VOMIT (victims of modern imaging technology)-an acronym for our times. *BMJ* 2003; **326**: 1273 [DOI: 10.1136/bmj.326.7401.1273]

2 **Shaikh U**, Lewis-Jones H. Commercial CT scans: VOMIT victim of medical investigative technology. *BMJ* 2008; **336**: 8 [PMID: 18174573 DOI: 10.1136/bmj.39435.572731.3A]

3 **Harisinghani MG**, McLoud TC, Shepard JA, Ko JP, Shroff MM, Mueller PR. Tuberculosis from head to toe. *Radiographics* 2000; **20**: 449-470; quiz 528-529, 532 [PMID: 10715343 DOI: 10.1148/radiographics.20.2.g00mc12449]

4 **Martini M**. Tuberculosis of the Upper-Limb Joints. Tuberculosis of the Bones and Joints. Switzerland: Springer, 1988: 80-110 [DOI: 10.1007/978-3-642-61358-6_10]

5 **Fukasawa H**, Suzuki H, Kato A, Yamamoto T, Fujigaki Y, Yonemura K, Hishida A. Tuberculous arthritis mimicking neoplasm in a hemodialysis patient. *Am J Med Sci* 2001; **322**: 373-375 [PMID: 11780697 DOI: 10.1097/00000441-200112000-00012]

6 **Gutiérrez-Polo RA**, López-Medina S, Cabrera-Pozuelo E, González-Vela C, Gutiérrez-Polo MD, Peña-Sagredo JL, Martinez-Taboada VM. Metastatic arthropathy report of two cases and review of the literature. *J Clin Rheumatol* 1997; **3**: 162-167 [PMID: 19078177 DOI: 10.1097/00124743-199706000-00011]

7 **Kotwal PP**, Khan SA. Tuberculosis of the hand: clinical presentation and functional outcome in 32 patients. *J Bone Joint Surg Br* 2009; **91**: 1054-1057 [PMID: 19651833 DOI: 10.1302/0301-620X.91B8.22074]

8 **Sawlani V**, Chandra T, Mishra RN, Aggarwal A, Jain UK, Gujral RB. MRI features of tuberculosis of peripheral joints. *Clin Radiol* 2003; **58**: 755-762 [PMID: 14521883 DOI: 10.1016/S0009-9260(03)00271-X]

9 **Hassan FO**. Tuberculous dactylitis pseudotumor of an adult thumb: a case report. *Strategies Trauma Limb Reconstr* 2010; **5**: 53-56 [PMID: 20360878 DOI: 10.1007/s11751-010-0080-1]

10 **Kobayashi K**, Bhargava P, Raja S, Nasseri F, Al-Balas HA, Smith DD, George SP, Vij MS. Image-guided biopsy: what the interventional radiologist needs to know about PET/CT. *Radiographics* 2012; **32**: 1483-1501 [PMID: 22977031 DOI: 10.1148/rg.325115159]

11 **FitzGerald R**. Radiological error: analysis, standard setting, targeted instruction and teamworking. *Eur Radiol* 2005; **15**: 1760-1767 [PMID: 15726377 DOI: 10.1007/s00330-005-2662-8]

12 **Jain SN**. Are radiologists true medical imaging gatekeepers? *Indian J Radiol Imaging* 2014; **24**: 315-316 [PMID: 25489123 DOI: 10.4103/0971-3026.143892]

P- Reviewer: Arcangeli S, Chow J, Gao BL **S- Editor**: Ji FF
L- Editor: A **E- Editor**: Lu YJ

Published by **Baishideng Publishing Group Inc**
7901 Stoneridge Drive, Suite 501, Pleasanton, CA 94588, USA
Telephone: +1-925-223-8242
Fax: +1-925-223-8243
E-mail: bpgoffice@wjgnet.com
Help Desk: http://www.f6publishing.com/helpdesk
http://www.wjgnet.com